TRANSPORTATION RESEARCH RECORD 1084

Pavement Roughness and Skid Resistance

TRB

TRANSPORTATION RESEARCH BOARD
NATIONAL RESEARCH COUNCIL
WASHINGTON, D.C. 1986

Contents

Strategies for Reducing Truck Accidents on Wet Pavements

DON L. IVEY, WALTER B. HORNE, and RICHARD D. TONDA

ABSTRACT

The discovery that heavy truck tires do hydroplane at vehicle speeds from 50 to 70 mph is explored in depth. Horne's prediction of this phenomenon is described in detail. The Texas Transportation Institute's testing program to verify this prediction is described and the results are compared with Horne's theory. An analysis of the Bureau of Motor Carrier Safety files on truck accidents for the years 1979 through 1981 shows the extreme overrepresentation of unloaded tractor semitrailers in wet weather accidents, supporting the thesis that tire hydroplaning of large unloaded vehicles is a major contributor to wet weather accidents. Finally, other elements of the problem are explored such as vehicle stability, braking system effects, low tire-pavement friction, and the speed increases associated with unloaded vehicles.

The recent prediction by Horne (1) and verification (2) that truck tires are subject to dynamic hydroplaning at highway speeds has dictated a reassessment of the causes of tractor semitrailer accidents in wet weather. Those concerned with highway safety have long noted the high frequency of single vehicle losses of control in wet weather. Although many reports have been published documenting this phenomenon and discussing low tire-pavement friction (3,4), reduced visibility (5), and hydroplaning (6) as influential factors, almost all this work has dealt primarily with automobiles. Large trucks have been considered an especially puzzling case. For example, some engineers have noted what appeared to be a comparatively frequent occurrence--unloaded trucks' loss of control during wet weather. Because it was understood that large truck hydroplaning at highway speeds did not occur, these losses of control were usually attributed to low tire-pavement friction, brake balance problems, and possibly excessive speed by lightly loaded trucks. This common understanding has now been shown to be in error and another influential factor must be added to the list--truck tire hydroplaning.

The addition of this new factor does not negate any of those previously known but it does complicate the loss of control phenomenon because there is now a new level of interactions between (a) visibility, (b) speed, (c) loading condition, (d) pavement surface properties, (e) brake system characteristics, and (f) hydroplaning.

The reduction of visibility during wet weather has been described in several reports (5,7) and is generally associated with a reduction in the time required for traction performance, at the time the availability of traction for either cornering or braking may be greatly reduced. Figures 1 and 2 show the influence of rainfall on visibility. Figure 3 shows how available tire-pavement friction is reduced on wet pavement (3). This reduction is maximum at high speed.

Although it remains to be proven, it appears probable that an inverse relationship exists between tractor semitrailer speed and load carried. The

D.L. Ivey and R.D. Tonda, Texas Transportation Institute, Texas A&M University System, College Station, Tex. 77843. W.B. Horne, Highway Safety Consultant, 192 Queens Drive West, Williamsburg, Va. 23185.
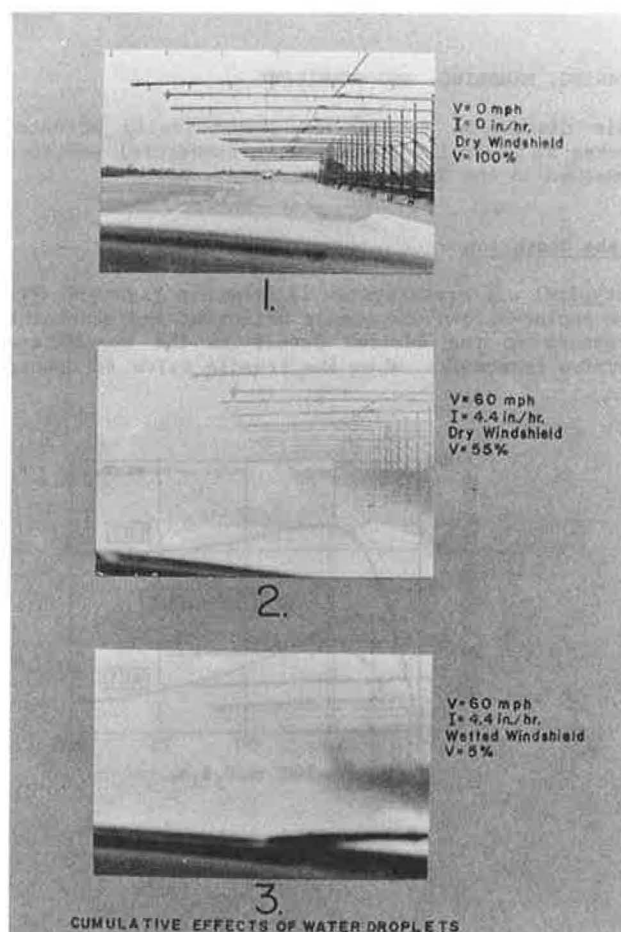
FIGURE 1 Progressive influence of rainfall on visibility as the intensity increases and as the windshield surface becomes covered with water.

obvious capability of some rigs to run faster under lightly loaded conditions points to this probability. It will be demonstrated in other sections of this paper that it is the lightly loaded truck tire that is susceptible to hydroplaning. Thus the likelihood of higher speeds under reduced load condition in-

FIGURE 2 Spray generated by tractor semi-trailer reduces visibility for drivers of following vehicles.

creases the probability of hydroplaning and makes the appropriate balance in the brake system more critical to vehicle control.

BRAKING, HANDLING, AND STABILITY

This discussion focuses on pneumatically actuated brakes as typically installed on commercial vehicles operated in the United States.

Brake Operation

A typical air brake system is shown in Figure 4 (8). The engine-driven compressor builds up and maintains pressure to the desired levels in the supply and service reservoirs. When the treadle valve is opened

by the driver's foot (under normal operation), it takes a certain length of time for the supply pressure to be achieved in the brake chambers. This response time depends on the system's arrangement, which can be fairly complicated as demonstrated in Figure 4. The volumes of each system component, orifice and valve sizes, and line lengths strongly influence the response time. In Figure 5, MacAdam et al. (9) shows time histories of trailer brake chamber pressure of three combination vehicles. The application times are measured from the instant of pressure increase at the treadle valve. This figure shows that, in an accident environment in which a great deal can occur in a few milliseconds, the response time of the trailer brakes may have a significant effect.

The air pressure in the system is converted into an actuation force on the brake by the brake chamber. Typically, the air pressure displaces a piston/diaphragm assembly through a distance called the stroke. This displacement actually produces the force necessary for brake application, which force can be ideally computed by the product of the pressure times the piston/diaphragm area. In practice, however, this ideal result is not obtained. Figure 6 shows the results of processing typical test data and plotting effective area as a function of stroke and pressure. This graph illustrates dramatically how significant shortfalls in design force can be experienced in maladjusted brakes. As the brakes are used (if they are not properly adjusted for the current state of lining wear) the chamber can run out of stroke. Also, as brakes are heated through use, drum expansion may increase the influence of marginally adjusted links so that a loss of torque capacity is realized.

In order to draw reasonable conclusions about the expected performance of a brake system, the components described earlier must be analyzed as a system. A detailed analysis is beyond the scope of this paper; however, excellent developments have been
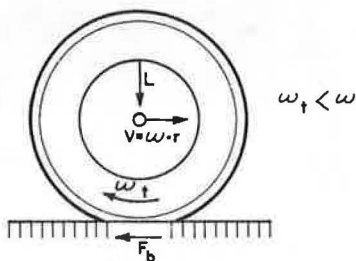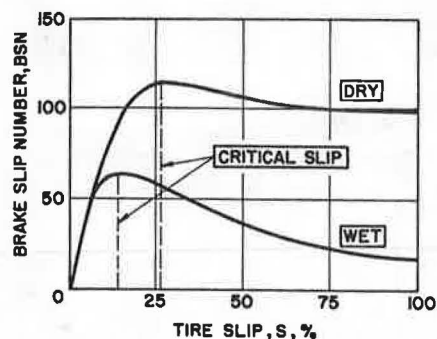
Operating in the Brake Slip Mode
(After Kummer and Meyer (3))
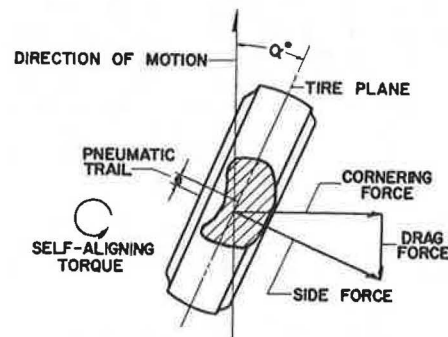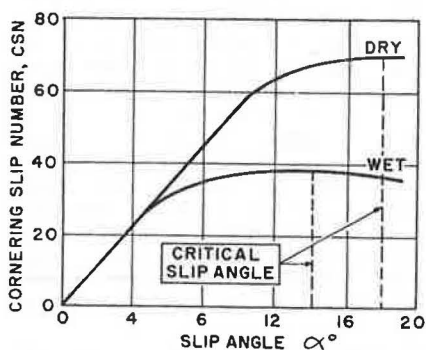
Operating in the Cornering Slip Mode
(After Kummer and Meyer (3))

FIGURE 3 Frictional characteristics of tires operating on typical wet and dry pavements.
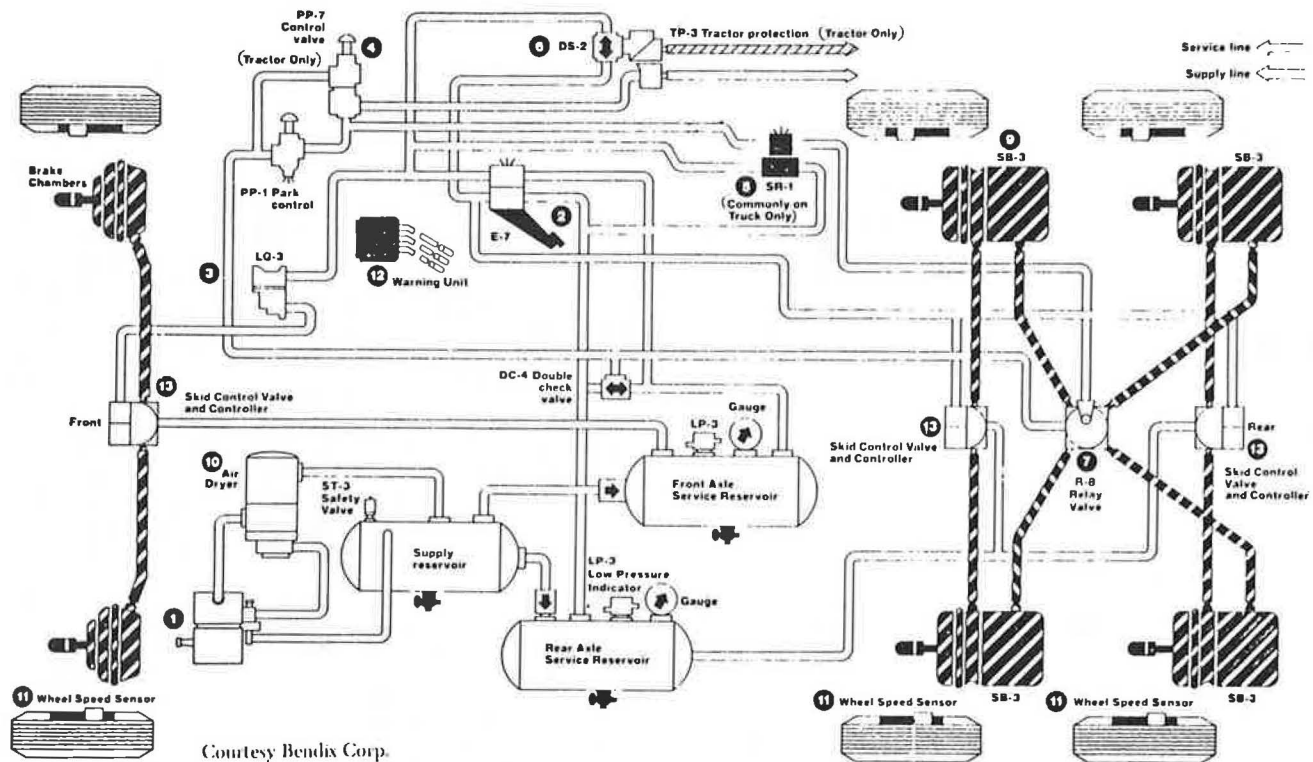
FIGURE 4   Air brake system.
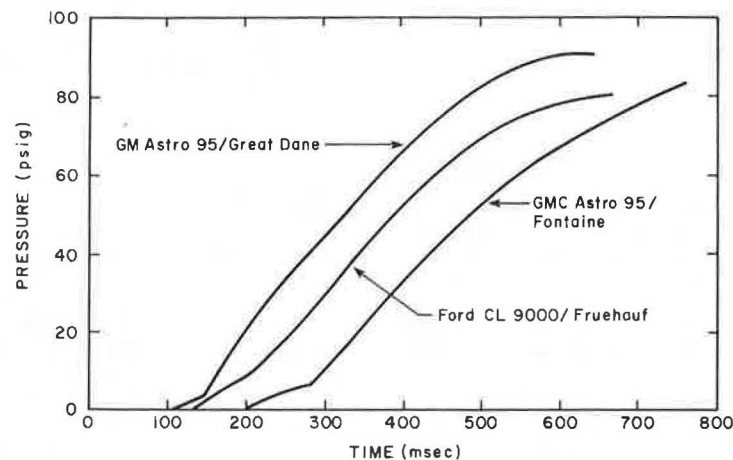
FIGURE 5   Response time histories, trailer brake chamber pressure.

reported (10,11) with a more general, less technical presentation (8).

The essential facts about truck brake operation as it relates to the current subject follow.

Proper brake diaphragm adjustment is essential to proper system operation. This effect, varying as described earlier, is at least as significant as the load variation on the assembly.

The S-cam and wedge-type brake mechanisms, although inherently self-energizing and hence potentially more appealing in normal operation, are more prone to fade, less consistent, and more susceptible to wear and adjustment malfunctions than their disc counterparts.

Conventional (nonlock control logic) brake systems must be designed for best compromise between fully loaded (high-temperature rise/drum expansion) and empty conditions. This can promote systems that either tend to lock at light loads (better heavily

loaded system) or systems that are marginal under full load (better brake stability and control when empty). In any event, brake adjustment is critical and must be accomplished on a regular basis or the system should incorporate automatic slack adjusters.

It is virtually impossible to adjust a brake system so that it is ideal for all conditions of load. If brake systems are adjusted for the full-load condition, they may be poorly adjusted during the light-load condition. This is why antilock brake systems are potentially so important.

Further complicating the problem is the fact that optimum braking would require a different balance for each level of tire-pavement available friction. Brake systems are not optimized for the occasional low friction levels that occur in wet weather.

The ideal combination of an antilock control logic and disc brake mechanism can exploit all the advantages of each, plus be adaptable to extremes in load
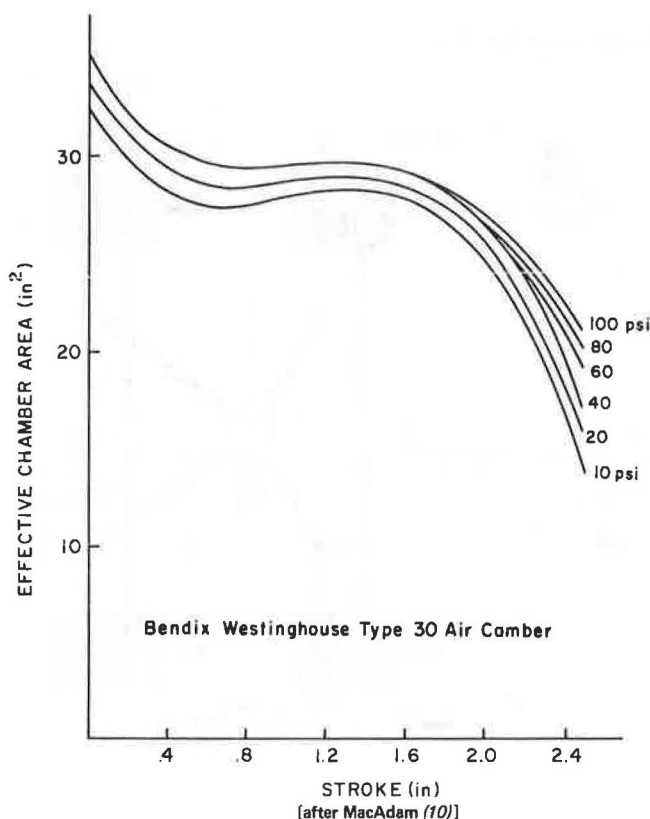
FIGURE 6   Brake chamber effective area versus stroke.

conditions much more readily than nonantilock systems.

Control Loss During Emergency or Extreme Maneuvers

Many reports have been written on how braking systems can be improved in order to achieve shorter stopping distances. Whether or not shortening truck stopping distances will increase highway safety is a question that has not been definitively answered. It does appear apparent that preventing wheels from locking during extreme braking maneuvers would prevent many losses of control.

Many of the emergency maneuver conditions that can lead to losses of control are defined in Table 1. Factors that initiate a loss of control during braking and cornering, or a combination of both, are described in the second column. The possible result of these attempted maneuvers is given in the third column, and possible ways of recovering from the developing loss of control situation are given in the final column. It is with reservation that this final column has been prepared. The instinct and reactions of an experienced and skilled driver cannot be put in tabular form by researchers. In many cases emergency maneuvers and reaction to the resultant dynamic conditions must take place in a time period that allows only instinctive reaction rather than adherence to appropriate learned responses.

The best judgment of the authors has been exercised in developing these possible methods of recovery, along with the counsel of Robert D. Ervin, Research Scientist at the University of Michigan Transportation Research Institute.

Many of the recovery methods are obvious. There are, a few that may warrant some discussion. Possible results of losses of control are tractor jackknifing, trailer jack-knifing, and rollover. These

conditions are shown in Figure 7. For example, when tractor drive wheels break traction and skid laterally during an excessive cornering maneuver, it would appear helpful to disengage the clutch. This reduces circumferential braking due either to drive torque or to engine drag and gives the tire more cornering capacity. The time factor may make this reaction impractical in most cases.

Some consideration has been given to the idea that activating the trailer brakes in a condition of excessive body roll or lateral acceleration could destroy or at least reduce the cornering capacity of the trailer tires and reduce the roll moment. Although this may be true it would also undoubtedly cause trailer swing. Thus one loss of control situation would be traded for another. In view of this, and a growing belief in the industry that individually activated trailer brakes (hand-lever trailer brakes) are an anachronism, the authors have declined to recommend the use of trailer brakes for any situation. Although there may be some specific situations when they could be of value, there appear to be many more situations in which their use would be counterproductive.

A few of the terms used in Table 1 may be unfamiliar; for example, "modulating" service brakes and "feeling" for the steering limit. Modulating brakes means simply the driver getting on and off the foot treadle valve in such a way as to prevent any wheels from locking and at the same time braking effectively. Feeling for the limit of cornering is probably not practical. Under a few conditions of almost steady-state cornering, a driver may be able to sense when the truck tires start to skid laterally and reduce and then add steering to approach the cornering limit.

It may remain for detailed dynamic handling and stability testing of a variety of rigs to determine the practicality of many of the suggested methods of recovery.

HYDROPLANING

It has been understood in the highway engineering community that large truck tires do not hydroplane at highway speeds. There were several reasons why this myth developed. In the early 1960s, Horne and his fellow engineers in the National Aeronautics and Space Administration (NASA) discovered and studied the phenomenon of hydroplaning as it related to aircraft tires. Because of the way aircraft tires are constructed, the shape of the contact patch remains much the same for a fairly wide variation of tire loads. The NASA group found that hydroplaning speed could be predicted as a simple function of tire pressure. This relationship predicted hydroplaning speed of tires with 60 to 100 psi inflation pressure well above that which could be achieved by highway vehicles. Because truck tires normally required pressures in this range, it was believed that they would not be subjected to speeds high enough to hydroplane.

Further work on automobile tires in the late 1960s confirmed that hydroplaning speeds would be extremely high at high levels of tire pressure. These studies of automobile tires, including research by Stocker and Gallaway at Texas Transportation Institute, suggested that tire loads were an unimportant variable. Those who interpreted this work to mean that truck tires could not hydroplane did not appreciate the following. Although an automobile tire for a 4,000-lb vehicle may have a normal range of loads from 800 to 1,200 lb, a truck tire may be operated with loads varying from 600 to 6,000 lb. With extremely wide

TABLE 1 Types of Control Loss During Emergency or Extreme Maneuvers and Possible Solutions

Maneuver	Factor Initiating Control Loss	Result	Possible Methods[a] of Recovery
Straight-line braking	Front tractor wheel lockup	Steering control is lost and vehicle may stay on a straight path in a stable condition.	Modulate[b] service brakes to regain steering.
	Tractor drive wheels lockup	Excessive tractor yaw may occur quickly. (Tractor jack-knifing.)	Modulate service brakes and steer in direction of movement (i.e., if tractor is rotating to left steer to right and vice versa).
	Trailer wheels lockup	Trailer swing may occur. (Trailer jack-knifing.)	Modulate service brakes and if reasonable, accelerate modestly.
	Tractor front wheels skid[c] laterally	Steering control is lost. Reduction in cornering capacity and drift of tractor front end outside of intended curve path.	Reduce steering and "feel" for steering limit of tire-cornering capacity.
	Tractor drive wheels skid[c] laterally	Reduction in cornering and probable drift of tractor drive wheels outside of intended curve path. Excessive tractor yaw may occur quickly. (Tractor jack-knifing.)	Reduce steering; steer in direction of movement and depress clutch.
Cornering	Trailer wheels skid[c] laterally	Drift of trailer wheels outside of intended curve path. Trailer swing may occur. (Trailer jack-knifing.)	Reduce steering.
	Excessive body, roll, or lateral acceleration	Rollover	Reduce steering.
	Tractor front wheels lockup and/or skid[c] laterally	Steering control is lost. Reduction in cornering capacity and probable drift of tractor front end outside of intended curve path.	Reduce steering and modulate service brakes.
Combined braking cornering	Tractor drive wheels lockup and/or skid[c] laterally	Reduction in cornering and probable drift of tractor drive wheels outside of intended curve path. Excessive tractor yaw may occur quickly. (Tractor jack-knifing.)	Reduce steering and modulate service brakes. Steer in direction of movement and depress clutch.
	Trailer drive wheels lockup and/or skid[c] laterally	Drift of trailer wheels outside of intended curve path. Trailer swing may occur. (Trailer jack-knifing.)	Release trailer brakes if they have been activated. Reduce steering and modulate service brakes.
	Excessive body roll or lateral acceleration	Rollover	Reduce steering.

[a] In some cases on pavements having low values of available friction, the result of attempted emergency maneuvers will occur so quickly the driver will not have time to provide other than an instinctive reaction. The time necessary for the theoretically best countermeasures will not be available or effective.
[b] Modulating the service brake means successively activating and releasing the foot treadle to prevent lockup while braking effectively.
[c] Lateral skidding means the cornering capacity of the tire is saturated, the tire may start to skid laterally and the cornering force may be greatly reduced.

TRACTOR
REAR WHEELS
LOCKED

[after Ervin (10)]

TRAILER
WHEELS
LOCKED

TRACTOR JACK-KNIFE   TRAILER JACK-KNIFE   ROLLOVER
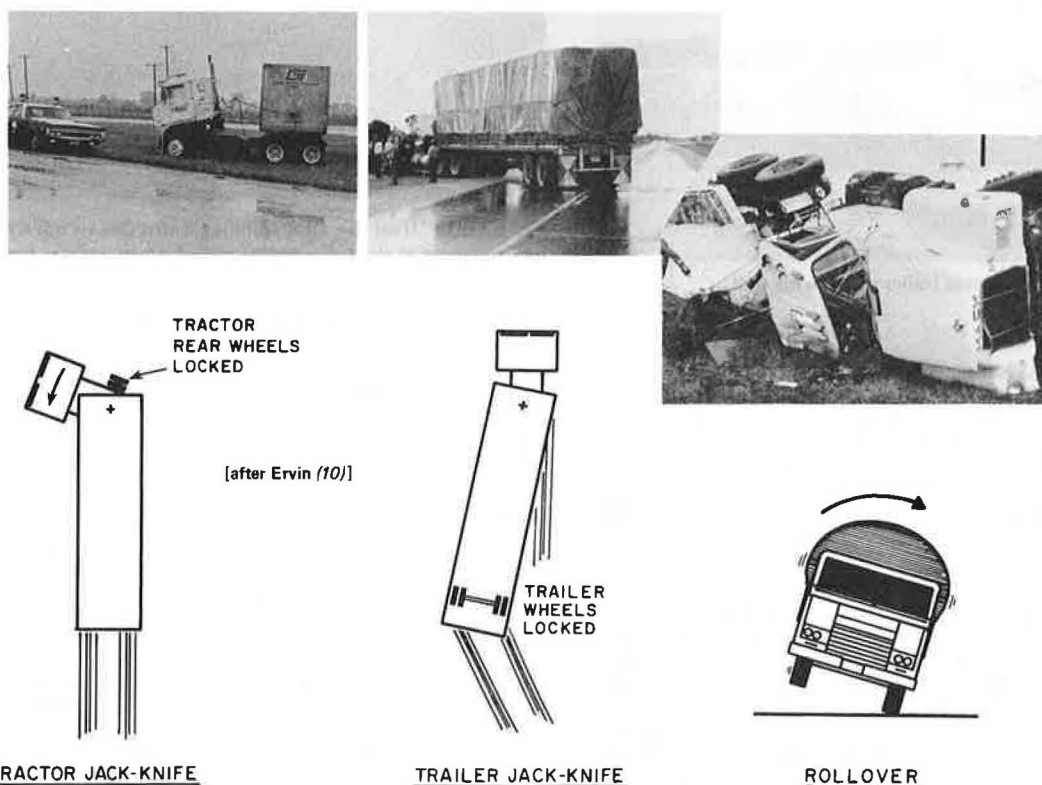
FIGURE 7 Loss of control responses of tractor semi-trailers.

load variation, the aspect ratio of a truck tire surface contact zone varies spectacularly, leading to hydroplaning conditions for a lightly loaded, albeit normally inflated, truck tire at speeds common to highway vehicles. This footprint aspect ratio is the ratio of the surface contact zone width to length.

At the meeting of the Committee on Surface Properties--Vehicle Interaction during the Transportation Research Board's Annual Meeting in January 1984, it was suggested that a task group be set up to look into the special problems of tractor-trailer loss of control. During the course of committee discussion, Horne disclosed that he had written a paper predicting that truck tires, in an extremely low load condition, will hydroplane at highway speeds and explained why this would occur. Horne was asked if this theory had been experimentally verified, as it was definitely contrary to conventional wisdom. Horne responded that it had not been so verified. Shortly after the meeting, Horne sent the Texas Transportation Institute (TTI) a copy of his forthcoming paper, scheduled for presentation at the meeting of ASTM E-17 in April 1984 (1). Horne's arguments, explanations, and predictions were compelling. Intrigued by the possibility of explaining why unloaded tractor-trailers are so prone to loss of control during wet weather, engineers at TTI constructed the test trailer shown in Figure 8. The hydroplaning trough used in this testing is shown in Figure 9, and the trailer used during testing in the trough is shown in Figure 10. The test data are summarized in Table 2.

FIGURE 9 Hydroplaning trough.

FIGURE 8 Hydroplaning test trailer and towing unit.

FIGURE 10 Test tire after spinning down due to full dynamic hydroplaning as the test wheel is pulled down a water trough.

At this time, only four data points have been determined. The lightest load available on the test tire was 940 lb. By imprinting the tire footprint (contact area on pavement surface) using carbon paper, it was determined that the aspect ratio (the nominal ratio of the footprint width to length) was 1.4 for tire pressure varying between 20 and 100 psi. This footprint is shown in Figure 11 at an inflation pressure of 75 psi.

By gradually increasing speed, the speed was determined (for a particular load and pressure condition) at which the tire began to spin down. That point selected was a reduction of apparent tire speed of 2 mph. By increasing speed beyond that value, large values of spin down could be achieved.

Figure 12 shows how the four data points compare to Horne's predictions. Within the range of practical truck tire pressures (60 to 120 psi) the comparison appears quite good. Horne's prediction is about 4 mph low (8 percent) at 60 psi, correct at 75 psi, and about 6 mph high (10 percent) at 100 psi. Because

TABLE 2 Tabulation of Test Conditions

Truck Tire	Wear Condition	Pressure (psi)	Load (lb)	w/ℓ	Hydroplaning Speed (mph)
10.00.20	New	20	940	1.40	43
10.00.20	Worn[a]	40	940	1.40	51
10.00.20	Worn[a]	75	940	1.43	58
10.00.20	Worn[a]	100	940	1.41	62
10.00.20	Worn[a]	70	3,600	0.95	Over 62[b]
10.00.20	Worn[a]	100	3,600	1.10	Over 62[b]

Note: Water depth about 1/4 in. ± 0.1 in.

[a]Worn to approximately 2/32 in. tread remaining.
[b]The top speed achievable was 62 mph. No spin down was detected at this speed.

there was no replication of the data achieved, this is probably within the range of experimental variation if such factors as tire construction, tire tread depth, water depth, and pavement texture are considered.

Horne's equation is

$$VEL = 7.95 \ (P)^{0.5} \ (1/w/\ell)^{0.5} \tag{1}$$
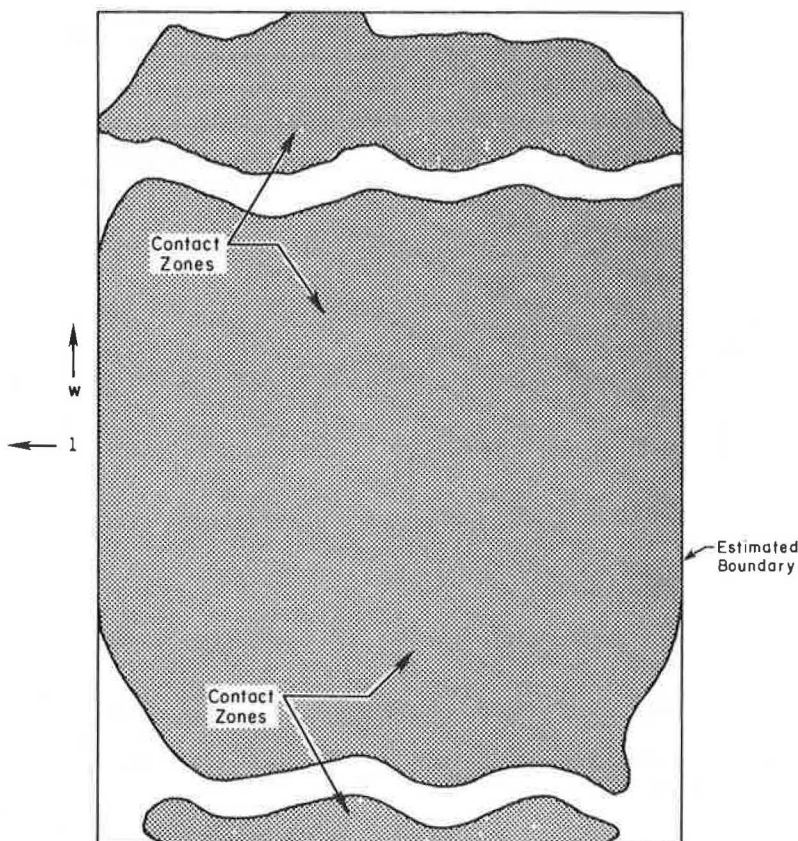
FIGURE 11   Footprint of test tire.
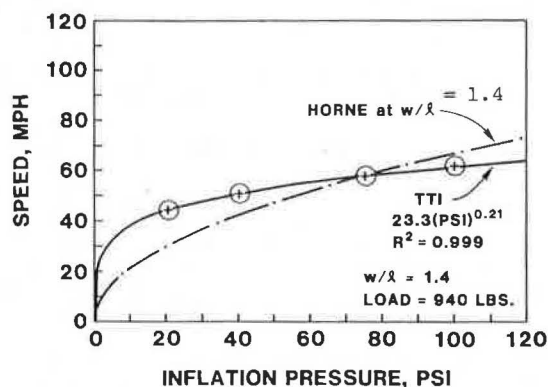
FIGURE 12   Comparison of TTI data points and Horne's predictions.
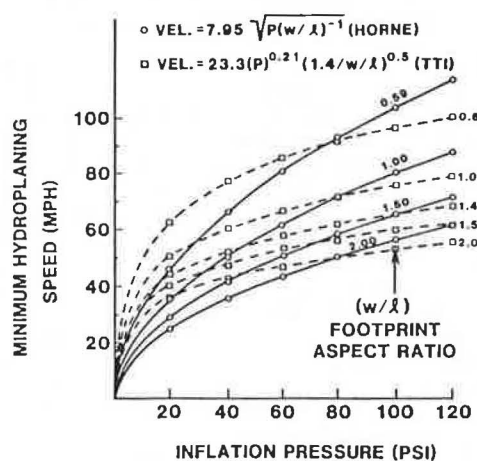
FIGURE 13   Comparison of Horne's and TTI's curves.

compared to an equation based on TTI's curve fit, normalized at the test aspect ratio of 1.4

$$VEL = 23.3 \ (P)^{0.21} \ (1.4/w/\ell)^{0.5} \qquad (2)$$

A comparison of the curves achieved using the two equations is shown in Figure 13. It must be considered highly presumptious to base an equation on four data points. In the future, TTI engineers expect to acquire more data at lower and higher tire loads. These data should allow the formation of a more reliable predictive equation. It is conclusive, however, that Horne's theoretical predictions are reasonably accurate at commonly used truck tire inflation pressures and that lightly loaded truck tires do hydroplane.

ACCIDENT DATA

Further support of the thesis that lightly loaded trucks are subject to loss of control due to hydroplaning was provided by Chira-Chavala (12). Using 1979 through 1981 Bureau of Motor Carrier Safety data for all Interstate Commerce Commission (ICC)-authorized truck accidents, Chira-Chavala determined that empty combination trucks were overrepresented in wet weather by a factor of 3 when compared to loaded rigs.

Demonstration of the hydroplaning phenomenon for lightly loaded tires and the overrepresentation of unloaded combination trucks during wet weather fit together to strongly indicate that truck tire hydro-

planing has a significant influence on vehicle handling and stability.

CONCLUSION

Controlling commercial tractor semitrailers on pavements that provide limited tire-pavement friction are a major problem during periods of wet weather. The characteristics of large truck tires contribute to this problem in that they also provide lower tire-pavement friction levels when compared with automobile tires. Complicating this already severe situation is the fact that truck tires on vehicles in a lightly loaded condition can undergo full dynamic hydroplaning when a significant layer of water covers the pavement surface. This can occur at speeds easily reached by many commercial rigs.

Commercial tractor semitrailers possess unique braking and handling characteristics. These characteristics, in combination with the wide range of load conditions experienced by these vehicles, especially the unloaded configuration, provide situations in which there is a significant probability that one or more of the following will occur:

1. Tractor jack-knifing under combinations of emergency or extreme braking or cornering, or both;
2. Trailer jack-knifing (trailer swing) under combinations of emergency or extreme braking or cornering, or both;
3. Tractor or trailer initiated rolling under conditions of emergency or extreme cornering (development of high values of lateral acceleration).

There are ways to avoid most of these situations by driving defensively, and possible ways to recover as critical dynamic conditions begin to develop that are described here. Reducing speed to 50 mph in wet weather should preclude hydroplaning of tires inflated to 80 psi or more.

Another complication is the problem of brake system design and maintenance. Without careful attention to brake maintenance, including adjustment, loss of braking effort between wheels can contribute to unstable braking. Although some authors believe there is a best sequence of wheel lockups in a severe braking maneuver, others remain unconvinced. Some believe that insufficient evidence currently exists to establish such a preferred sequence. The problem of brake system design under major load variations has traditionally dictated compromise. If the system is designed for the fully loaded condition, it will not be optimum when the rig is unloaded. This is a compelling argument for antilock systems--the one system all authorities appear to agree is preferable to any sequence of wheel lockup.

Because of the wide variation in the loading conditions of tractor semitrailer combinations, the peculiar handling characteristics of these articulated vehicles and the manner in which the braking characteristics and the loading variations affect those handling characteristics, the authors are convinced that reliable, effective antilock brake systems will become the norm in all such vehicles in the near future. The advent of low-cost microprocessor technology with its companion sensor and actuator development, leaves little doubt of the viability of this concept. The mid-1980s is witnessing the application of this technology to high-end passenger cars in both Europe and the United States. Its use in the vehicles discussed in this paper is more compelling for safety reasons and far more easily justified on a benefit-cost basis.

DEDICATION

This paper is dedicated to Louis Homer Hart, trucker, who died in the iron arms of an 18 wheeler trying to avoid a jack-knifed rig on a rain-slick south Texas highway, November 22, 1947.

REFERENCES

1. W.B. Horne. Predicting the Minimum Dynamic Hydroplaning Speed for Aircraft, Bus, Truck and Automobile Tires Rolling on Flooded Pavements. Presentation to ASTM Committee E-17, College Station, Tex., June 5, 1984.
2. D.L. Ivey. Truck Tire Hydroplaning--Empirical Verification of Horne's Thesis. Presentation to the Technical Seminar on Tire Service and Evaluation, ASTM Committee F-9, Akron, Ohio, Nov. 1984.
3. H.W. Kummer and W.E. Meyer. Tentative Skid Resistance Requirements for Main Rural Highways. NCHRP Report 37, HRB, National Research Council, Washington, D.C., 1967, 80 pp.
4. D.L. Ivey, I. Griffin, III, T.M. Newton, and R.L. Lytton. Predicting Wet Weather Accidents. Accident Analysis and Prevention, Vol. 13, No. 2, June 1981, pp. 83-99.
5. D.L. Ivey, E.K. Lehtipuu, and J.W. Button. Rainfall and Visibility--The View from Behind the Wheel. Journal of Safety Research, Vol. 7, No. 4, Dec. 1975, pp. 156-169.
6. B.M. Gallaway et al. Pavement and Geometric Design Criteria for Minimizing Hydroplaning. Report FHWA-RD-79-31. FHWA, U.S. Department of Transportation, 1979.
7. R.S. Morris et al. Field Study of Driver Visual Performance During Rainfall. Report DOT-HS-5-01172. NHTSA, U.S. Department of Transportation, 1976.
8. Motor Truck Engineering Handbook. J.W. Fitch Publisher, Anacortes, Wash., 1983.
9. C.C. MacAdam et al. A Computerized Model for Simulating the Braking and Steering Dynamics of Trucks, Tractor-Semitrailers, Doubles, and Triples Combinations, User's Manual-Phase 4. Report UM-HSRI-80-58. Highway Safety Research Institute, University of Michigan, Ann Arbor, Sept. 1, 1980.
10. Mechanics of Heavy-Duty Trucks and Truck Combinations. Proc., Engineering Summer Conference, University of Michigan Transportation Institute, Ann Arbor, June 1984.
11. R.W. Radlinski, S.F. Williams, and J.M. Machey. The Importance of Maintaining Air Brake Adjustment. SAE Publication SP-574. Truck and Bus Meeting and Exposition, SAE, Warrendale, Pa., Nov. 1982.
12. T. Chira-Chavala. Problems of Combination Trucks on Wet Pavements: An Accident Analysis. In Transportation Research Record 1068, TRB, National Research Council, Washington, D.C., 1968, pp. 70-75.

Methodology for Computing Pavement Ride Quality From Pavement Roughness Measurements

MICHAEL S. JANOFF

ABSTRACT

The objective of this paper is to report on the development of a methodology
for computing pavement ride quality from pavement roughness measurements. This
methodology is based on a statistical transform between physical profile mea-
sures and subjective panel ratings that allows the mean panel rating for a given
pavement section to be accurately predicted from the profile measure of the
pavement section. The physical profile measure, denoted the Profile Index (PI),
is a measure of pavement roughness in the frequency band extending from 0.125
to 0.630 cycles/ft (10 to 51 Hz at 55 mph). A second transform has been devel-
oped from a pavement section's mean panel rating that provides an accurate pre-
diction of its need for repair.

The objective of this paper is to report on the
development of a methodology for predicting pavement
ride quality from pavement roughness measurements.
This methodology is based on research performed by
Ketron, Inc., for the Transportation Research Board
National Cooperative Highway Program (NCHRP) (1).
The goals of the research were to (a) develop a
scale that accurately reflects the public's percep-
tion of pavement roughness, (b) develop transforms
that relate pavement profiles to this scale, and (c)
show how roughness statistics produced by various
response-type road roughness measuring systems
(RTRRMS) relate to this scale.

BACKGROUND

During the AASHO Road Test, serviceability was de-
fined as the ability of a pavement to serve the
traveling public (2). The most commonly used objec-
tive measure of serviceability, the present service-
ability index (PSI), is derived from measurements
made with response-type road roughness measuring
systems. However, this PSI only approximates the
original panel rating concept and is recognized as
having shortcomings. Whether the public's perception
of serviceability is the same today as it was 20
years ago is questionable. Vehicles, highway charac-
teristics, and travel speeds have changed, and ser-
viceability, as originally defined, is not exclu-
sively a measurement of pavement ride quality or
rideability, but is confounded by the inclusion of
factors for surface defects.

For management of pavement inventory, it would be
better to have separate measures of rideability and
surface defects. Therefore, there is a need to de-
velop a new pavement rating scale to ensure that
objective pavement evaluations are directly and rea-
sonably related to the public's perception of ride-
ability. Rideability or ride quality is defined as
the subjective evaluation of pavement roughness.
Roughness, or more specifically longitudinal rough-
ness, is defined as the longitudinal deviations of a
pavement surface from a true planar surface with
characteristic dimensions that affect vehicle
dynamics, ride quality, and dynamic pavement loads
(Project Statement, NCHRP Project 1-23).

Pavement roughness and ride quality involve three
related items: subjective measures, objective or
physical measures, and statistical comparisons. It
is far too complicated, time consuming, and expen-
sive to rely on subjective ratings alone. The phys-
ical measurements, in combination with appropriate
statistical transformations, are clearly preferred.
However, the accuracy and validity of the physical
correlates must be determined before they can be
used as a replacement or surrogate for the subjec-
tive but more realistic human responses.

DEFINITIONS AND CONCEPTS

In addition to rideability and roughness, defined in
the preceding section, a number of related concepts
should be explained.

For the physical roughness data, a profilometer
was used to compute a profile index (PI) defined as
the square root of the mean square of the profile
height, with units in inches. PI is defined in this
paper for specific frequency bands of roughness.

For the subjective rideability data, two terms
were used: (a) a mean panel rating (MPR) of a given
pavement section, which is the mean value (i.e., the
average) of a group of subjective panel ratings for
a given test section, and (b) a pavement section's
rideability number (RN), which is equivalent to its
MPR but is derived from a pavement section's PI by
using a statistical transformation. One additional
concept is the needs repair rating (NR), which
represents the percentage of the driving public that
believes a given pavement section should be repaired.

In the later part of this paper it is demonstrated
how the concepts PI, RN, MPR, and NR are related.

RESULTS

Main Panel Rating Experiment

The main panel rating experiment was designed with
the following components:

1. Fifty-two test sections including all three
surface types [bituminous concrete (BC), portland
cement concrete (PCC), and composite] and spanning a
wide range of roughness.

FIGURE 1 Rater form.

2. Thirty-six panel members spanning a wide range of ages and driving experience.

3. The Weaver/AASHO rating scale (Figure 1), including the subjective rating of rideability and a secondary two-alternative forced choice (i.e., one of two boxes must be checked for each site by each panel member) to subjectively evaluate whether or not each pavement section requires repair or maintenance.

4. A detailed set of instructions that were uniformly given to all panel members (Figure 2).

5. A carefully designed and controlled experimental protocol.

6. Data reduction and analysis methods.

This experiment was implemented in the fall of 1983 in the Columbus, Ohio, area with the cooperation and help of the Ohio Department of Transportation (DOT).

Concurrent with the experiment, the Ohio DOT obtained profile information measuring each test section using a profilometer and a Mays meter. The experimental design is summarized as follows:

Test sections	52 test sections, 1/2 mi each in Columbus, Ohio, area, including 18 BC, 17 PCC, and 17 composite, spanning a range of roughness of 32.6 to 661.3 in./mi
Panel members	36 employees of Ohio DOT with 1 to 50 years of driving experience
Test vehicles	Four K-cars of similar age and mileage
Rating scale	Weaver/AASHO plus secondary rating (Figure 1)
Instructions	Figure 2
Profilometer	KJ Law noncontact
RTRRMS	Mays meter
Time	2 days per group (12 subjects) 6 days total

Data Analysis

The primary objective of the data analysis was to identify the frequency band at which MPR is most highly correlated with PI and then to derive a regression equation relating MPR and PI (i.e., a statistical transform) that can be used to predict

Highway Improvement Study

Purpose
    To survey typical Ohio drivers in order to determine what they think of the
    quality of the ride provided by the roads in the state. The Ohio DOT will
    use this information to help decide which roads it should improve first
    with the limited funds available to make highway improvements.

Object of Ketron's Study
    We are going to drive you over a number of roads that we believe are repre-
    sentative of the roads as they exist throughout the state. We will then ask
    you to make two judgments concerning each road. First, we want you to rate
    the roughness or smoothness of the ride provided by each road on a scale of
    0 to 5, and second, we want you to indicate whether or not you think an
    effort should be made to improve the ride quality of each road.

Making Your Ratings of Ride Quality

(A facsimile of the rating scale was shown to the subjects for this section.)

    The first thing we want you to consider as you drive down a road is the
    roughness or smoothness of the ride provided by the road and then to rate it
    on this scale (illustrated), which ranges from 0 to 5. You will indicate your
    rating by placing a small mark across the vertical line of the scale at the
    place that you believe best describes the ride provided by each road.

Definitions of Endpoints

    All the roads that you drive over in this survey will be between two ex-
    tremes. That is, somewhere between impassable and perfect.

Impassable:
    A road that is so bad that you doubt that you or the car will make it to
    the end at the speed you are traveling--like driving down railroad tracks
    along the ties.

FIGURE 2 Panel instructions.

Perfect:
   A road that is so smooth that at the speed you are traveling you would
   hardly know the road was there. You doubt that if someone made the surface
   smoother that the ride would be detectably nicer.

   Because these roads probably do not exist you will probably not consider
any road to be worse than impassable or better than perfect.

   In order to help you make your rating, we have included a number of words
along the scale that could be used to describe how the riding sensation ap-
pears to you. For example, if you should encounter a road for which you could
describe the ride as Fair but not quite good, place your mark just below the
line labeled 3 (illustrated). On the other hand, if you think the next road is
still fair, but somewhat worse than the previous road, place your mark at a
point that you think is the appropriate distance down in the Fair category. To
indicate small differences between the ride quality provided by the roads, you
may place your mark anywhere you like along the scale.

   Note: We are not asking you to place roads into one of five cate-
   gories! You should use small differences in the position of your marks
   to indicate small differences between the ride quality provided by the
   roads. You may place your mark anywhere you like along the scale.

Indicating the Need for Improvement

   After you have made your rating of the degree of ride quality provided by
any particular road, we want you to check the appropriate box alongside the
rating scale to indicate whether or not you think the state should improve the
ride quality of the road.

   When making this decision you should take into account the fact that because
the state only has a certain, fixed amount of money each year to make road
improvements, it must determine which roads should be improved first. There-
fore, before deciding on the need for improvement, you should not only consider
how rough a ride is provided by each road, but whether you believe the road is
important enough to be placed high on the state's list of roads needing im-
provement. For example, you may ride across two roads that give identically
rough rides but, if you had your choice, you would rather see only one of them
improved because the type or character of that road appears to you to make it
more worthy of improvement.

Procedure for Survey

   • For this survey we are going to ask you to evaluate 81 road sections.

   Note: You will not be rating an entire road for its ride quality. We
   have carefully selected small test sections to represent each road. It
   is these sections that we want you to rate for ride quality.

   • As you approach each section, the driver will call out the number
of the section. Be sure you have the proper numbered form.
   • When the driver says START, begin concentrating on what the rating
of ride quality should be, based on how the ride feels to you.
   • It will only take about 30 seconds to drive over each section, so
maintain your concentration until the driver says STOP. At that point,
place your rating mark on the scale.
   • Next, while taking into account both the roughness of the ride
through the representative test section, as well as the nature and type
of the entire road, indicate whether or not you think the ride quality
needs to be improved by checking the appropriate box next to the rating
scale.
   • Because some sections are only 3 to 4 minutes apart, make your
decisions quickly and pass your forms to the person sitting in the front
right seat.
   • This procedure will be repeated for each site.
   • We will be driving over a predetermined course in an ordinary pas-
senger car. The trip will take 6 hours the first day and 5 hours the sec-
ond.

Special Instructions

   • When making your rating of ride quality, do not consider any of
the road before or after a test section. We are only interested in a rat-
ing for a small section of road.
   • When making your decision concerning the need for improvements

FIGURE 2 (continued)

assume that the ride provided by the entire road is the same as that for the test section.

• Concentrate only on the ride quality provided by the roads. Do not let the appearance of the road surface influence your ratings. Judge only how the road feels!

• Do not be distracted by conversations in the car or by pretty scenery.

• Do not reveal your ratings to the other raters. There is no right or wrong answer, so do not "cheat." We are interested only in your opinion, which is as valid as anyone else's.

• Be critical about the ride quality provided by the roads. If they are not absolutely perfect as far as you are concerned, be sure to give it a rating on the scale that you think best reflects the diminished quality of the ride.

• Be aware that there are many ways that the ride could be considered less than perfect. The road could (a) be so bumpy that it rattles your bones and makes your teeth chatter, (b) have bumps or undulations that makes the car heave up and down as if it were a roller coaster, or (c) have other imperfections in the surface that you believe detract from the ride quality.

FIGURE 2 (continued)

RNs from PIs measured in this frequency band. Secondary objectives included development of statistical transforms between response-type roughness measures and RNs and between NR and RN.

To meet the primary objective, the PI for each profile for each of the 26, one-third octave bands of frequencies were computed from 0.0025 to 0.8 cycles/ft (0.2 to 64 Hz at 55 mph). The PI values were then correlated with the MPRs for each test section, for all three surfaces combined, and for the three types of surfaces individually. Figure 3 shows the results for all three surfaces combined [the results for the three individual surface types are similar and available in NCHRP Report 275 (1)]. [Note that the graph in Figure 3 was extended beyond 0.8 cycles/ft (dashed line) using data collected with the Pennsylvania State University profilometer. The upper limit of the Ohio DOT profilometer was 0.8 cycles/ft.]

The abscissa in Figure 3 shows the 26 different frequency bands and the ordinate shows the correlation coefficient that results when PI in an individual band is correlated with MPR for the test section. From the figure it can be seen that between the frequencies 0.125 and 0.63 cycles/ft (10 to 51 Hz at 55 mph), the correlation coefficients (r) re-

main better than -.85 but that outside this band the correlation coefficients decline rapidly.

If PI is computed for each profile within this entire band of frequencies (0.125 to 0.630 cycles/ft) and correlated with MPRs, the resulting correlation coefficient is -.85. When the raw data are plotted (Figure 4) it is evident that an exponential curve is revealed and a log transform of the PI measures increases the correlation to -.94. The resulting equation

$$MPR = -1.74 - 3.03 \log (PI) \qquad (1)$$

accounts for 88 percent of the variance. This equation is shown in Figure 5.

The NR rating was also found to be highly correlated with MPR ($r = -.93$) and yielded a regression equation

$$NR = 132.6 - 33.5 \ MPR \qquad (2)$$

This equation is shown in Figure 6.

Note that Equations 1–4 are based on only the Ohio data; in other states they could change slightly. [See NCHRP Report 275 (1).]
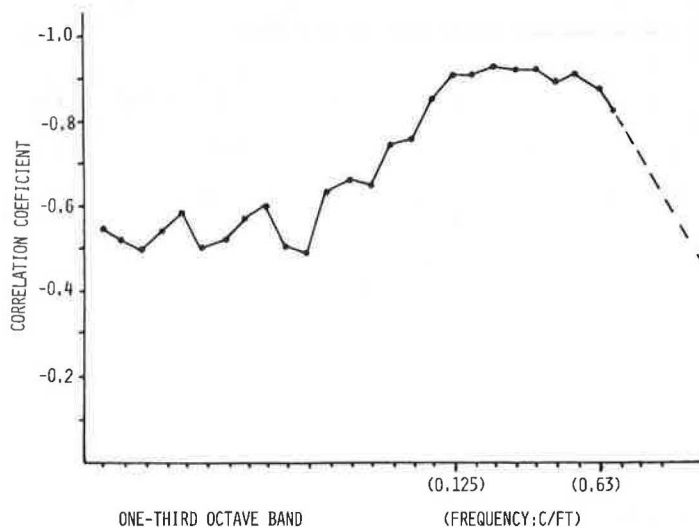
FIGURE 3 Correlation of MPR with PI for all surfaces.
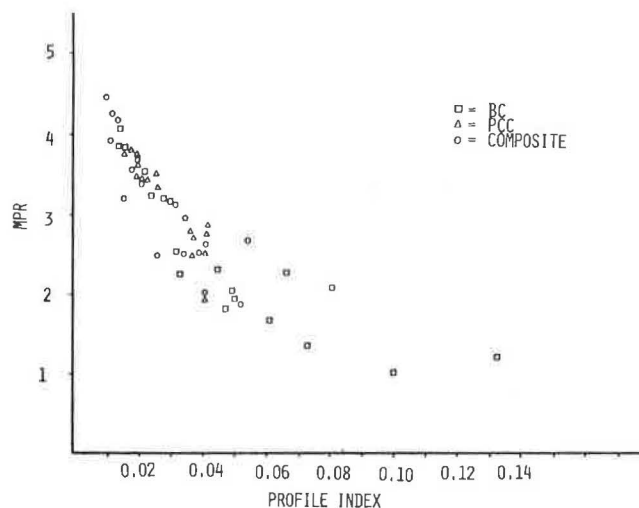
FIGURE 4   Profile index versus MPR, all surface types.
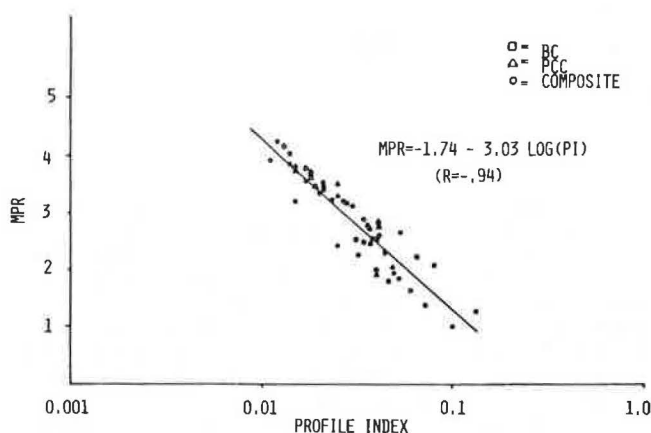
FIGURE 5   Log transform of raw data.
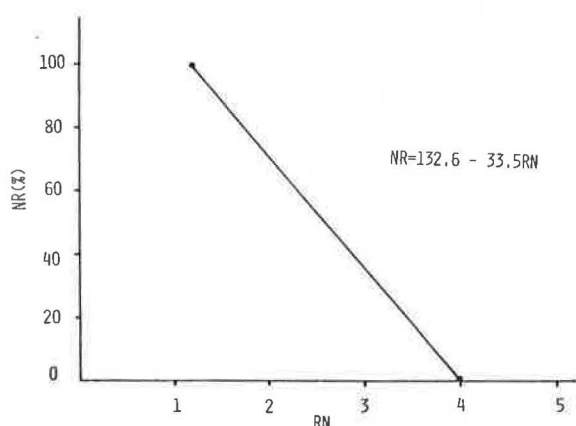
FIGURE 6   Needs repair versus ride number.

CONCLUSION

The implications of the primary analysis are that assuming an agency is able to compute PI for the band of frequencies 0.125 to 0.63 cycles/ft, then by applying the transform

$$RN = -1.74 - 3.03 \log (PI) \qquad (3)$$

it can compute the ride number of a given pavement section. The ride number is an accurate approximation of the true mean panel rating of the pavement section ($r = -.94$).

From RN, NR can be computed by using

$$NR = 132.6 - 33.5 \, RN \qquad (4)$$

to determine the exact percentage of the driving public that believes a given pavement section should be repaired.

ACKNOWLEDGMENT

The work reported in this paper was sponsored by the American Association of State Highway and Transportation Officials, in cooperation with the Federal Highway Administration, U.S. Department of Transportation, and was conducted by the National Cooperative Highway Research Program, Transportation Research Board of the National Research Council.

REFERENCES

1. M.S. Janoff et al. Pavement Roughness and Rideability. NCHRP Report 275, TRB, National Research Council, Washington, D.C., 1985, 69 pp.
2. W.N. Carey and P.E. Irick. The Pavement Serviceability Performance Concept. In HRB Bull. 250, TRB, National Research Council, Washington, D.C., 1960, pp. 40-58.

Discussion

R. M. Weed and R. T. Barros*

This discussion is not intended to detract from the author's excellent work but, instead, to suggest how the choice of more appropriate mathematical models might enhance it further.

From examination of the raw data in Figure 4, the author notes that an exponential function of some sort is suggested. He then proceeds to do a log transformation on the X-axis data (PI) and obtains Equation 1 by linear regression. The relatively high correlation coefficient of -0.94 indicates that a good fit of the data has been obtained.

In spite of this good fit, there are some drawbacks to the mathematical model that has been used. As shown conceptually in Figure 7, if the model is

*New Jersey Department of Transportation, 1035 Parkway Avenue, Trenton, N.J. 08625.
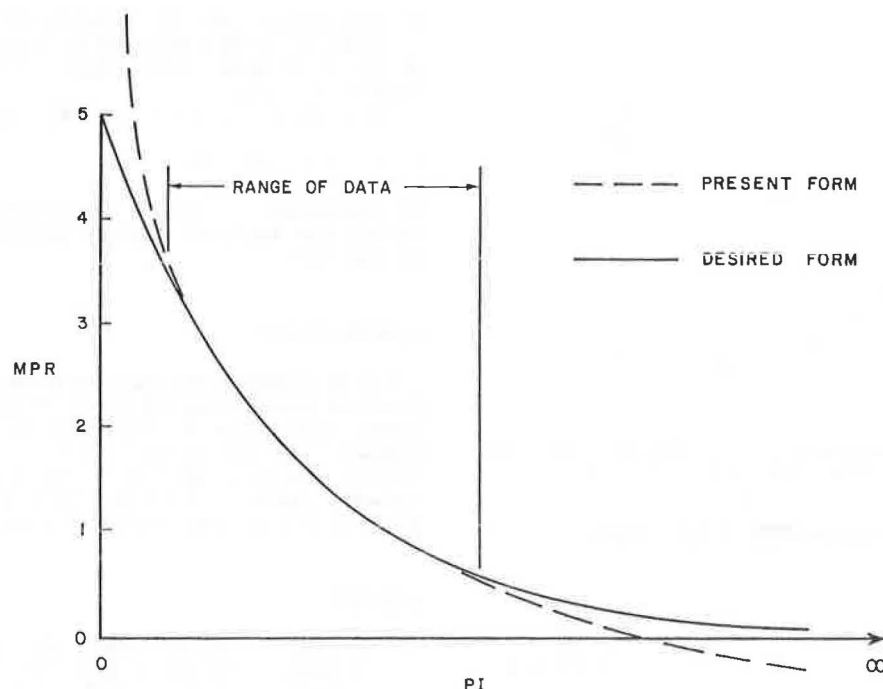
FIGURE 7   Comparison of two conceptual models.

extended beyond the range of the data, it violates two known constraints: (a) it rises above MPR = 5 at low PI values and (b) it eventually goes below MPR = 0 at very high PI values. This is the result of doing the log transformation on the X-axis data rather than on the Y-axis data. Although this model may be empirically useful within the range of the data, better models are available that do not violate these basic constraints.

The primary goal is to find the mathematical model that most accurately describes the process being investigated. To this end, it is appropriate to use every resource available, including any prior knowledge of that process. In this particular case, it is known that PI = 0 must correspond to MPR = 5 because both these points represent the best that can be obtained on the two scales. At the other extreme, there is essentially no difference between a very high PI value and a still higher PI value; for all practical purposes, both would correspond to MPR = 0. This suggests that the appropriate curve will originate at PI = 0, MPR = 5 and fall exponentially to eventually become asymptotic to the X-axis. As a check, visual inspection of Figure 4 strongly supports this conclusion.

A basic exponential decay function that is capable of satisfying the known constraints is given by Equation 5. Two additional candidate models are given by Equations 6 and 7. These models are capable of assuming the general shapes shown in Figure 8, depending on the values of the coefficients that are used. For this particular application, it can be seen by inspection that the first coefficient must be A = 5 in order for the curves to originate at the point x = 0, y = 5.

$$y = Ae^{Bx} \tag{5}$$

$$y = Ae^{Bx^C} \tag{6}$$

$$y = Ae^{Bx^{C+Dx}} \tag{7}$$

The next step is to fit these models using least-squares techniques. There are two ways that this can be done and one is somewhat preferable to the other. The less desirable method is to do a logarithmic transformation (two transformations are required for Equations 6 and 7) followed by linear regression and a transformation back to the original parameters. This method is considered less desirable because the least-squares technique may not be fully optimal when operating on transformed data. A preferable technique is the use of nonlinear regression, a standard feature included in SAS ($\underline{1}$) and other computerized statistical analysis packages. With nonlinear regression, the least-squares procedure is applied directly to the raw data after first imposing the appropriate constraints. The data in Table 1 compare the author's results with those obtained by nonlinear regression.

TABLE 1   Comparison of Four Models

Model	Form	Equation	Residual Sum of Squares
Equation 1	$y = A - B \log x$	$MPR = -1.74 - 3.03 \log PI$	4.33
Equation 5	$y = Ae^{Bx}$	$MPR = 5e^{-17.4\ PI}$	5.39
Equation 6	$y = Ae^{Bx^C}$	$MPR = 5e^{-10.6PI^{0.852}}$	4.75
Equation 7	$y = Ae^{Bx^{C+Dx}}$	$MPR = 5e^{-304PI^{1.55+8.29\ PI}}$	4.17

The "goodness of fit" of the four models, as measured by comparatively low residual sums of squares, has been included in Table 1 as a matter of interest. This should not be the primary factor of consideration, however, when deciding among competing models. When it is possible to identify fundamental mathematical constraints, these constraints should be satisfied before any statistical procedures are applied. By this reasoning, any of the alternate models (Equations 5-7) is preferable to Equation 1, although

only Equation 7 produces a lower residual sum of squares.

The three alternate models are compared to the author's original model in Figures 9–11. All three satisfy the known constraints and Equation 7, in particular, appears to provide an exceptionally good fit of the data.

In summary, the primary goal is to obtain the mathematical model that best describes the physical process. To accomplish this, it is necessary to impose any known constraints before regression analysis, or any other statistical technique, is applied. There are two advantages to this approach. First, by satisfying these constraints, it is more likely that a fundamentally correct model will be obtained. Second, because the equation may eventually be applied by users unfamiliar with its development, it will be more likely to produce correct results if it should subsequently be used outside the range of data from which it was derived.
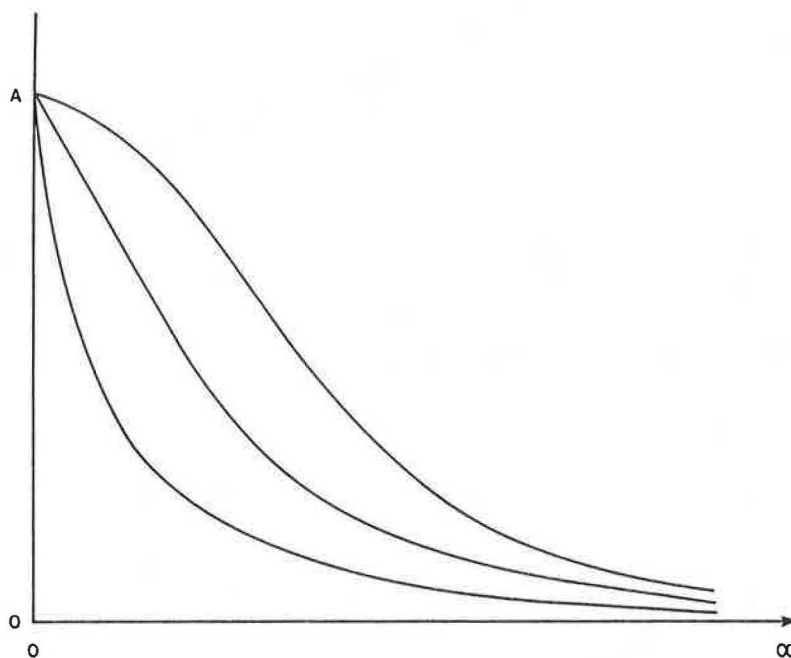
FIGURE 8   Various forms of exponential decay curves.
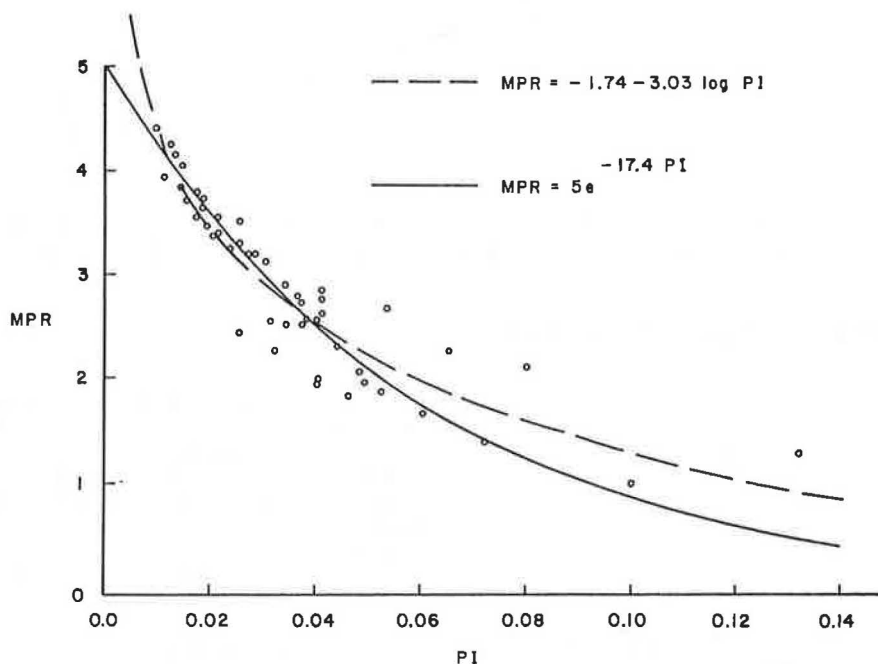
FIGURE 9   Equation 5 compared with Equation 1.
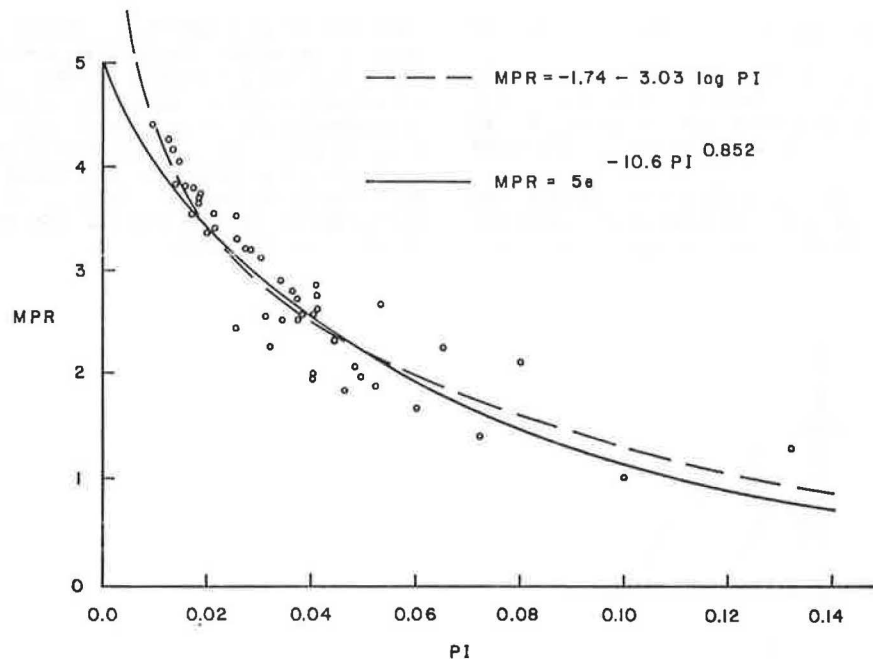
FIGURE 10   Equation 6 compared with Equation 1.
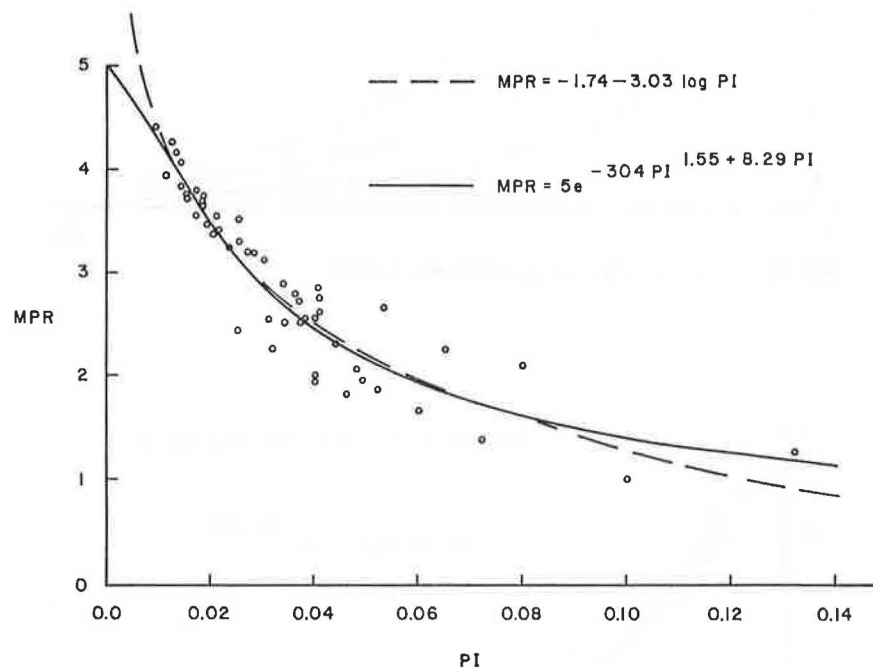
FIGURE 11   Equation 7 compared with Equation 1.

REFERENCE

1. SAS User's Guide. SAS Institute, Cary, N.C., 1979.

Author's Closure

I would like to thank Weed and Barros for their discussion of my paper. Although their comments are valid, I believe that a response on my part is necessary for completeness.

Their comments primarily address my choice of model and the fact that my model does not accurately predict ride quality (RN) either less than 1.0 or greater than 4.5. Their analysis develops a model that is theoretically correct (i.e., from an engineering point of view) for all levels of ride quality.

A number of points should be noted:

1. My research (NCHRP Project 1-23) has indicated that on roads with ride quality less than 1.0, 100 percent of the raters agree that the road should be repaired; for ride quality greater than 4.5, 100 percent of the raters agree that the road requires

no repair at all. Hence, from a practical viewpoint (e.g., to make a decision concerning whether a specific road should be repaired), only the range from 1.0 to 4.5 is important; what happens outside this range is not important.

2. Extrapolation to predict values (of RN) outside the range of the empirical data can lead to inaccuracies; none of us knows how the data will behave outside the (RN) range of 1.0 to 4.5. Although their assumptions concerning behavior at the extremes of the curve appear reasonable, neither they, nor I, have any validation of them.

3. Their point concerning application by unfamiliar users is well taken. However, there are methods other than nonlinear that are far simpler to apply to alleviate this problem. Restricting the range of the equation (a simple "if" statement, for example) is one of them.

I believe that the analysis accomplished by Weed and Barros is important in providing more insight into the entire process that describes the relationship between psychological ride quality and physical roughness. However, their results, like mine, still leave questions to be answered. I hope that additional research will be undertaken to answer these questions.

Critical Evaluation of the Calibration Procedure for Mays Meters

BOHDAN T. KULAKOWSKI

ABSTRACT

A procedure for calibrating Mays meters using a standard quarter-car model is reviewed. Uncertainties of the calibration method caused by lateral nonuniformity of the road surface and differences between the dynamics of calibrated and standard vehicles are discussed. The results of a statistical analysis of experimental data used for Mays meter calibration are presented. Investigation of the effects of the number of raw data on the accuracy of calibration leads to some practical recommendations for the number and length of the calibration test sites.

Mays meters are the most common equipment used by state transportation agencies to measure road roughness. The output generated by the Mays meter represents an accumulated displacement between the rear axle and the body of the vehicle. In order to calibrate the system, the scale of the output signal in terms of road roughness has to be determined by comparison with a standard. The calibration procedure for Mays meters was the subject of an extensive study conducted by Gillespie et al. (1). In the study a reference standard system—a quarter-car model of specified parameters—was introduced, and various calibration methods were evaluated. The research findings reported (1) provided the basis for the new standard calibration procedure that will be introduced by ASTM in the near future. The results presented by Gillespie et al. have undoubtedly been very helpful to the transportation agencies now developing reliable and accurate calibration proce-

dures, yet many important questions remain unanswered.

The objective of this paper is to address some of these questions: How good or how certain is the standard system used in Mays meter calibration? Are there any important uncertainties affecting the accuracy of calibration? How extensive should the raw data set be to assure good correlation with the standard system, and, in particular, how many test sites should be used and of what length? Are multiple tests on each road site necessary? Although definite answers to some of these questions have not been found at this point, raising them should bring researchers closer to a better, more accurate calibration procedure.

UNCERTAINTIES OF THE STANDARD QUARTER-CAR MODEL

Every calibration procedure requires a standard (reference) against which a calibrated system may be compared. It is necessary that the uncertainties of the standard be considerably less than those of the system to be calibrated in order to assure high ac-

Pennsylvania Transportation Institute, Pennsylvania State University, Research Building B, University Park, Pa. 16802.

curacy of measurement. In the calibration of Mays meters, a model of a quarter-car, shown in Figure 1, is used as a standard. The model is well defined and probably as certain as a mathematical model can be. However, it is not the quarter-car model itself but the model-generated roughness data that are used as the reference in calibrating Mays meters.
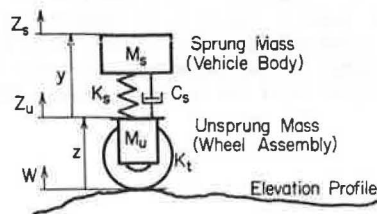
$K_s/M_s = 62.3\ s^{-2}$　　$M_u/M_s = 0.15$
$K_t/M_s = 653.0\ s^{-2}$　　$C_s/M_s = 6.0\ s^{-1}$

FIGURE 1　Standard quarter-car model.

The quarter-car roughness index values are calculated for a given input signal representing a road profile. It is assumed that exactly the same input signal is applied to the calibrated and calibrating vehicles. This in general is not quite true, but it is hoped, at least, that the difference between the two signals is insignificant.

Is it insignificant? Consider the structure of the calibration system. The idealized and actual system structures are shown in Figure 2. The wheelpaths of the calibrating and calibrated vehicles are never exactly the same. The differences between the profiles are represented in Figure 2 by random signals v' and v" for the left and right wheelpaths, respectively. Mathematically the relationship between the profiles can be described by Equations 1 and 2

$$w'_{MM} = w'_{QC} + v' \tag{1}$$

$$w''_{MM} = w''_{QC} + v'' \tag{2}$$

where

　w_{MM} = road profile in Mays meter wheelpath,
　w_{QC} = road profile in profilometer wheelpath, and
　　v = signal representing difference in profiles between the two paths.

Superscripts ' and " are used to denote the left and right wheel signals, respectively. The disturbances v' and v" appear to be a result of the lateral nonuniformity of the road surface. In order to evaluate the extent of this lateral nonuniformity, actual roughness index values for the left and right wheelpaths on 20 road sites, each 0.6 mi long, were compared. The height sensor ʾnd accelerometer data for the left and right whee. were collected with the Pennsylvania Transportati ʾ Institute (PTI) profilometer, and the roughness index values for the two wheels, R'_{QC} and R''_{QC}, were calculated. The roughness index is defined as

$$R_{QC} = 1/L \int_0^L |z(x)|\ dx \tag{3}$$

where

　$z(x)$ = axle-body displacement of the quarter-car model, inches;
　　x = longitudinal distance variable, miles; and
　　L = length of the road site, miles.

The values of R'_{QC} and R''_{QC} were obtained for 0.05-mi increments from the computer program developed by Watugala (2) on a DEC LSI 11/23 computer. Two conclusions, shown graphically in Figure 3, can be drawn from the results. First, the lateral nonuniformity of road roughness is considerable as is indicated by large differences between the right and left wheelpath values on many sites. This means that the inputs to the calibrated and calibrating systems may be significantly different because they never follow exactly the same path. One of the most important requirements for a highly accurate calibration, namely, that inputs to the two systems be identical, is therefore not met. The magnitude of the error caused by the lateral nonuniformity of the road surface, however, is difficult to assess.

The second conclusion from a comparison of the roughness data for the two wheels is that the values for the right wheel are higher than those for the left wheel on most road sites, as is indicated by the clustering of the data points below the line of unity slope in Figure 3. It was found that the average roughness index value in the right wheelpath was 83.37 in./mi, whereas in the left wheelpath it was only 75.60 in./mi, about 10 percent lower. The difference was more pronounced for rougher roads having a roughness index value greater than 50 in./mi. The high value of the correlation coefficient, r = 0.96,

FIGURE 2　Idealized (a) and actual (b) structures of the calibration system.

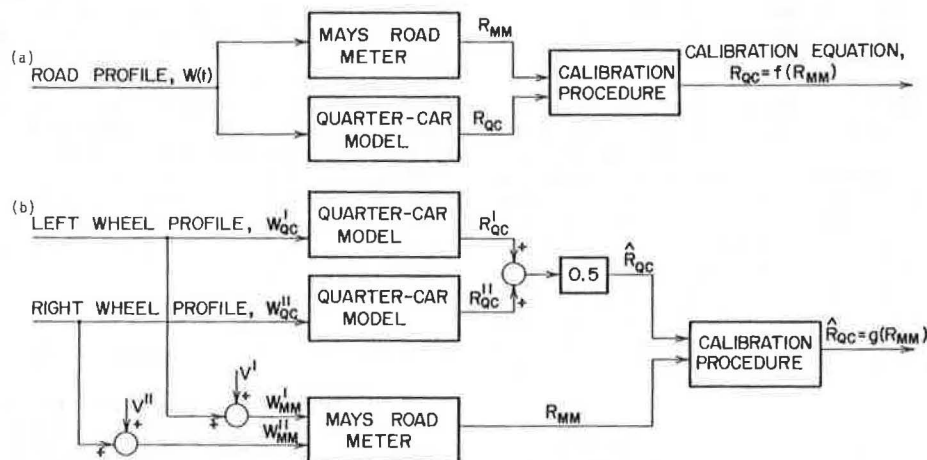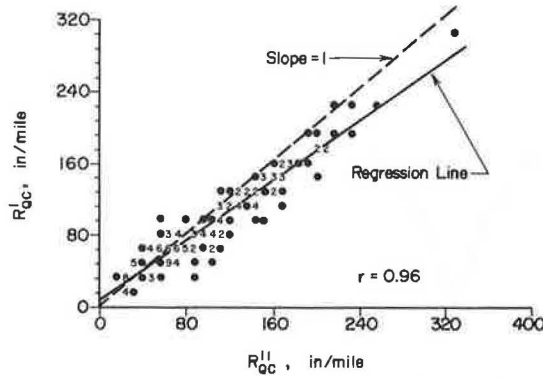FIGURE 3 Comparison of road roughness index values calculated with a standard quarter-car model from left, R'_{QC}, and right, R''_{QC}, wheelpath data.

confirms that the relationship is not coincidental. In fact, a statistically meaningful linear regression model was obtained relating roughness index values in two wheelpaths:

$$R'_{QC} = 5.83 + 0.837 \, R''_{QC} \tag{4}$$

The standard deviation between the model (Equation 4) and the raw data was relatively low--12.55 in./mi. As mentioned before, the magnitude of the inaccuracy of the calibration formula caused by the lateral nonuniformity of the road is difficult to evaluate, but it can be as much as 5 to 10 percent. The closer are the wheelpaths of the calibrated and calibrating vehicles, the smaller is the effect of the lateral nonuniformity. The error can be entirely eliminated only if calibration is conducted on test facilities closed to road traffic.

PHYSICAL VERSUS STATISTICAL VALIDITY OF THE LINEAR CALIBRATION FORMULA

A linear regression equation is commonly used as a calibration formula relating road roughness index values obtained with Mays meters and with the standard quarter-car model. The form of this equation is

$$R_{QC} = \alpha_0 + \alpha_1 R_{MM} \tag{5}$$

where

   R_{QC} = roughness index value calculated using standard quarter-car model,

   R_{MM} = roughness index value measured with Mays meter, and

   α_0, α_1 = constant parameters.

Both R_{QC} and R_{MM} are numerical measures associated with the responses of two dynamic systems, the quarter-car model and the Mays meter, to a dynamic road profile input. Therefore, the relationship between the two system outputs is dynamic, depending on the frequency spectrum of the input signal, and can only be approximated by the static formula (Equation 5) with a limited accuracy.

Consider the dynamics of the Mays meter-quarter-car relationship in more detail. First of all, assume that both the Mays meter and the standard quarter-car model are described by the set of two linear differential equations

$$M_s \ddot{z}_s + C_s (\dot{z}_s - \dot{z}_u) + K_s (z_s - z_u) = 0 \tag{6}$$

$$M_u \ddot{z}_u - C_s (\dot{z}_s - \dot{z}_u) - K_s (z_s - z_u) = K_t (w - z_u) \tag{7}$$

where the meaning of the symbols used in these equations is explained in Figure 1. By applying a Fourier transformation and rearranging Equations 6 and 7, the relative axle-body displacement, $z = z_s - z_u$ can be expressed in terms of model parameters, profile w, and frequency ω as follows:

$$z(j\omega) = M_s K_t \omega^2 / [M_u M_s \omega^4 - j(M_u + M_s)C_s \omega^3 \\ - (M_u K_s + M_s K_s + M_s K_t)\omega^2 + jC_s K_t \omega \\ + K_s K_t] \, w(j\omega) \tag{8}$$

The magnitude of the axle-body displacement, which is used to calculate the road roughness index from Equation 3 can be derived from Equation 8 as

$$|z(j\omega)| = b_2 \omega^2 / (a_8 \omega^8 + a_6 \omega^6 + a_4 \omega^4 \\ + a_2 \omega^2 + a_0) \tag{9}$$

where

   $b_2 = K_t / M_u$

   $a_0 = K_s K_t / M_s M_u$

   $a_2 = (C_s K_t / M_s M_u)^2 - 2(K_s K_t / M_s M_u) \\ [K_s / M_s + (K_s + K_t)/M_u]$

   $a_4 = [K_s / M_s + (K_s + K_t)/M_u]^2 + 2K_s K_t / M_s M_u \\ - 2(C_s K_t / M_s M_u)(C_s / M_s + C_s / M_u)$

   $a_6 = (C_s / M_s + C_s / M_u)^2$

   $a_8 = 1.0$

It can be seen that the relationship between the two measures of roughness determined by the ratio of magnitudes $|z(j\omega)|$ integrated and averaged over the road length is a complex function of frequency. The problem is illustrated in Figure 4, which shows how the ratio of the magnitude of the axle-body displacement of the standard quarter-car model versus that of the Mays meter quarter-car model represented by the 1962 Chevrolet Impala varies with the frequency of the road profile. An attempt to approximate the relationship between the roughness indices generated with the two models by the linear calibration formula (Equation 5) is hardly justified if roads of different frequency spectra are to be analyzed.

On the other hand, the statistical parameters of linear calibration equations are usually rather encouraging: high correlation coefficient, relatively small standard deviations. This happens because most roads have similar frequency spectra of their profiles. However, great care should be exercised if roads of unusual frequency characteristics are to be tested.

The frequency spectrum of the profile, as observed by a vehicle, changes not only from site-to-site but it also changes with the vehicle speed on the same site. It can thus be concluded from the earlier discussion that the road roughness index is a speed-related quantity. It is therefore proposed that the speed at which the roughness measurements are made always be indicated; for example, I/M_{40} or I/M_{25} would denote the road roughness index values at 40 and 25 mph, respectively.

SELECTION OF THE NUMBER AND LENGTH OF ROAD TEST SITES

Calibration of Mays road meters is a statistical procedure designed to produce the best mathematical model of the relationship between a calibrated system subject to random disturbances and a standard. The form of the model is assumed a priori to be linear with constant coefficients as shown in Equation 5. With the specified form (Equation 5) the problem reduces to an estimation of the parameters α_0, α_1, which is commonly accomplished by using a linear regression method. It is usually considered that the number of raw data must be sufficiently
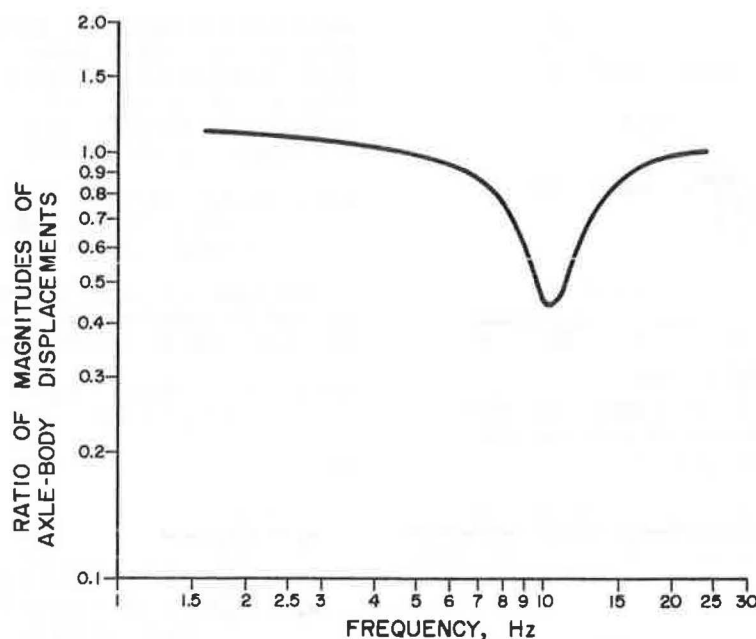
FIGURE 4 Ratio of magnitudes of axle-body displacement of the standard quarter-car model versus Mays meter quarter-car model represented by a 1962 Chevrolet Impala.

large, whatever that means, in order to ensure accurate results. The term sufficiently large, is usually interpreted as the larger the better, which essentially is true if the cost of calibration is not taken into account. Some state transportation agencies have developed extensive (and expensive) data collection procedures for calibrating their Mays meters. The effect of the number of data on the accuracy of Mays meter calibration was investigated in a study sponsored by the Pennsylvania Department of Transportation (3). The raw data base used in this study contained road roughness index values measured in 0.05-mi increments on 20 road sites, each 0.6 mi long. The calibrated Mays meter was run five times on each site. A total of 1,200 data were therefore collected. The calibration formula obtained from the original set of data was

$$R_{QC} = 14.3 + 0.693 \ R_{MM} \qquad (10)$$

Next, the raw data were averaged over 0.10, 0.20, 0.30, and 0.60-mi increments. The results of the calibration for the different distance increments are given in Table 1. Increasing the distance increment eliminates high frequency noise and thus has a smoothing effect on the data, which causes the standard deviation to decrease. On the other hand, with an increased distance increment, the range of the roughness data is narrowed; as a result the regres-

sion line fits the data better around the center of the range, but the accuracy for extreme values of roughness gets worse. A compromise selection of a distance increment between 0.2 and 0.3 mi appears to be the best choice.

As mentioned earlier, the data were collected five times on each site in order to eliminate random measuring errors. Additional computations were performed to determine calibration equations based on data obtained after one, two, three, and four repetitions. The results are given in Table 2 where it can be seen that the calibration parameters are almost totally independent of the number of repetitions. This observation can be explained by the fact that even with a single test on each road site, the total number of data collected was sufficiently large to ensure good accuracy of calibration. It should be noted that by reducing the number of runs from five to one, the extent of the calibration testing program is reduced by 80 percent without loss of accuracy.

Next, the problem of test site selection was examined. Calibration computations initially made for 20 sites were repeated for 15, 10, and 5 sites selected from the original set. The data were averaged over 0.25 mi, which gives two data points from each 0.5-mi section. The distribution of raw data and the calibration lines of the standard quarter-car, R_{QC}, versus Mays meter roughness index, R_{MM}, are shown in graphical form in Figures 5 through 8. The numerical results are given in Table 3. In addition to the data presented here, the same experiment was conducted for three other Mays road meters yielding very similar results (3). It can, therefore, be concluded that as few as 5 sites can be used instead of 20 to obtain sufficient accuracy of calibration.

Finally, the conclusions regarding the number of sites and the number of repetitions were combined, and the calibration was conducted for the drastically reduced set of data containing roughness index values from five sites, each obtained in a single test. The sites selected were 0.5 mi long and the distance increment was 0.25 mi, which gives a total of 200 data points in the full set against 10 data points

TABLE 1 Effect of Distance Increment on the Results of Calibration

Distance Increment, Mile	Calibration Formula, Equation 5		Correlation Coefficient	Standard Deviation, in./Mile
	Intercept, α_0	Slope, α_1		
0.05	17.5	0.629	0.91	19.3
0.10	15.8	0.647	0.94	14.7
0.20	14.4	0.659	0.96	12.1
0.30	14.4	0.660	0.97	10.4
0.60	14.6	0.658	0.98	9.1

TABLE 2   Results of Calibration for Different Numbers of Test Runs on Each Site

Speed	Parameter	No. of Repetitions				
		5	4	3	2	1
25 mph	Intercept, α_0	14.3	14.4	14.3	14.4	14.3
	Slope, α_1	0.693	0.693	0.693	0.693	0.698
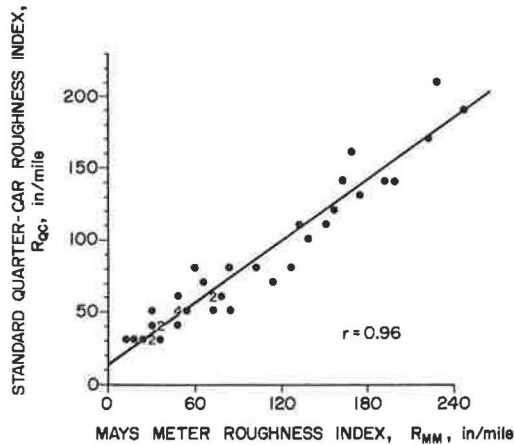
FIGURE 5   Calibration data for 20 sites.
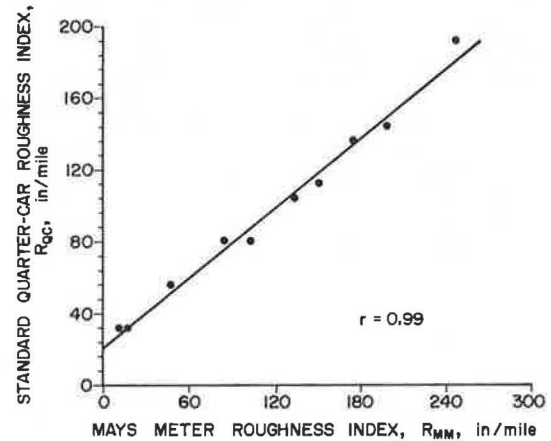
FIGURE 8   Calibration data for 5 sites.
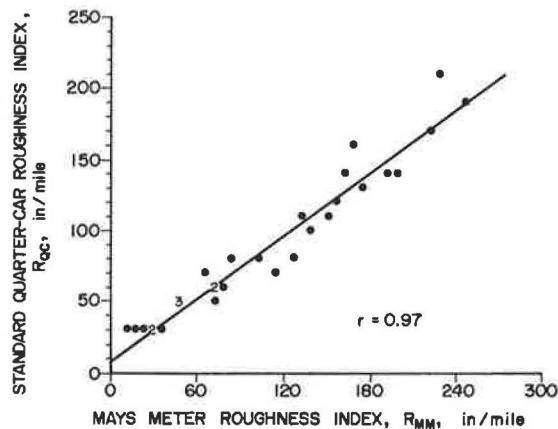
FIGURE 6   Calibration data for 15 sites.

TABLE 3   Results of Calibration for Different Number of Test Sites

Speed	Parameter	No. of Test Sites			
		20	15	10	5
25 mph	Intercept, α_0	12.8	8.61	10.3	20.1
	Slope, α_1	0.708	0.734	0.719	0.649

in the reduced data set. The calibration lines obtained for the reduced and full sets of data at 25 mph are shown in Figure 9. A rule of thumb often used in least-squares parameter estimation states that a minimum of 5 to 10 raw data points per estimated parameter are needed to ensure meaningful results. Thus at least 10 to 20 raw data points are necessary for Mays meter calibration because two parameters, α_0 and α_1, are being estimated, which roughly agrees with the conclusions set forth.

FIGURE 7   Calibration data for 10 sites.
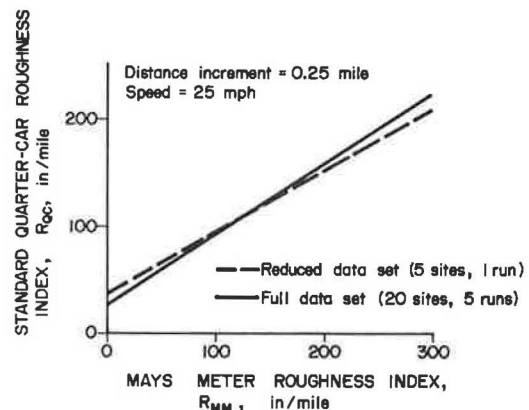
FIGURE 9   Calibration lines obtained from the full set of data and from the reduced set of data.

SUMMARY

Mays meter users, in their efforts aimed toward obtaining maximum accuracy of calibration, should be aware of the fundamental conceptual and technical problems associated with the calibration of the Mays meters against a standard quarter-car model. These problems include lateral nonuniformity of the road surface, which means that the input signals applied to the calibrated and calibrating systems are never identical. The difference between the dynamic characteristics of the Mays meter and those of the standard quarter-car is another problem limiting the accuracy of calibration. The lateral nonuniformity of road surface and the differences between the dynamic behavior of the calibrated and the calibrating vehicles cause inherent uncertainties in the calibration procedure that cannot be eliminated by increasing the amount of test data. The results of the statistical analysis presented in this paper should be useful in developing accurate, low-cost testing procedures for the calibration of Mays road meters.

REFERENCES

1. T.D. Gillespie, M.W. Sayers, and L. Segel. Calibration of Response-Type Road Roughness Measuring Systems. NCHRP Report 228. TRB, National Research Council, Washington, D.C., 1980, 81 pp.
2. G.K. Watugala. Determination of Road Roughness from Inertial Profilometer Data. Ph.D. dissertation, The Pennsylvania State University, University Park, 1984.
3. B.T. Kulakowski. Correlation of Road Roughness Measurements Obtained with the 1962 Chevrolet Impala and with the Standard Quarter-Car Model. Final Report, Pennsylvania Department of Transportation, Harrisburg, July 1985.

Computation and Analysis of Texture-Induced Contact Information in Tire-Pavement Interaction

T. G. CLAPP and A. C. EBERHARDT

ABSTRACT

In tire-pavement interaction, road surface texture is an important parameter that influences many factors such as tire noise, skid resistance, vehicle performance, and rolling resistance. Efforts to understand and quantify the texture effects in tire-pavement interaction have been limited because of the difficulties in experimentally and theoretically determining the many individual contact areas and contact pressures produced by irregularly shaped asperities indenting the tire tread. A numerical method is developed and incorporated into a computational algorithm to approximate contact pressure resulting directly from road surface texture in tire-pavement interaction. Only 2-D road surface profile geometry and tire inflation pressure are required as input parameters. The purpose of this paper is to demonstrate application of the method. Several types of surface textures are analyzed using the contact approximation method. The road surfaces are characterized by analyzing the individual pressure distributions, contact lengths, and tire deformations that make up the pressure profiles. The contact length information is combined with the surface profile geometry to approximate the geometry of the deformed tire surface. Analysis of the deformed tire geometry provides information concerning factors such as void area and depth of penetration. Two-dimensional pressure profiles associated with the 2-D surface texture profiles are computed and transformed into force time-histories of tire input excitation.

The interaction between a rolling tire and a road surface has been a topic of wide research interest for many years. As the popularity and demand for automotive transportation have increased, research has been conducted by tire and pavement designers to understand and improve tire-pavement interaction for two primary reasons: vehicle performance and safety. The tremendous growth of the nation's transportation system and the ever present need to conserve energy have produced additional reasons for addressing the topic of tire-pavement interaction such as tire noise and rolling energy loss. Current research of tire-pavement interaction is directed toward understanding the contact forces that affect tire noise, vehicle performance, safety, and rolling resistance.

Road surface texture is an important parameter in the analysis of tire-pavement contact. Surface texture has always been an important consideration in the design and construction of pavements with good skid resistance characteristics (1). Surface texture is also shown to affect tire noise, a primary environmental noise source, by up to 6 dB on dry pavements and up to 15 dB on wet pavements (2). Surface texture also affects tire rolling resistance, an important component of vehicle fuel consumption, by up to 30 percent (3). The recent design of small, lightweight vehicles has increased the significance of the structure-born vibration and acoustic radi-

ation affecting passenger comfort (4). Road surface texture creates fluctuating forces that excite the tire structure, resulting in vibrational response.

Sophisticated tire models are being developed to understand and predict the response of tires in contact with a variety of road surfaces. These models require an input excitation that reflects the true nature of tire-pavement contact. The contact information resulting from road surface texture must be included in the excitation mechanism.

Efforts to understand and quantify the texture effects in tire-pavement interaction have been limited as a result of difficulties encountered in experimentally or theoretically determining the many individual contact areas and pressures produced by irregularly shaped asperities indenting the tire tread. Global contact pressure and contact area associated with the tire footprint have been investigated (5), but the influence of surface texture is lost when averaged over the contact region. This global contact information is not sufficient to model the random, fluctuating forces that excite the tire structure and affect many factors related to tire-pavement interaction. This texture-induced contact information is required to represent realistic excitation forces produced by actual road surfaces.

Research has been performed to develop a method for predicting the normal contact forces that are created as a direct result of surface texture (6). Because the texture-induced contact information influences many topics of interest, a basic goal of the research has been to develop a method that is available to the tire and pavement research community.

The purpose of the research described here is to

T.G. Clapp, Textile Engineering and Science Department, P.O. Box 8301, North Carolina State University, Raleigh, N.C. 27695-8301. A.C. Eberhardt, Department of Mechanical and Aerospace Engineering, P.O. Box 7910, North Carolina State University, Raleigh, N.C. 27695-7910.

demonstrate the usefulness of the method by computing texture-induced contact pressure and length information from a variety of road surfaces. This contact pressure information is used to analyze individual peak pressures and construct force time-histories that excite tire models for predicting vibrational response and rolling resistance. The contact length information is used to approximate tire envelopment into the surface texture. This information contains skid-resistance parameters such as void area and depth of penetration resulting from surface texture geometry.

Researchers investigating topics such as skid resistance, tire noise, rolling resistance, and vehicle performance have an interest in the contact pressure and length information resulting directly from road surface texture in tire-pavement interaction. An analysis of experimental methods used to characterize pavement skid resistance by measuring texture-related parameters has demonstrated a need to define other surface texture parameters, such as microtexture, to adequately predict pavement skid resistance (7). In this paper information available from the approximation method developed for use by the general research community is described.

APPROXIMATION OF TEXTURE-INDUCED CONTACT PRESSURE

The development of an approximation method is based on an analysis of individual contact areas that are combined to form the total contact between a tire and a road surface. A contact model is developed to approximate the contact stress or pressure associated with individual contact areas. The contact stress produced by the model is mathematically described using the classical theory of elasticity (8,9). Contact pressure is approximated based on the model formulation and known input parameters.

An individual contact area associated with a surface asperity and the tire tread is modeled as a rigid indenter in contact with an elastic half-plane as shown in Figure 1. A line of continuous contact between points a and b is used to provide a two-dimensional model of the contact area. Working in two-dimensions reduces the complexity of the modeling process and is justified by the randomness of the road surface profile and the independence of parallel paths (10). The line of contact is called the displacement function, $f(x)$, and is assumed to be a known parameter. The vertical component of stress along the half-plane boundary is equal and opposite to the applied vertical pressure, $p(x)$, in the region of contact and equal to zero outside the contact region. This contact model provides the foundation on which tire-pavement contact is modeled.

The mathematical foundation used to develop the

pressure distribution associated with tread-pavement contact is based on plane problems in the theory of elasticity. Galin (8) performed an exhaustive study on the topic of contact problems of the theory of elasticity. Specifically, Galin developed an analytic solution for a two-dimensional contact problem that is based on the same assumptions as the model for the tire-pavement contact problem. In that development, the following equation occurs:

$$\pi E f(x)/2(1 - \nu^2) + C0 = \int_a^b (\sigma_y)_{y=0} \ln|t - x| dt \quad (1)$$

where

$$E = 1/2 \text{ plane modulus of elasticity,}$$
$$\nu = 1/2 \text{ plane Poisson's ratio,}$$
$$t = \text{dummy variable of integration,}$$
$$x = \text{horizontal contact position,}$$
$$a, b = \text{contact end points,}$$
$$(\sigma_y)_{y=0} = \text{normal contact stress, and}$$
$$f(x) = \text{contact displacement function.}$$

C0 is a constant that describes the vertical distance from the half-plane boundary line to the initial point of contact. This formulation contains the displacement function, $f(x)$. Discrete samples that describe the road surface geometry are used to represent the displaced half-plane contact length, $f(x)$. The normal stress, σ_y, in the y-direction and on the half-plane boundary is equal and opposite to the externally applied vertical pressure, $p(x)$,

$$(\sigma_y)_{y=0} = -p(x) \quad (2)$$

Equation 2 is substituted into Equation 1 to obtain

$$\pi E f(x)/2(1 - \nu^2) + C0 = -\int_a^b p(t) \ln|t - x| dt \quad (3)$$

Equation 3 is in terms of the displacement function, $f(x)$, which is described by 2-D road surface profiles.

With $f(x)$ previously defined, the problem becomes that of finding the corresponding pressure distribution, $p(x)$. The physics of the problem require the existence of a pressure distribution. Although unknown, the pressure is assumed to be some function with unknown coefficients that approximate the true pressure distribution.

The contact pressure distribution is approximated by a sequence of third-order polynomials connected by appropriate boundary conditions as shown in Figure 2.

The pressure distribution, $p_i(x)$, for each spline, i, is represented as follows:

$$p_i(x) = B_{i0} + B_{i1}x + B_{i2}x^2 + B_{i3}x^3 \quad (4)$$

where $X_i \leq x \leq X_{i+1}$. The coefficients, B_{in}'s, are unknown, and X_i and X_{i+1} are spline end points. Equation 4 is substituted into Equation 3 to determine the pressure distribution over an individual spline of contact length with end points X_i and X_{i+1}. The pressure is approximated over the entire contact length by a series of cubic splines to obtain

$$\pi E f(x)/2(1 - \nu^2) + C0 = -\sum_{i=1}^{I} \sum_{n=0}^{3} B_{in}$$
$$\int_{X_i}^{X_{i+1}} (t - X_i)^n \ln|t - x| dt \quad (5)$$
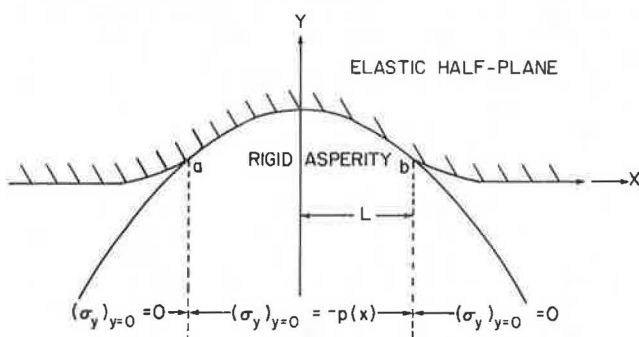
FIGURE 1 Two-dimensional model of the contact and boundary conditions between an elastic half-plane and a rigid object.
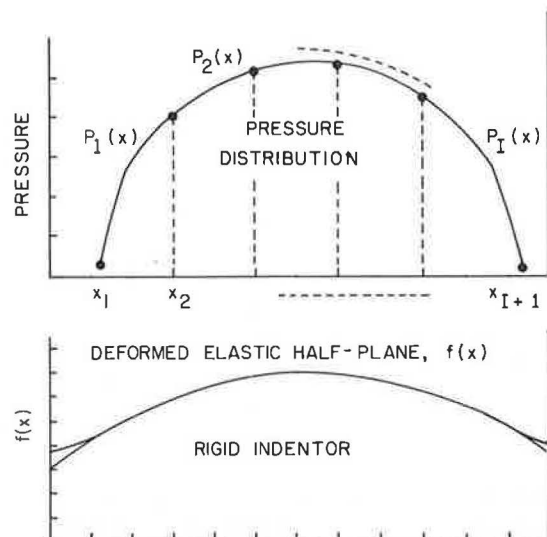
FIGURE 2 Sketch of the spline approximation of contact pressure associated with a deformed elastic half-plane.

FIGURE 3 Typical section of 2-D road surface profile geometry.

where I is the total number of splines.

The splines are combined using appropriate interface conditions. Splines can be combined by imposing restrictions on the continuity of the pressure distribution, or restrictions on first, second, or third derivatives of the distribution (11). The interface condition imposed on combining splines is that the pressure must be continuous, this means that

$$B_{(i+1)0} = B_{i0} + B_{i1}h_i + B_{i2}h_i^2 + B_{i3}h_i^3 \qquad (6)$$

where $i = 1, I - 1$ and $h_i = X_{i+1} - X_i$. This restriction assures a continuous distribution without introducing complexities that increase solution time and coefficient storage.

The unknowns in Equation 5 are C0 and the spline coefficients B_{in} (i = 1, I; n = 0, 3) to total 4 I + 1unknowns. With the interface conditions applied, there is a total of 3I + 2 unknowns. A total of 3 I + 2 equations are generated by selecting 3 I + 2 x-values along the contact length that correspond to discrete displacement values, f(x). A coefficient matrix formed by the 3 I + 2 equations is analyzed by using a singular value decomposition to decompose the matrix into singular values and vectors (12,13). The decomposed matrix information is used to compute the unknown spline coefficients. With the spline coefficients determined, the pressure distribution is approximated.

The method developed for approximating contact pressure also approximates the true contact length by producing negative pressures in the regions along the assumed contact length where no contact exists.

The approximation method is validated and incorporated into a computational algorithm to compute the contact information resulting directly from road surface texture in tire-pavement interaction (6). The input requirements for the algorithm consist of discrete samples that represent a two-dimensional road surface profile, as shown in Figure 3, and tire inflation pressure. The size and detail of the surface texture to be analyzed is limited primarily by the sample spacing of the surface profile. The algorithm computes multiple contact sections along the 2-D surface profile to incorporate the effects of adjacent asperities.

The algorithm computes the contact pressure and length information associated with 2-D surface tex-

ture profiles. The contact information consists of a series of individual contact lengths and pressure distributions associated with a 2-D road surface profile to form a 2-D pressure profile that characterizes the road surface. The pressure profile provides the basic contact information used to describe the effect of road surface texture in tire-pavement interaction. The amount of contact information produced by the algorithm is demonstrated by analyzing a variety of road surfaces. Details of the algorithm's computational process are included in the analysis.
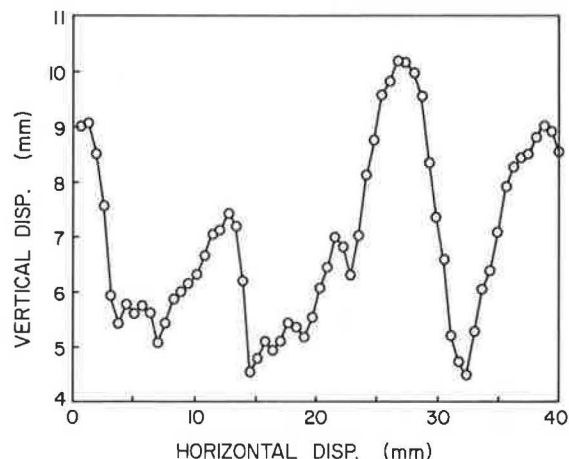
APPLICATION OF COMPUTATIONAL ALGORITHM USING ROAD SURFACE TEXTURE

Surface profiles from four selected pavements are analyzed to predict the 2-D contact pressure profiles that contain the force and contact length information. Profile information was collected in previous research from four road surfaces located at Texas Transportation Institute (TTI), College Station, Texas (10). These surfaces are referred to in this report as Test Pads 2, 4, 7, and 8 to maintain consistency with previous research. The construction and skid resistance of the test surfaces are well-documented (14) and are given in Table 1.

TABLE 1 Pavement Description

Pad	SN_{40}	Description
2	18 ± 3	Asphaltic concrete with jennite flush seal
4	42 ± 5	Crushed gravel hot-mix asphaltic concrete
7	60 ± 5	Lightweight aggregate asphaltic chip seal
8	50 ± 5	Lightweight aggregate hot-mix asphaltic concrete

For each of the four pavements, 21 two-dimensional surface profile traces were collected using a profilometer developed at North Carolina State University (10). Each trace contains 560 points that describe the surface geometry. These points have a sampling increment of 0.635 mm (0.025 in.) over a total profile length of 35.56 cm (14 in.). Examples of the reproduced profiles from each pavement are shown in Figure 4. This figure shows the wide texture range investigated and the necessity of using a narrow sampling increment to accurately describe the profile geometry. The contact information is approxi-
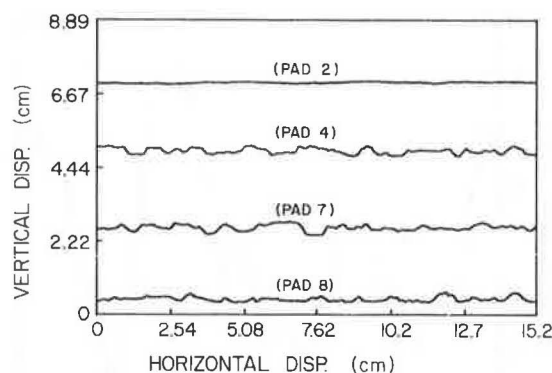
FIGURE 4 Computerized TTI pavement profile
(vertical scale offset 2.22 cm).

mated for each road surface using the profile infor-
mation as input into the computational algorithm.

The penetration or contact depth is determined by
assuming total envelopment, computing the pressure
profile, and comparing the average pressure of the
profile to an equilibrium pressure. The depth of
penetration is estimated based on the difference in
pressure values. The iterative process is continued
until the approximated average pressure is within 5
percent of the equilibrium pressure. If the average
contact pressure of the total profile is less than
the equilibrium or inflation pressure, then the sur-
face is considered totally enveloped, and no modifi-
cations to the profile data are necessary. A partic-
ular example using a truck tire inflation pressure
of 517 kPa (75 psi) is selected as the equilibrium
pressure. The smoothest surface, Pad 2, has a totally
enveloped average pressure of 131 kPa (19 psi) and
is the only surface that is considered totally envel-
oped. Test Pads 4, 7, and 8 have average pressures
of 1241 kPa (180 psi), 1344 kPa (194 psi), and 1034
kPa (150 psi). Because these average pressures, as-
suming total envelopment, are above the equilibrium
pressure, Pads 4, 7, and 8 are considered only par-
tially enveloped, and the depth of penetration must
be determined.

Once the contact depth is determined for one sur-
face profile, an empirical formula is constructed
based on the mean surface depth and some fraction of
the standard deviation to include the local vari-
ations in estimating the depth of penetration. The
estimation of the penetration depth dramatically re-
duces the computation time and produces average
pressures that are within 10 percent of the equilib-
rium pressure.

When the penetration depth is estimated for a
particular surface profile, the profile data are
modified by setting to zero displacement values be-
low the contact depth equal to the contact depth
value as shown in Figure 5. The modified profiles
provide the necessary input into the approximation
method to predict the contact information associated
with each particular road surface.

COMPUTATION AND ANALYSIS OF CONTACT INFORMATION

Twenty-one pressure profiles from each of the four
test pavements are generated by inputting the modi-
fied road surface profiles into the approximation
algorithm. The texture-induced contact information
is characterized by analyzing the contact length in-
formation, the individual pressure distributions,
and the spectral content contained in the pressure
profiles.
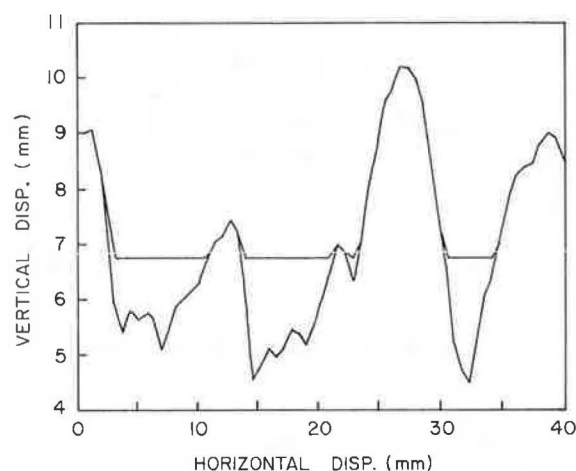
FIGURE 5 Modified surface profile based on an
estimated depth of penetration over the original profile.

The area of contact associated with each pavement
is contained in the approximated pressure profiles
as indicated by the lengths of the profile over
which positive pressure exists. The displacement in-
formation associated with each individual contact
length is known and is used to construct an approxi-
mated enveloped half-plane. This information pro-
vides a means of understanding and quantifying the
surface texture effect on parameters such as void
area, percent contact length to total length, depth
of penetration, and pressure distribution. Each test
pavement is characterized by these parameters using
the contact length information.

Pad 2, the smoothest pavement, is assumed to be
totally enveloped, achieving full depth of penetra-
tion. The percent contact length to total length is
56 percent, which indicates that a large portion of
the road surface is not in contact with the half-
plane. An examination of the enveloped and original
surface profiles shown in Figure 6 provides an ex-
planation. Pad 2 contains low amplitude microtexture
that produces a fluctuating pressure distribution as
shown in Figure 7. The negative portions of the high
frequency distribution are areas in which no contact
exists, resulting in the 56 percent contact value.

Figure 6 also shows that the enveloped profile is
practically identical to the surface profile. The
area between the curves is called the void area and
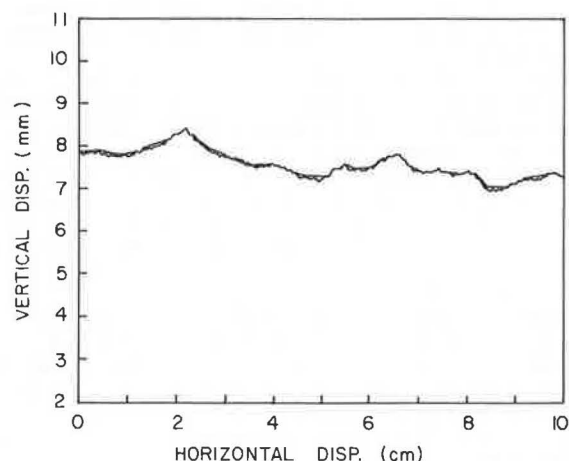
FIGURE 6 Comparison of original and enveloped surface
profiles from Pad 2.
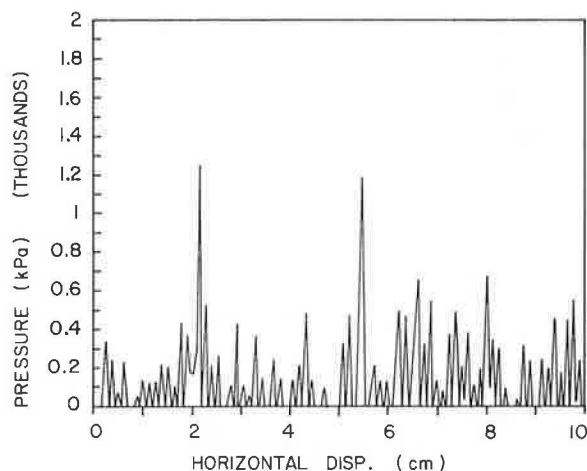
FIGURE 7 Contact pressure profile for Pad 2.

is an important safety consideration in pavement design. A large void area is desired to provide a path for water to exit from the tire-pavement contact region in wet highway conditions. Pad 2 has a very small average void area of 0.0010 cm²/cm (0.0004 in²/in.) that is measured in centimeters squared per centimeter of horizontal surface length. This small void area is a contributing factor in the low skid number of 18 ± 3.

The pressure profile for Pad 2 contains many low amplitude distributions. Analysis of the individual pressure distributions produces an average pressure of 180 kPa (26 psi) with average peak pressure of 380 kPa (55 psi).

Pads 4, 7, and 8 are partially enveloped as shown by the enveloped and original surface geometries in Figures 8 through 10. The figures show the different characteristics that describe each pavement. Pad 4 has widely spaced contact areas with similar depths of penetration. Pad 7 has widely spaced contact areas, but the depth of penetration varies from asperity-to-asperity because of the height variation of the asperities. Pad 8 has many sharp asperities in contact with the half-plane.

The pressure distributions associated with the enveloped profiles for Pads 4, 7, and 8 are shown in Figures 11 through 13. The microtexture roughness is reflected in the pressure profiles by the multiple peaks in the pressure distributions over individual

FIGURE 9 Comparison of original and enveloped surface profiles from Pad 7.
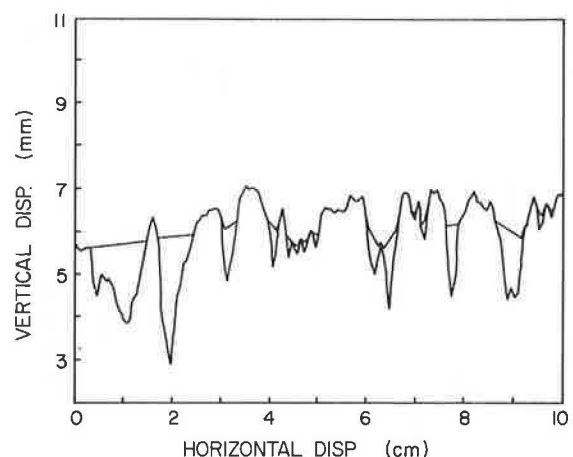
FIGURE 10 Comparison of original and enveloped surface profiles from Pad 8.

contact lengths. Pad 8 reflects much more microtexture roughness than Pads 4 or 7. Additional information about the individual pressure distributions is given in Table 2, along with other parameters that characterize the three pavements.

Pads 4, 7, and 8 all have high peak and average pressure values. Pad 8 contains 50 percent more peaks per centimeter than Pads 4 or 7, which may be reflected by the relatively higher skid number. Sharp peaks in the pressure distribution tend to improve tire-road surface adhesion by breaking the water film, thus diminishing the lubricating properties of the film. Pads 4 and 7 have a similar number of peaks and pressure values, but Pad 7 is superior to Pad 4 in terms of stopping traction as indicated by their skid numbers. The skid number difference is believed to be a result of the depth of penetration generated by the surfaces.

It is also assumed from this observation that handling (lateral tractive response) is also improved to some extent as the skid number increases. The primary resistive force that prevents skidding at high speeds in wet conditions is the hysteresis component of friction caused by the elastic half-plane material being deformed over the road surface asperities. Pad 7 is embedded approximately 32 percent deeper than Pad 4. This additional penetration increases the resistive forces that are created

FIGURE 8 Comparison of original and enveloped surface profiles from Pad 4.
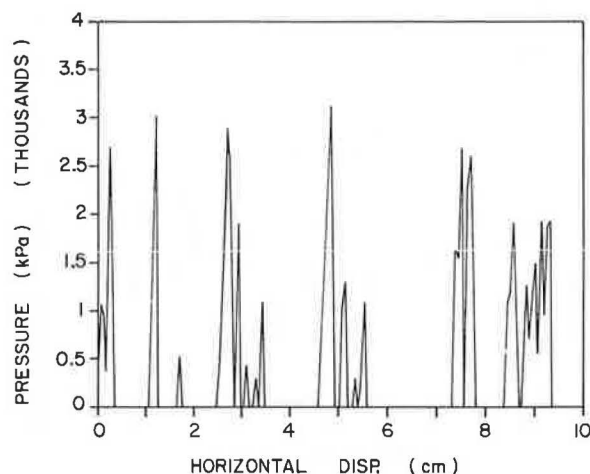
FIGURE 11 Contact pressure profile for Pad 4.
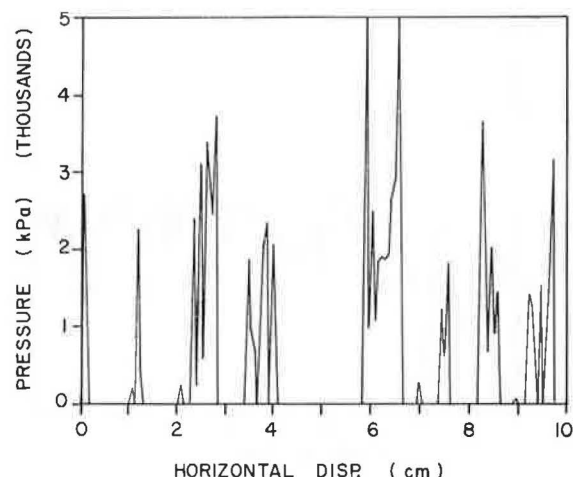
FIGURE 12 Contact pressure profile for Pad 7.
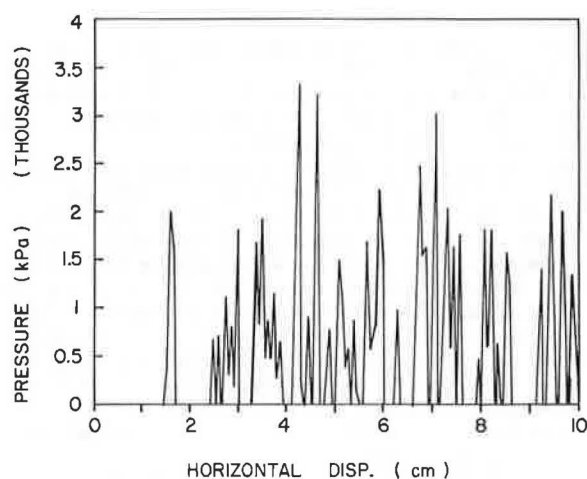
FIGURE 13 Contact pressure profile for Pad 8.

under sliding or skidding conditions. A detailed investigation of the contact information from many road surfaces can provide a definitive relationship to predict pavement skid resistance based on the analysis of road surface geometry using the methodology developed in this paper.

TABLE 2 Contact Information Analysis Results

	Pad 4	Pad 7	Pad 8
Individual avg. pressure, kPa	1179	1234	1055
psi	171	179	153
Individual peak pressure, kPa	2165	2227	1882
psi	314	323	273
No. peaks/cm	2.6	2.4	3.9
in.	6.6	6.2	9.8
Avg. depth of penetration, mm	1.17	1.55	0.89
in.	0.046	0.061	0.035
Standard deviation of penetration, mm	0.71	0.97	0.38
in.	0.028	0.038	0.015
Percent contact	32.4	32.0	45.3
Void area, cm^2/cm	0.10	0.10	0.036
in.^{2}/in.	0.04	0.04	0.014
Skid number (SN$_{40}$)	42 ± 5	60 ± 5	50 ± 5

The pressure profiles are transformed into force time-histories by multiplying the pressure times incremental areas to obtain incremental forces, and dividing the displacement increment by vehicle velocity to obtain a time increment. The two-dimensional time-histories can be combined to produce a three-dimensional forcing function that can be used to excite the tire-pavement contact region.

The force time-histories are also transformed into the frequency domain to determine the spectral energy contained in each road surface. Examples of each pavement's spectral energy in 1/3-octave bands are shown in Figure 14. This spectral energy can be used to characterize road surfaces and excite tire models.
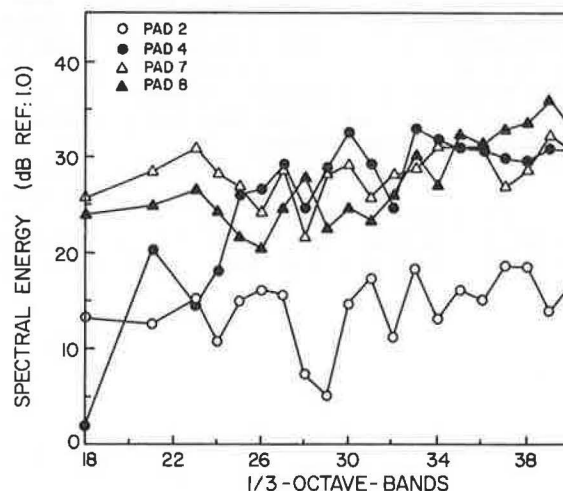
FIGURE 14 Comparison of 1/3-octave-band power spectra of the four test pad contact pressures.

Other contact information can also be extracted from the contact pressure profiles and the enveloped tire geometry as required to provide insight into factors influenced by road surface texture in tire-pavement interaction.

SUMMARY

Demonstrated in this paper are the capabilities of a computational algorithm for approximating contact

information resulting directly from road surface texture in tire-pavement interaction. The methodology incorporated in the algorithm is developed to operate on a microcomputer and to use input information that is accessible, or obtainable, by the research community. The texture-induced contact information produced by the algorithm can be applied to understand and predict factors influenced by surface texture such as tire noise, pavement skid resistance, rolling resistance, and vehicle performance.

Current research is directed toward incorporating the computational algorithm into a generally available software package that can be implemented by the research community to compute texture-induced contact information given the road surface profile data and relate this information to factors such as skid resistance, tire noise, and rolling resistance. Efforts are also directed toward predicting the total forcing function in the tire-pavement contact region by combining the texture-induced forces with the effects of tread pattern and global pressure distribution over the tire footprint.

ACKNOWLEDGMENTS

REFERENCES

1. D.F. Moore. The Friction of Pneumatic Tyres. Elsevier Scientific Publishing Co., Amsterdam, The Netherlands, 1975.

2. A.C. Eberhardt. An Experimental and Analytical Investigation of the Vibration Noise Generation Mechanism in Truck Tires. Report DOT-HS-8-02020. U.S. Department of Transportation, 1981.

3. L.W. DeRaad. The Influence of Road Surface Texture on Rolling Resistance. SAE Paper 780257. Society of Automotive Engineers, Warrendale, Pa., 1978.

4. S.K. Jha. Identification of Road/Tyre Induced Noise Transmission Paths in a Vehicle, International Journal of Vehicle Design and Components, Vol. 5, No. 1-2, Jan. 1984, pp. 143-158.

5. A. Browne, K.C. Ludema, and S.K. Clark. Contact Between the Tire and Roadway. Mechanics of Pneumatic Tires. NHTSA, U.S. Department of Transportation, 1981.

6. T.G. Clapp. Approximation and Analysis of Tire-Pavement Contact Information Resulting from Road Surface Roughness. Ph.D. dissertation, North Carolina State University, Raleigh, 1985.

7. T.J. Yeager and F. Buhlmann. Macrotexture and Drainage Measurement on a Variety of Concrete and Asphaltic Surfaces. Pavement Surface Characteristics and Materials. ASTM STP 763. C.M. Hayden, ed., American Society for Testing and Materials, 1982, pp. 16-30.

8. L.A. Galin. Contact Problems in the Theory of Elasticity. Department of Mathematics, North Carolina State University, Raleigh, Oct. 1961.

9. N.I. Muskhelishvili. Some Basic Problems of the Mathematical Theory of Elasticity. P. Noordoff Ltd., Groningen, The Netherlands, 1953.

10. T.G. Clapp. Spectral Correlation of the Surface Profile in the Development of a Tire and Pavement Interaction Force Model. Master's thesis, North Carolina State University, Raleigh, 1983.

11. A. Ralston and P. Rabinowitz. A First Course in Numerical Analysis, McGraw-Hill Book Co., New York, 1978.

12. J.E. Dennis and R.B. Schnabel. Numerical Methods for Unconstrained Optimization and Nonlinear Equations. Prentice-Hall, Inc., Englewood Cliffs, N.J., 1983.

13. G.H. Golub and C.F. VanLoan. Matrix Computations. Johns Hopkins University Press, Baltimore, Md., 1983.

14. R.D. Kilmer. Truck Noise I-C. Report DOT-TST-76-48. U.S. Department of Transportation, 1975.

Influence of Pavement Edge and Shoulder Characteristics on Vehicle Handling and Stability

DON L. IVEY and DEAN L. SICKING

ABSTRACT

Described in this paper is an analytical approach to predicting the steer angle of a vehicle, which is necessary to mount a pavement edge from the scrubbing condition. This steer angle is dependent on a new concept, the effective edge height, pavement edge geometry, travel lane friction and shoulder friction, tire geometry, and tire-cornering characteristics. It is demonstrated how this steer angle prediction can be combined with a vehicle simulation such as highway vehicle object simulation model (HVOSM) to predict vehicle movements, stability, and controllability. It is concluded that this combination of analyses used with driver performance characteristics now allows the study of a variety of factors. These would include all vehicle characteristics defined by HVOSM and many highway properties. Principal among these highway properties are pavement, shoulder and edge surface friction, and edge height and shape.

The possibility of a driver losing control after the vehicle goes off the paved surface onto a shoulder has caused highway engineers great concern. Why this occurs and under what conditions it can occur has been the subject of research efforts by Klein et al. (1), Nordlin and Stoughton (2,3), and Zimmer and Ivey (4). These efforts have been summarized in TRB State-of-the-Art Report 1, "The Influence of Roadway Surface Discontinuities on Safety" (5). Recently Graham and Glennon have tried to use computer simulation to study the phenomenon of vehicle loss of control due to pavement edges (6). In all these efforts no one has tested a large group of drivers. This is a recognized shortcoming, but the necessary resources were simply not available. To alleviate this problem, the Transportation Research Board is sponsoring a new study at the University of Michigan Transportation Research Institute and Texas Transportation Institute. Testing of a wide spectrum of drivers in highway environments is being conducted to better define driver performance. This work includes edges of different sizes and shapes. Still, there will not be enough funding to test all edge conditions of interest.

The work presented here is an effort to provide an analytical approach to the evaluation of a variety of edge conditions using the most reliable vehicle handling simulation--that venerable code developed by McHenry et al.--highway vehicle object simulation model (HVOSM) (7). The difficulty in using HVOSM directly has been in simulating tire edge interaction with reasonable accuracy. In this paper that difficulty is overcome by the development of an analysis that predicts the steer angle necessary to mount a specific edge from the scrubbing (4) condition. Once that value is determined as a function of edge height, edge shape, tire size, tire-pavement cornering characteristics, and other physical parameters, it can be used as one input parameter to HVOSM to define initial conditions. HVOSM, in an unmodified

form, will then define vehicle response as a function of vehicle and driver performance characteristics. Presented in this paper in abbreviated form is the analytical development to predict initial steer angle, and the use of HVOSM is demonstrated to determine subsequent vehicle response. The results are most encouraging. This technique can be used to extrapolate driver performance characteristics now being observed in the TRB study to a variety of physical situations and to define parametrically the influence of specific factors on vehicle handling and stability.

ABBREVIATED THEORETICAL DEVELOPMENT

Consider an automobile with one set of wheels off the pavement edge but with the inside of those wheels brushing that edge as shown in Figure 1. As the driver turns the steering wheel in an effort to mount the edge to return to the paved surface, the steering angle of the front wheels, α, is gradually increased. As α gets larger, the vehicle will finally climb the edge when the right front wheel reaches the critical value of α, α_c. Further, the right rear tire will finally mount the edge when the yaw of the vehicle has increased to approximately α_c. The vehicle speed, yaw, and yaw rate at this predictable vehicle position, along with the driver's reaction time and counter steering capability will then dictate whether the vehicle can be successfully controlled. The critical steer angle, α_c, is therefore of major importance in predicting vehicle controllability. This abbreviated derivation is an attempt to predict that critical steer angle. The complete derivation is available on request from the authors.

FORCES ACTING ON THE FRONT TIRES

As a vehicle in the edge scrubbing condition has its wheels gradually turned into the pavement edge surface, a state of equilibrium exists between the
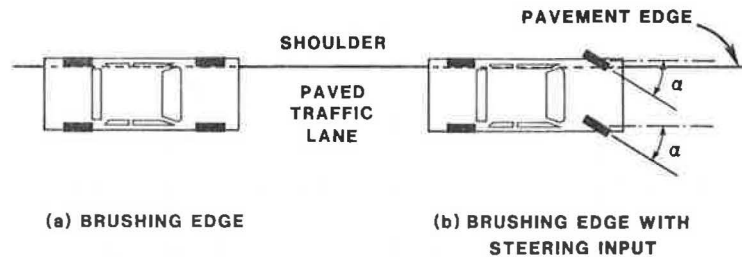
FIGURE 1   Vehicle gradually turning toward a pavement edge.
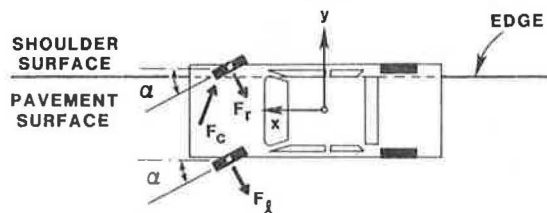
FIGURE 2   Equilibrium of forces acting on vehicle front tires.

W_{zr} = the weight of and on the right front wheel,
N_b = the normal force on the bottom contact path,
N_e = the normal force acting at the contact zone of the tire
with the pavement edge, and
F = the friction force acting on the tire-edge contact zone.

FIGURE 3   Forces on the tire in contact with the pavement edge.

FIGURE 4   Reduction of N_b as the effective edge height increases.

cornering forces on the two front wheels and the resisting force generated by the edge, as shown in Figure 2.

A summation of the forces acting on the front tires in the y direction yields

$$\vec{F}_r + \vec{F}_\ell = \vec{F}_c \qquad (1)$$

where F_r is the cornering force exerted on the right front tire, F_ℓ is the cornering force exerted on the left front tire, and F_c is the force exerted by the pavement edge on the right front tire.

The cornering forces can be determined by knowledge of the lateral force generation characteristics of the tires in contact with specific surfaces, the vertical load at the pavement or shoulder surface on each front tire, and the slip angle, α, of each front tire.

The definition of the magnitude and direction of the edge force, F_c, is somewhat more difficult. First, it will be assumed that the edge force, F_c, is the resultant of two forces. These are N_e, a force acting normal to the undeformed surface of the tire at the center of the area of tire-edge contact, and F, the friction force acting at the tire and edge contact zone. This friction force must act in opposition to the relative velocity between the tire and edge surface and in the plane of the contact zone, assuming further that plane is defined by the undeformed surface of the tire. These forces are shown in Figure 3. A summation of forces vertically yields

$$\vec{N}_b + \vec{N}_e + \vec{F} = \vec{W}_{zr} \qquad (2)$$

The normal force, N_b, acting on the bottom contact patch of the tire is difficult to deal with analytically. At some point, this force obviously becomes zero for the larger edge heights as mounting starts. This variation of N_b with edge height was assumed to vary as shown in Figure 4. An n value of 4.5 was tentatively selected to give an appropriate fit of test data. This will be discussed further in the final section. Using this approximation for N_b, Equation 2 can be written

$$\vec{W}_{zr}/e^{\Delta e/n} + \vec{N}_e + \vec{F} = \vec{W}_{zr}$$
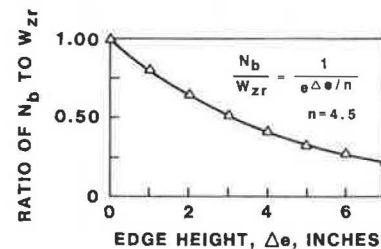
In the full derivation it has been shown that Equations 1 and 2 can be expressed in terms of the geometric characteristics of the tire and the pavement edge and two unknowns N_e and α_c. With these equations, N_e can be eliminated and the slip angle, α_c, necessary to climb a specific pavement edge, may be calculated.

EFFECTIVE EDGE HEIGHT

It is intuitively appealing that more gradually sloped edges are easier for a tire to mount than sharp, abrupt edges, just as it is easier to walk up a gradual incline than to climb a cliff. If it is noted how a tire makes contact with edges of different shapes, as shown by Figure 5, it becomes apparent that the relative ease or difficulty a tire encounters in traversing a particular edge may be explained by the idea of effective edge height. The effective edge height is defined as the height above the lower surface (usually considered the shoulder surface) at which the tire makes predominant contact with the edge. In earlier discussions this has been called the contact zone, and is defined as the area at which the normal force, N_e, and the friction force, F, act. As observed in Figure 5, a right-angle

VIEW FROM REAR OF TIRES
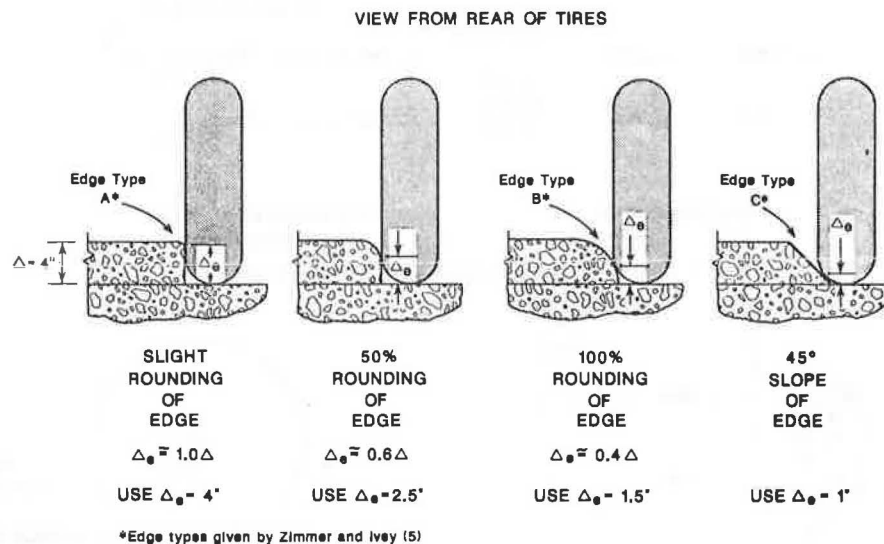
FIGURE 5 Effective edge heights for different edge shapes.
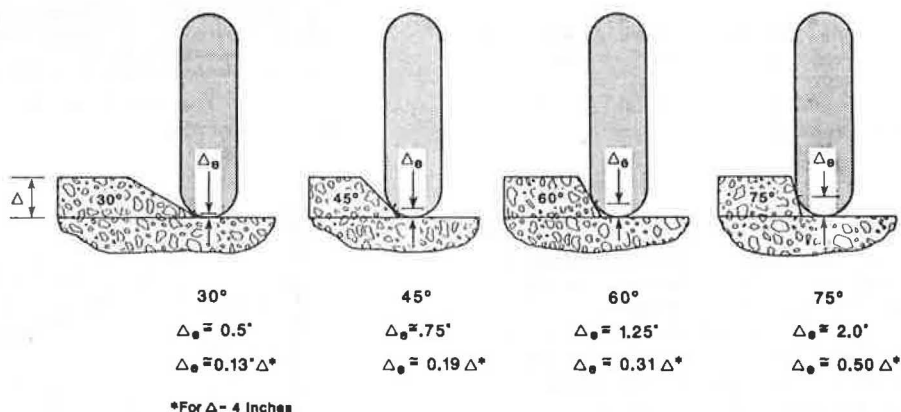
FIGURE 6 Effective edge heights for different edge slopes.

edge has an effective height, Δ_e, roughly equivalent to the total vertical distance, Δ, between the two major plane surfaces (i.e., the pavement surface and the shoulder surface). As different edge shapes are considered, it is apparent that the effective height becomes smaller as the edge becomes more rounded, and finally sloped at an angle of 45 degrees. Both empirical testing and the theory presented here, demonstrate conclusively the greater ease of traversing more rounded and more gradually sloped edges (1-4).

Figure 6 shows the influence of different edge slope angles on the effective height, and Figure 7 shows the complete variation from an edge slope of zero degrees, which must certainly correspond to a zero effective height, to a slope of 90 degrees, which is just as certainly an effective height, Δ_e, equal to the total height, Δ.

A range of angles probably exists between 60 and 90 degrees where the concept of effective height less than the total height breaks down. This is due to tire deformation producing tire surface compliance with edge geometry and the simplified geometry attributed to the tire cross section in this development.

The effective height is only slightly influenced by the steer or slip angle, α, in the range of importance, from 0 to 15 degrees. This small variation may be considered of only academic interest.
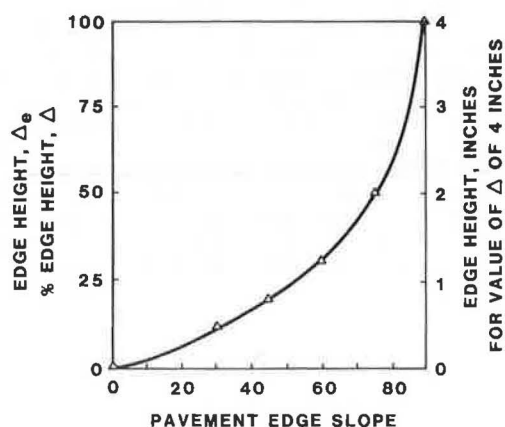
FIGURE 7 Effective edge height variation with edge slope.

It appears compelling then that the concept of effective height explains in simple geometric terms the resistance a tire (or vehicle) encounters in traversing edges of the same total height but of quite different shape. In subsequent sections, the concept of effective height will be used, along with
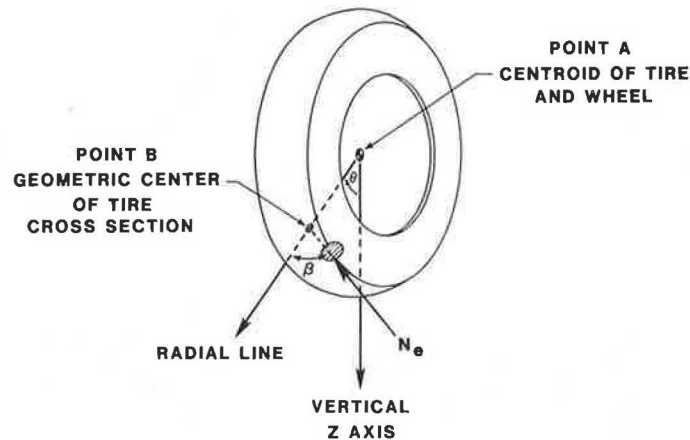
FIGURE 8 Perspective of tire.
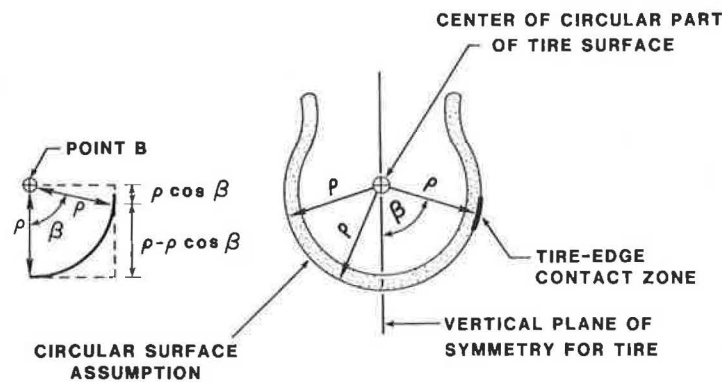
FIGURE 9 Cross section of tire.

the theoretical analysis to calculate those resistances.

NORMAL FORCE

Figure 8 is a perspective view of the tire and wheel showing the direction of the normal force, N_e, that is developed between the tire and the edge. The normal force is assumed to act in a direction normal to the undeformed surface of the tire. A further simplification is that the surface of the tire cross section is circular and is defined by a radius, ρ, about point B (see Figure 9). Although it is recognized that tires are not circular in cross section, the authors believed that the circular simplification would not seriously compromise accuracy. The results appear to bear this out.

The following geometric measurements were used to resolve the normal force into transverse and vertical components.

θ, the angle between the vertical plane, including the wheel axis and a second plane defined by the wheel axis and the tire-edge contact zone.

r, the radial distance from the wheel axis to the contact zone.

r_t, the undeformed tire radius.

r_r, rolling radius of the tire (note this can be approximated by r_t when the tire starts to mount the pavement edge).

Δ_e, the effective height of the pavement edge (i.e., the height of the tire-edge contact zone above the lower surface).

ρ, the approximate radius of curvature of the tire cross section as shown in Figure 9.

β, the angle in the plane of the tire cross section between the central plane cross section and the edge contact zone. (See Figures 8 and 9.)

The transverse component of N_e sin is found to be N_e sin β and the vertical component of N_e is N_e cos β cos θ.

FRICTION FORCE

Now the friction force, F, acting in the tire-pavement edge contact zone will be considered. Figure 10 is a side view of the tire-edge contact patch showing the velocity components V_ℓ and $\dot{\theta}_r$ and the resultant velocity V_r. These geometric and dynamic parameters may be used to define the transverse and vertical components of the force F. Thus the transverse com-
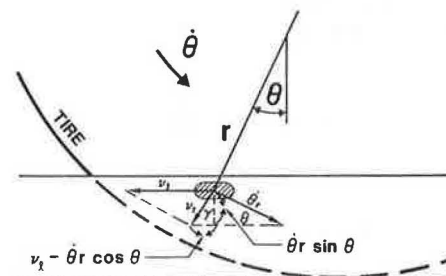
FIGURE 10 Relative velocity between tire and pavement edge.

ponent of F is F cos γ cos β and the vertical component of F is F cos γ sin β.

DETERMINATION OF TIRE-CORNERING FORCE

In determining the conditions under which a tire will mount an edge, it is necessary to estimate the tire-cornering force when the slip angle, α, is equal to the critical slip angle, α_c. This is done by calculating the slope of a line between zero slip angle and points on the side force, slip angle curve. Figure 11 shows how this is done. If these slopes C'_α are estimated from the side force, slip angle curve for a particular tire, surface, and tire load, a curve relating C'_α to α can be plotted in Figure 12. By dividing all values of C'_α by the load at which the test was conducted, C'_α can be made dimensionless and the two lines, A and B, can be expressed.

$C_\alpha = K_1 - K_2\alpha$, $0 < \alpha \leq \alpha_d$ (Line A)

$C_\alpha = K_3 - K_4\alpha$, $\alpha > \alpha_d$ (Line B)
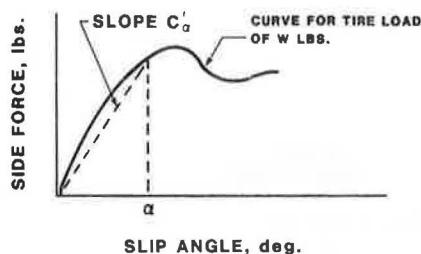
FIGURE 11 Side force, slip angle curve.
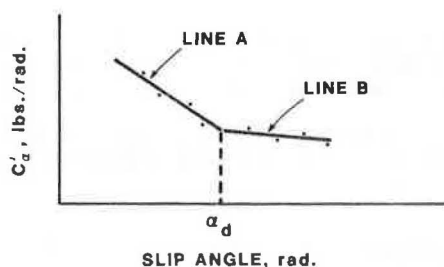
$C_\alpha = K_1 - K_2 \alpha$, $0 < \alpha \leq \alpha_d$ (LINE A)

$C_\alpha = K_3 - K_4 \alpha$, $\alpha > \alpha_d$ (LINE B)

FIGURE 12 Slope—slip angle and straight-line approximation.

Sakai used Figure 26 in "Characteristics of Japanese ESV Tires" (8) to calculate values for K_1 through K_4. For a 6.45-14-4PR (5J-14 rim) conventional tire, the K values calculated were

$K_1 = 8.04$
$K_2 = 17.1$ One line was sufficient to adequately
$K_3 = 8.04$ describe the data.
$K_4 = 17.1$

EQUILIBRIUM EQUATIONS

In reading the equations in this section the reader will see that static equations have been used and the inertial terms needed to define the dynamic

equilibrium of an accelerating body have been neglected. It was believed that this would not compromise accuracy for the following reason. In the instant before edge mounting begins, a vehicle in an edge scrubbing condition at a constant speed does not have significant accelerations imposed on any element. This obviously neglects the random accelerations caused by surface roughness. The authors have a philosophy of problem solving that does not respect sophistication for its aesthetic properties. It is thus submitted that the static treatment is adequate for the purposes of this analysis.

With the resolution of the normal and friction forces acting on the pavement edge, it is now feasible to write Equations 1 and 2 in different terms.

First considering Equation 1 and noting that the cornering force on each wheel can be represented by

$W_z\ C_\alpha\ \alpha$

where W_z is the weight on a particular wheel contact patch and C_α is the unit cornering stiffness at a slip angle α, Equation 1 can be written

$$W_{zr}\ S\ C_{\alpha_c} + W_{z\ell}\ C_{\alpha_c}\ \alpha_c = N_e \sin\beta\ \cos\alpha_c$$
$$+ F \cos\gamma \cos\beta \cos\alpha_c \quad (3)$$

If the coefficient of friction between the pavement edge and the tire is μ_e, F can be replaced by $\mu_e N_e$. S is the reduction of C_{α_c} due to lower shoulder friction, and the term $e^{\Delta e/n}$ produces a reduction in N_b as the effective edge height, Δ_e, becomes larger. Note that n is an empirically determined constant. This equation can be rewritten

$$(W_{zr}/e^{\Delta e/n})\ S\ C_{\alpha_c}\ \alpha_c + W_{z\ell}\ C_{\alpha_c}\ \alpha_c =$$
$$N_e \sin\beta \cos\alpha_c + \mu_e N_e \cos\gamma\ \beta \cos\alpha_c \quad (4)$$

Equation 2 can also be rewritten

$$N_e \cos\beta \cos\theta + \mu_e\ N_e \cos\gamma \sin\beta =$$
$$W_{zr} - W_{zr}/e^{\Delta e/n} \quad (5)$$

By solving Equation 5 for N_e and substituting that value into Equation 4, the result is one equation with one unknown, α_c. The value of α_c may be calculated by successive approximation.

For a BR 60SR14 (6Jx14 rim) the K values calculated were

$K_1 = 15.6$ }
              Line A coefficients
$K_2 = 74.0$ }

$K_3 = 8.04$ }
              Line B coefficients
$K_4 = 17.1$ }

If C_α calculated in this way is multiplied by the weight supported by the tire and the slip angle in radians, the result is the cornering force for the value of α used in either the Line A or Line B equations. If the critical value of slip angle, α_c, is used, the cornering force on the nonmounting front tire may be calculated.

COMPARISON WITH EMPIRICAL OBSERVATIONS

Independent observations of the steer angle necessary to climb a pavement edge from the scrubbing condition were provided in a 1976 paper by Klein et al. (1). They made observations on four vehicles shown in the
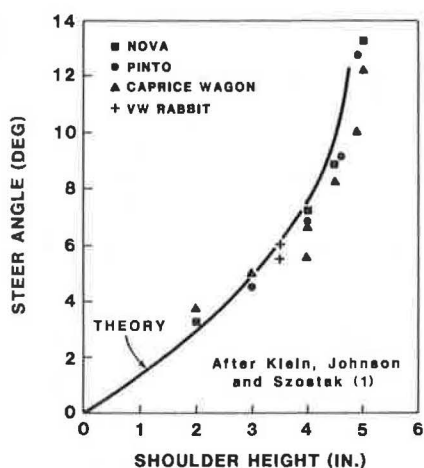
FIGURE 13 Steer angle required to climb various edge heights from a scrubbing condition for four cars compared with theoretical predictions.

FIGURE 15 Influence of N_b reduction factor.

legend of Figure 13 and came to the conclusion that the steer angle was somewhat independent of vehicle and tire size, at least within the range tested and testing accuracy.

To compare the theory with the empirical observations shown in Figure 13, the following parameters were used: A nominal 14-in. tire, roughly comparable to the "conventional tire" given by Sakai ($\underline{8}$). (See Figure 14.) The tire radius, r_t, was taken at 12.5 in.; the rolling radius r_r, at 12.0 in.; the tire cross-section radius, ρ at 3.6 in.; and nominal values of K_1, K_2, K_3, and K_4 were 9, 18, 9, and 18, respectively. These values are very close to those derived from the conventional tire side force, slip angle data, although the surface in the Sakai ($\underline{8}$) tests was different from that in Klein et al. ($\underline{1}$). The tire-edge friction coefficient, μ_e, was 0.7; the shoulder-friction reduction factor, S, was 0.8; and n the vertical force, N_b, reduction factor was 4.5.

FIGURE 14 Side force—slip angle curves for three tires.

Based on these estimates, the theory curve shown in Figure 13 was generated. Although these results appear to be excellent because the factors used appear to be reasonable estimates of the conditions of the tests, it must be recognized that the factor, n, the vertical force reduction factor was selected to give an appropriate fit of the data. Figure 15 shows that the relationship produced by the theory is heavily dependent on the value of n selected. That is, the slip angle predicted to climb a specific

edge is heavily dependent on the amount of the weight borne by the tire-shoulder surface contact zone at the time mounting occurs.

In order to objectively assess the predictive accuracy of the theory, it would be necessary to experimentally determine the following factors: (a) μ_e, (b) S, (c) n, and (d) k_1 through K_4.

The appropriate equations developed in this study were programmed for solution and for graphics display by Robert Streckfus. The program listing is available to any interested party. The results of Streckfus' study of the influence of several different parameters is shown in Figures 16 through 19.

In Figure 16, the curves from left to right above the 6-degree steering angle line are for values of the pavement edge friction of 0.3, 0.7, and 0.9, respectively.
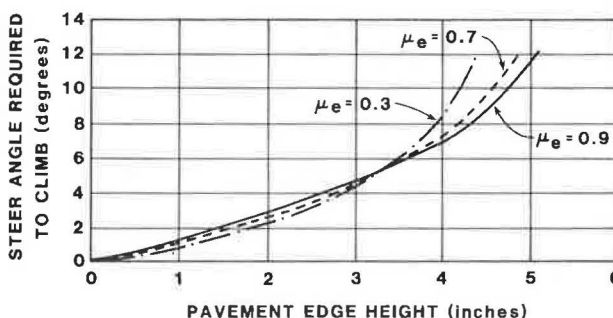
FIGURE 16 Influence of pavement edge friction.

Figure 17 shows the influence of the shoulder friction reduction factor as it varies from 0.1 to 1.0. An icy shoulder might be represented by an S factor as low as 0.1. If the pavement friction is 0.7, the icy shoulder friction would be 0.1 times 0.7 or 0.07. That situation would be more critical
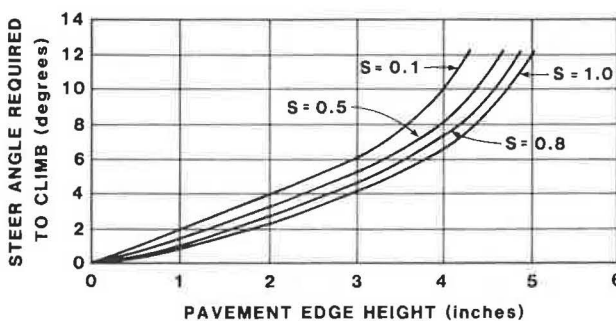
FIGURE 17 Influence of shoulder friction reduction factor.

than the shoulder conditions under which more friction could be developed. It is surprising that it is not more influential until it is considered that only a portion of the wheel weight, N_b, is active on the shoulder surface when mounting occurs. By saying a shoulder has little effect on the steer angle to mount, it does not follow that the influence on vehicle loss of control is also small. The contrary is actually true.

Figure 15 shows that the value of N_b, and the rate it is reduced, as dictated by the factor n, is most important. From left to right, the orange curves are shown using n values of 3.0, 4.5, and 6.0, respectively. The value of 4.5 is believed to give the most appropriate, albeit slightly conservative, representation of the data developed by Klein et al. (1).

Figures 18 and 19 show how the tire-cornering force coefficients influence the solution. Larger K_1 and K_3 values give higher values of cornering force. These curves, from left to right in Figure 18, show the sensitivity of the theory as K_1 and K_3 vary from 7 to 11. Smaller values of K_2 and K_4 give larger values of tire-cornering force. Figure 19 shows the influence from left to right of values of K_2 and K_4 of 21, 18, and 15, respectively.
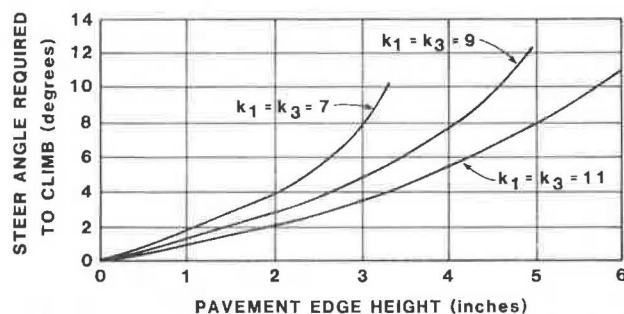
FIGURE 18 Influence of tire-cornering force coefficient.
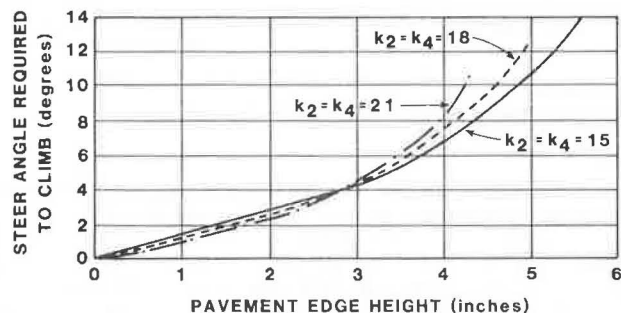
FIGURE 19 Influence of tire-cornering force coefficient.

The base reference values of the five coefficients for these sensitivity studies are

$$\mu_e = 0.7$$
$$S = 0.8$$
$$n = 4.5$$
$$K_1 = K_3 = 9.0$$
$$K_1 = K_4 = 18.0$$

These are the same values used to produce the comparison between theory and test data shown in Figure 13.

These results show a high probability that the theory developed here can provide meaningful predic-

tions of the tire-cornering slip angles necessary to mount defined pavement edges. It is a relatively easy step to move from this prediction to the assessment of safety for various edge conditions. Models such as the relatively simple one given by Klein et al. (1), or HVOSM (7), can be used to estimate automobile response subsequent to mounting a pavement edge at a specific condition of cornering slip angle. In the final section, HVOSM will be used to demonstrate how driver and vehicle performance can be assessed by using this combination of analyses.

VEHICLE MOVEMENT SUBSEQUENT TO EDGE MOUNTING

To demonstrate how the foregoing development can be used to study vehicle movements HVOSM was used. This code was selected as the most comprehensive and reliable of the codes available. It was developed by McHenry et al. (7) in the late 1960s, and has been widely used in the highway safety field since that time.

The vehicle selected for this demonstration was a 1974 Chevrolet Luv Pickup. The data used to simulate that vehicle and the various maneuver conditions are available but are not presented here. Nine edge conditions were selected and are given in Table 1, along with the value of critical steer angle, α_c, used as an initial condition.

Conditions 1, 2, and 3, were selected to show the effect of progressive degrees or rounding on vehicle responses after an edge climb. In order to determine vehicle response, an additional set of input parameters was required.

1. Initial steer angle. This was determined as follows: First an effective edge height was determined using the methods described previously. For example, the effective edge height for Conditions 1, 2, and 3, can be taken from Figure 5. They are 4.0, 2.5, 1.5, and 1.0 in. (Actually 0.75 in. was used instead of 1.0, as showing the more accurate value from Figure 8.) The values of Δ_e, effective edge height, were taken from Figure 7 for Conditions 4 through 9.
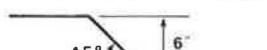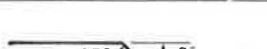
2. Using the value of Δ_e defined, the steer angle was determined using Figure 13. These values of steer angle are given in the final column of Table 1.

3. Driver control characteristics were required for each test run. On the basis of data developed by Zimmer and Ivey (4) and new data from the ongoing UMTRI/TTI study, values of a combined perception reaction time and a front wheel turning speed were selected. Approximate mid-range values of these performance characteristics were 0.5 sec and 16 degrees per sec. That is, the driver would start moving the steering wheel 0.5 sec after the right front tire mounted the edge from a scrubbing condition, and the rate of wheel movement would be 16 degrees per sec.

4. With these values of initial steer angle and driver control characteristics, the nine program runs given in Table 1 were produced.

Example output data selected from Condition 1 are given in Table 2. The initial speed on all runs was 50 mph (73.33 fps). The time elapsed after edge mounting begins is given in the first column. The position of the vehicle's center of gravity (c.g.) is given in the next three columns (x' = forward, Y' = lateral, and Z' = down). The sprung mass rotational orientation is given by the next three columns (Phi = roll, Theta = pitch, and Psi = yaw). The lateral, vertical, and forward speeds are given in the last three columns. The resultant velocity of the vehicle is the vector sum of these three velocities.

TABLE 1   Pavement Edge, Effective Edge Heights, and Initial Steer

Condition	Pavement Edge Profile	Effective Edge Height, Δ_e, inches	Initial Steer Angle, α_c degrees
1	4″ vertical drop	4.0 (From Figure 5)	7.5[a]
2	2″ / 4″	2.5 (From Figure 5)	3.8[a]
3	4″ / 4″ rounded	1.5 (From Figure 5)	2.1[a]
4	45° / 6″	0.75 (From Figure 7)	1.1[a]
5	45° / 4″	0.75 (From Figure 7)	1.1[a]
6	45° / 2″	0.75 (From Figure 7)	1.1[a]
7	45° / 4″	0.75 (From Figure 7)	1.1[a]
8	30° / 4″	0.50 (From Figure 7)	0.7[a]
9	15° / 4″	0.20 (From Figure 7)	0.5[a]

[a] These values determined from the effective edge height and Figure 15.

TABLE 2   Selected Computer Program Results (Condition 1)

Time (sec)	Position (in.)			Sprung Mass c.g. Orientation (deg)			Velocity (fps)		Forward Speed (fps)
	X′	Y′	Z′	Phi	Theta	Psi	Lateral	Vertical	
.0000	500.00	1,174.44	−25.71	4.93	.00	.00	.00	.00	73.33
.5500	980.34	1,171.78	−26.78	2.3	0.91	−1.71	1.20	0.76	72.15
1.1000	1,450.99	1,147.37	−27.16	6.35	−0.31	−18.63	14.10	−1.96	68.71
1.725	1,941.65	1,032.10	−27.45	6.66	−0.10	−49.78	31.96	−3.79	55.30
2.2750	2,301.60	864.80	−27.51	6.65	−0.07	−76.27	40.06	−4.69	39.11
2.5000	2,425.33	786.10	−27.54	6.58	0.00	−86.87	41.20	−4.76	32.02

Using these data from each condition run, Figures 20–22 were plotted. The only values needed to make these figures were X′ and Y′, movements of the c.g., and the yaw angle.

Figure 20 shows the influence of edge rounding. A sharp edge (Condition 1) 4 in. high throws the vehicle completely out of control. Progressive rounding (Conditions 2 and 3) rapidly reduces the problem. Some license has been taken with the vehicle plots of Condition 1. The final view of the vehicle on its side was not predicted by HVOSM. This was done to illustrate that a vehicle in an 86-degree lateral drift certainly has the potential of rolling.

Figure 21 shows the influence of edge height for a 45-degree sloped edge. Although the 6-in. edge (Condition 4) allows the vehicle to barely remain within its lane, the 4- and 2-in. edge allow progressively greater margins of safety. The primary difference in vehicle control in these three runs stemmed from the fact that the 0.5 sec perception-reaction time was not programmed to begin until the right front tire had reached the top of the 45-degree surface. This is probably a conservative assumption; that is, many drivers would begin their perception before fully mounting the edge.

The influence of edge slope is shown in Figure 22. As the slope is reduced from 45 to 15 degrees, the margin of safety, as illustrated by how much of a 12-ft lane is needed for the maneuver, becomes progressively larger.

When elements of Figures 20–22 are compared with driver and vehicle performance given in the literature (1–4), and with testing from the ongoing UMTRI/TTI project, good agreement is noted with the mid-range of driver performance. It is therefore submitted that the combination of the analytical pre-
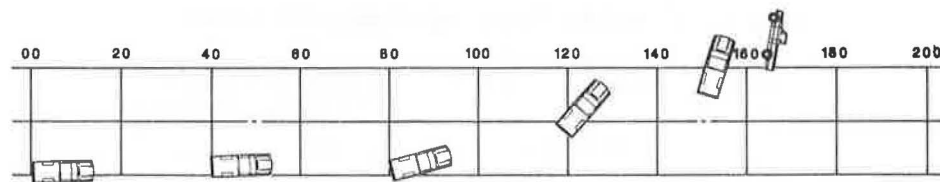
Condition 1 4 inch edge, no rounding
(Predicted steer angle, 7.5 degrees)
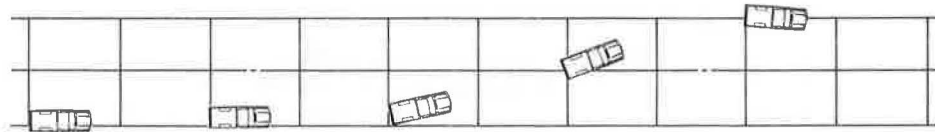
Condition 2 4 inch edge, 2 inch radius of edge rounding
(Predicted steer angle, 3.8 degrees)
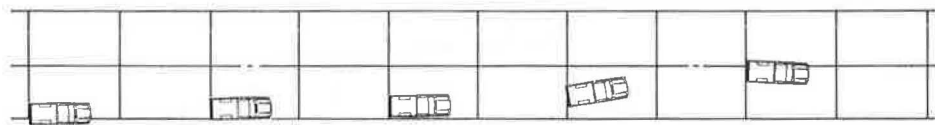
Condition 3 4 inch edge, 4 inch radius of edge rounding
(Predicted steer angle, 2.1 degrees)

FIGURE 20   Conditions 1, 2, and 3.
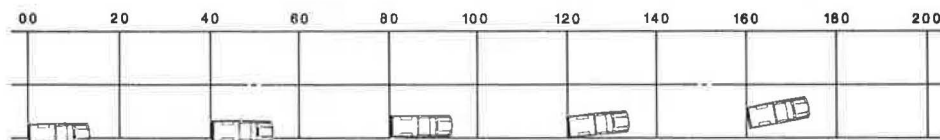
Condition 4 6 inch edge, 45 degree edge slope
(Predicted steer angle, 1.1 degrees)
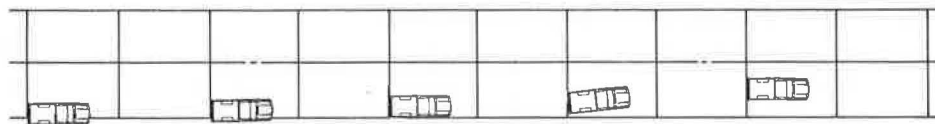
Condition 5 4 inch edge, 45 degree edge slope
(Predicted steer angle, 1.1 degrees)
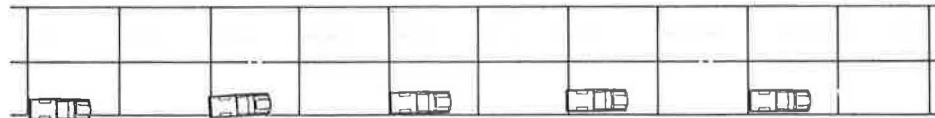
Condition 6 2 inch edge, 45 degree edge slope
(Predicted steer angle, 1.1 degrees)

FIGURE 21   Conditions 4, 5, and 6.

diction of initial steering angle and HVOSM has the potential of extrapolating the economically limited full-scale testing programs to analytically estimate the influence of such factors as

1. Vehicle characteristics
    a. Geometry
    b. Inertial properties
    c. Tire geometry
    d. Tire-surface cornering force characteristics

2. Highway properties
    a. Pavement surface characteristics (friction development potential)
    b. Shoulder surface characteristics
    c. Edge height and shape
    d. Edge surface characteristics

Based on the driver performance characteristics now being determined, these analyses can be conducted using as broad a spectrum of driver performance as is reasonable. With this combination, continually

Condition 7 4 inch edge, 45 degree edge slope
(Predicted steer angle, 1.1 degrees) (Same as Condition 5)

Condition 8 4 inch edge, 30 degree edge slope
(Predicted steer angle, 0.7 degrees)

Condition 9 4 inch edge, 15 degree edge slope
(Predicted steer angle, 0.5 degrees)

FIGURE 22   Conditions 7, 8, and 9.
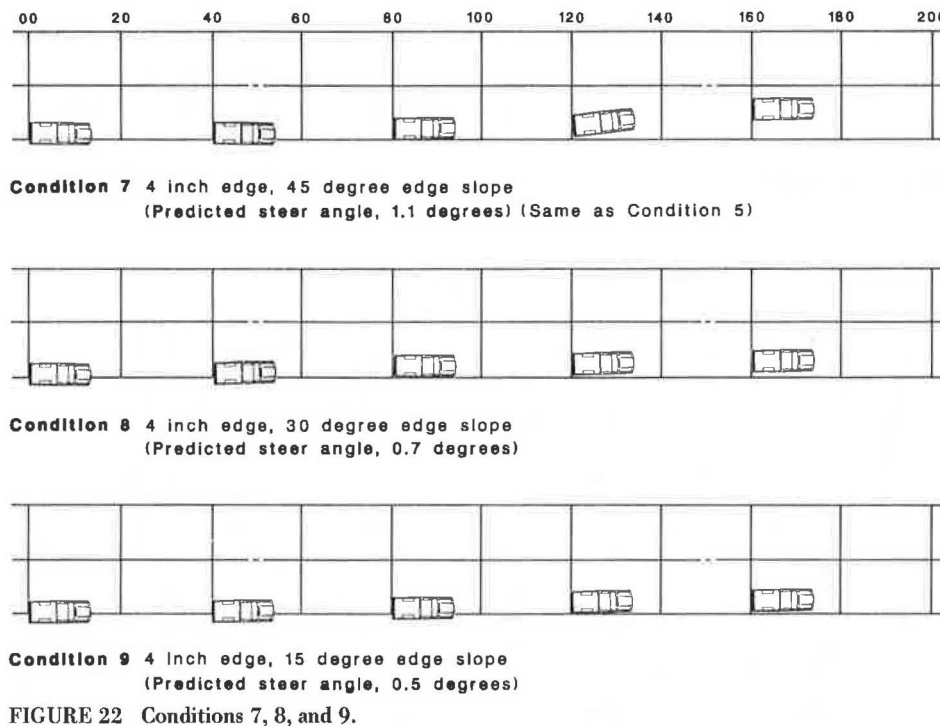
checking for agreement with full-scale testing, the full spectrum of highway conditions can be studied and specific situations may be evaluated.

REFERENCES

1. R.H. Klein, W.A. Johnson, and H.T. Szostak. Influence of Roadway Disturbances on Vehicle Handling. DOT HS-802 210. U.S. Department of Transportation, 1976.
2. E.F. Nordlin et al. The Effect of Longitudinal Edge of Paved Surface Drop-Off on Vehicle Stability. CALTRANS Report CA-DOT-TL-6783-1-76-22. Sacramento, Calif., March 1976.
3. R.L. Stoughton et al. The Effect of a Broken A.C. Pavement Drop-Off Edge and Muddy Shoulder on Vehicle Stability and Controllability. CALTRANS Memorandum Report, Sacramento, Calif., July 1978.
4. R.A. Zimmer and D.L. Ivey. Pavement Edges and Vehicle Stability--A Basis for Maintenance Guidelines. Presented at 61st Annual Meeting of the Transportation Research Board, Washington, D.C., Jan. 1983.
5. D.L. Ivey et al. The Influence of Roadway Surface Discontinuities on Safety. State of the Art Report 1, TRB, National Research Council, Washington, D.C., 1984, 45 pp.
6. J.L. Graham and J.L. Glennon. Work Zone Design Considerations for Truck Operations and Pavement/Shoulder Drop-Offs. Midwest Research Institute, Report 7020-S. Kansas City, Mo., Feb. 1984.
7. R.C. McHenry, D.J. Segal, and N.J. DeLays. Determination of Physical Criteria for Roadside Energy Conversion Systems. Cornell Aeronautical Laboratory, Cornell University, Buffalo, N.Y., July 1967.
8. H. Sakai. Characteristics of Japanese ESV Tires. Japan Automobile Research Institute, Inc. Fifth International Conference on Experimental Safety Vehicles, London, England, 1974.

Development of a Procedure for Correcting Skid-Resistance Measurements to a Standard End-of-Season Value

DAVID A. ANDERSON, WOLFGANG E. MEYER, and JAMES L. ROSENBERGER

ABSTRACT

The wet skid resistance of a pavement can vary significantly from one day to another and from one season to another. A general decay in skid resistance occurs from the spring to the fall with day-to-day perturbations superimposed over the general decay. The seasonal decay and the day-to-day perturbations may individually be as many as 10 to 15 skid numbers. These variations are of concern when skid resistance measurements are made for survey purposes. A general statistical model developed by others was used as a prediction equation to adjust skid measurements made on any given day to an end-of-season value. In the prediction equation, day-to-day variations are accounted for by the recent rainfall history (0 to 7 days) and the air temperature at the time of test. The general decay in skid resistance that occurs over the season is accounted for by the Julian calendar day and the average daily traffic. Adjusted end-of-season values for the data obtained in New York, Pennsylvania, and Virginia were such that 90 percent of the adjusted end-of-season values were within approximately +3.6 to -3.6 skid numbers of the measured end-of-season value. Additional research is needed to develop a fundamental understanding of the mechanisms that cause changes in skid resistance. This is necessary so that a more rational model can be developed to account for the site specificity of the changes in skid resistance that were observed.

The wet skid resistance of a pavement can vary significantly over time. Temporal changes in wet skid resistance occur over the life of a pavement, from one season to another and from one day to another (1). The mechanisms that cause these changes are not well understood; however, there is empirical knowledge of the factors that cause these changes.

The skid resistance of bituminous pavements increases in the first 1 or 2 years as the bitumen at the surface is worn away. After this conditioning period, the skid resistance tends to decrease over the years depending on factors such as traffic, mixture design, aggregate properties, and the environment. In the northern climates of the United States, seasonal changes are superimposed on the long-term skid resistance changes. During the fall and winter seasons skid resistance increases, followed by a loss of skid resistance over the late spring and summer months. Traffic polishes the pavement surface in the summer while alternate freezing and thawing of the aggregate and the use of antiskid materials and studded tires cause roughening of the surface (2).

Superimposed on the seasonal changes of skid resistance are day-to-day changes that have been attributed to short-term weather changes, principally rainfall and temperature. On bituminous surfaces, extended dry periods and periods of increasing temperature tend to decrease skid resistance. A typical sample of a plot of skid resistance versus time for a single season is shown in Figure 1. The short-term variations range as high as 10 to 15 skid numbers with a similar decrease in skid number during a single testing season.

The changes that occur in the skid resistance of portland cement concrete pavements are not as pronounced: there is no appreciable conditioning period during the first few years, and the seasonal and day-to-day variations tend to be smaller. However, the skid resistance of portland cement concrete can change dramatically as the pavement wears through the surface finish, the sand matrix, and into the coarse aggregate.

FHWA requires state agencies to make periodic measurements of skid resistance for inventory purposes. Because skid resistance can vary over a testing season by as many as 10 to 15 skid numbers, it would simplify inventorying procedures if skid numbers obtained on any given day could be corrected to some reference condition, such as the end-of-season minimum skid number. The objective of this study was to develop a procedure for correcting skid numbers made on any arbitrary day to an end-of-season minimum skid number. Because the procedure was designed for pavement management purposes, only those measurements that can be readily obtained in survey tests at 40 mph were included in the procedure. Such a procedure should also be useful for reconstructing the skid resistance on some given day from measurements taken on a later day as, for example, in reconstructing the conditions that existed at the time of a traffic accident.

Two predictor models were used in this study as algorithms for making short- and long-term corrections in measured skid resistance values. These predictor models, referred to as the mechanistic and statistical models, were developed by Henry et al. (3). In order to validate these models and to determine the most practical set of variables for use with the models, a sensitivity analysis was performed with an extensive 1979-1980 data set obtained previously by the Pennsylvania Transportation Institute. Final validation was done with a new data set obtained in New York, Pennsylvania, and Virginia in the summer of 1983. A single model was developed that contains only variables that can be readily measured by a survey crew making skid tests at 40 mph or obtained from highway agency records or weather stations. This

Nittany Engineers and Management Consultants, Inc., 736 Cornwall Road, State College, Pa. 16803.
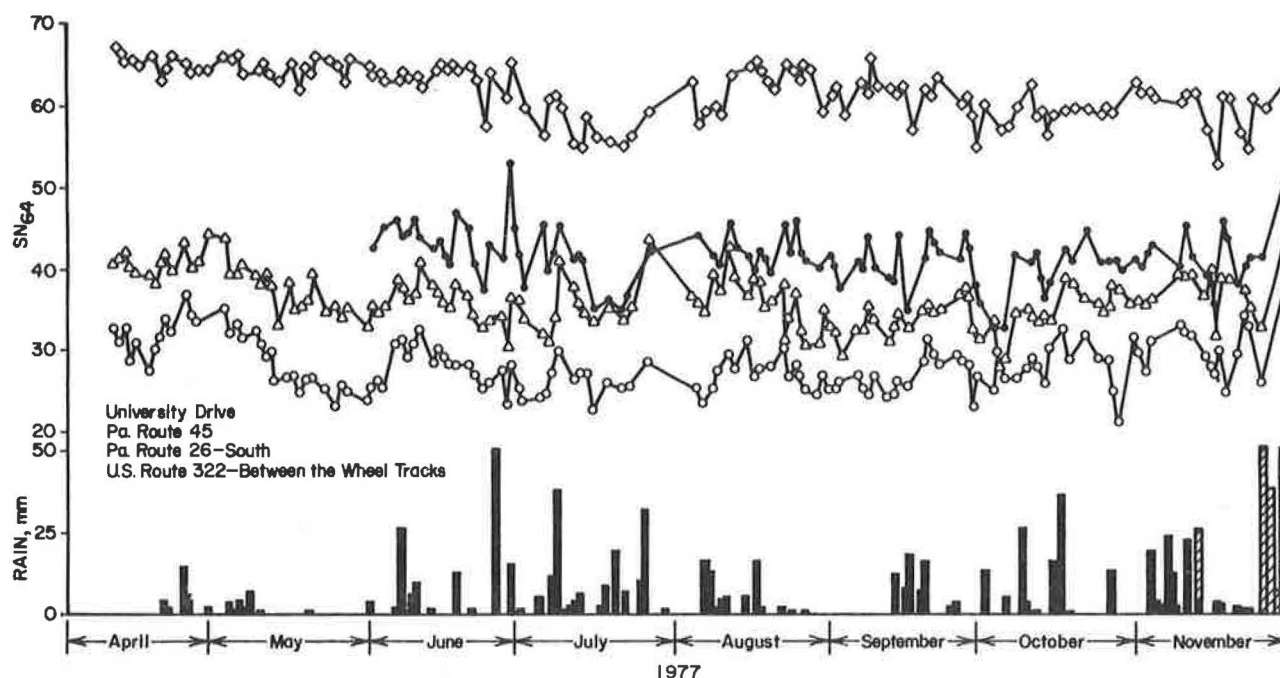
FIGURE 1 Skid number (SN_{64}) and rainfall data for the 1977 test season.

approach obviates the use of variables such as the British Portable Number (BPN) or texture depth measures, which require that traffic be stopped.

SENSITIVITY ANALYSIS USING THE 1979-1980 DATA

Data that had been obtained in Pennsylvania during 1979 and 1980 from 25 asphalt and portland cement concrete pavement sites (3) were used in the preliminary analyses. Two proposed prediction models were considered. The first, referred to as mechanistic model (3), is based on the assumed dependency of skid resistance on microtexture and macrotexture:

$$SN_{64} = SN_0 e^{-0.64PNG} \qquad (1)$$

where

    SN_{64} = skid resistance measured at 64 km/h (40 mph);
    SN_0 = skid number-speed intercept (i.e., skid resistance extrapolated to zero speed);
    PNG = percent normalized skid-resistance gradient, defined as $- 100/SN \cdot [d(SN)/dV]$; and
    SN = skid resistance at any velocity V.

The SN_0 and the PNG terms are highly correlated with microtexture and macrotexture, respectively. Macrotextrue is defined as texture with asperities greater than 0.1 mm, whereas microtexture is defined as texture with asperities of 0.1 mm and smaller. The mechanistic model has been proposed as a predictor of both long- and short-term variations in skid resistance. In this model both SN_0 and PNG may be expressed as a function of time. Because it is a function of macrotexture, PNG can be expected to experience little change over a single testing season. However, in order to determine the end-of-season value for SN_0, it is necessary to have polishing and texture data that would typically have to be obtained from laboratory tests. Therefore, this model

was considered inappropriate for the objectives of this study.

The sensitivity analyses were then focused on the generalized model

$$\ell nSN_{64} = b_0 + b_1DSF + b_2TEMP + b_3T30 + b_4JDAY$$
$$+ b_5AGE + b_6ADT + b_7SN_{64}F + \varepsilon \qquad (2)$$

where

    SN_{64} = a skid-resistance measurement made in accordance with ASTM E274 at 64 km/h (40 mph) using the ASTM Standard Test Tire E501;
    DSF = dry spell factor, $\ell n(t_r+1)$, where t_r is number of days since last daily rainfall of 0.1 in. (2.5 mm) or more, $t_r < 7$ and DSF < 2.08;
    TEMP = average of daily maximum and minimum temperature on the day of test;
    T30 = weighted temperature history defined as

$$1/30 \sum_{i=1}^{30} \left\{ [(29/30)^i T_{j-1}] \right\}$$

where T_{j-i} is the average of the maximum and minimum air temperatures on the Julian calendar day i days before the date of interest (3);

    JDAY = Julian calendar day;
    AGE = age of the pavement surface, years;
    ADT = average daily traffic;
    $SN_{64}F$ = the measured skid number at the end of the season;
    $b_0, \ldots, b_i$ = regression coefficients; and
    ε = random error term associated with regression.

In this model, the dry spell factor (DSF), median daily air temperature (TEMP), and the weighted aver-

age temperature (T30) account for the short-term weather effects, whereas the Julian calendar day (JDAY), pavement age (AGE), and end-of-season skid number ($SN_{64}F$) account for the seasonal effects. Thus the model describes changes in skid resistance that occur day-to-day and throughout the season.

Final end-of-season skid numbers were obtained from the data by plotting the data and observing trends. Linear regression was then used to calculate the coefficients, $b_0, \ldots, b_i$, in Equation 2. The following regression equation was obtained for the asphalt concrete sites that were measured in 1979 and 1980 (3):

$$\ln SN_{64} = 3.12 - 0.0371 \text{ DSF} + 0.0 \text{ TEMP} - 0.0028 \text{ T30} \\ - 0.00047 \text{ JDAY} - 0.0041 \text{ AGE} + 0.0 \text{ ADT} \\ + 0.0244 \text{ } SN_{64}F + \text{error} \qquad (3)$$

Equation 3 was then used to calculate values of the natural logarithm of the skid resistance ($\ln SN_{64}$), and these values were compared with the measured skid resistance values. This was done for each site and day of test in the data set. The differences between observed and predicted values, the residuals, were analyzed statistically for their magnitude and trends.

The significance of each of the terms in Equation 3 can be realized by multiplying the range of each of the variables by their respective model coefficient. This is given in Table 1 where both the absolute range (maximum value-minimum value) and the interquartile range (the range containing 50 percent of the observations) are used. The effect of each of these variables is small, less than four skid numbers, except for the variable $SN_{64}F$, which yields changes of 36 skid numbers. Although, except for $SN_{64}F$, the individual change attributable to any one of the variables is small, in combination, the changes can be significant, as shown in Figure 1.

Typical examples of the residuals for the predicted values of SN_{64} are shown in Figures 2 through 4. The residuals are not randomly distributed about zero but show systematic changes throughout the year. Further, the trend of the residuals over the testing season is not consistent from one year to the next as shown by comparison of Figures 3 and 4 (1979 versus 1980). This implies that the model coefficients are both site and year specific. To test for site-specific trends, a dummy site-specific variable was added to Equation 2, and this variable was shown to be highly significant (3). Quite obviously, from the statistical analyses and Figures 2 through 4, there are site-specific trends in the 1979-1980 data that are not accounted for by the model of Equation 2.

SELECTION OF TEST VARIABLES FOR 1983 TEST SEASON

The analysis of the 1979-1980 data showed that the dry spell factor (DSF), median air temperature on the day of test (TMEAN), 30-day weighted average air temperature (T30), pavement age (AGE), Julian calendar day on the day of test (JCD), and end-of-season skid number ($SN_{64}F$) are all statistically significant variables in the predictor model. Therefore, the 1983 validation testing program was developed to accommodate as wide a range as possible in these variables. Pavement and air temperature at the time of test were included because the skid tester that was used was equipped to collect this information.

Although the average daily traffic variable was not significant in the model with the 1979-1980 data set, engineering judgment dictates that it should be. It was reasoned that it was not significant because the 1979-1980 data did not have a sufficient range in ADT. Therefore, it was decided to retain ADT as a variable and to seek a wider range in ADT for the 1983 validation testing.

During the sensitivity analysis, other temperature variables were tried as a substitute for T30 because of the large amount of data required to calculate T30. The single 5-day average of the maximum and minimum temperature was found to be just as effective as T30, and data were collected to calculate this variable.

Because the preliminary model (Equation 2) did not completely account for temporal site-specific variations in skid resistance, blank tire (ASTM E524) skid resistance measurements were included in the 1983 test program. This decision was based on the hypothesis (4) that a comparison of blank and ribbed skid-resistance measurements would provide insight into the texture of the pavement surface at each site. Ribbed and blank tire measurements were made by testing each of the sites with one tire, changing tires, and then repeating the tests. Combined blank and ribbed tire data would be relatively easy to obtain with a two-wheel skid trailer, whereas site-specific texture measurements would be complex and costly with existing test equipment. It should be noted, however, that the use of the two-wheeled trailer to simultaneously measure blank and ribbed skid numbers was done at the peril of measuring two different pavement populations. Research by others has shown that the skid resistance can be significantly different in the two tire tracks (4). A more acceptable procedure would be to modify existing equipment to allow the blank and ribbed tire to be used in areas on the same tester.

1983 TEST PROGRAM

Skid-resistance testing was conducted in New York, Pennsylvania, and Virginia in the summer of 1983, providing a range of climates and surface types. Because both short-term and long-term variations in skid resistance were to be modeled, data were gathered on a daily basis during four different weeks in each of the three states. Testing was conducted

TABLE 1 Changes in Predicted Skid Resistance Due to Changes in the Independent Variables

Independent Variable	Model Coefficient, b_i	Range R	$\Delta SN_{64}^{\sim}$ Due to Range[a]	Interquartile Range (Q3–Q1)	$\Delta SN_{64}^{\sim}$ Due to Interquartile Range[a]
DSF, days	−.0371	2.08	−2.79	1.26	−1.70
T30, °F	−.0028	24.4	−2.46	10.8	−1.09
TEMP, °F	0	49.5	0	18.0	0
JDAY, day	−.00047	210.0	−3.59	106.0	−1.81
AGE, years	−.0041	11.0	−1.63	4.0	−.58
ADT, vehicles/day	0	3,650.0	0	23.5	0
$SN_{64}F$	.0244	39.2	36.1	18.0	16.1

[a] $\Delta SN_{64}^{\sim}$ is the change in the predicted value of SN_{64} due to a change in the independent variable equal to the range or interquartile range.
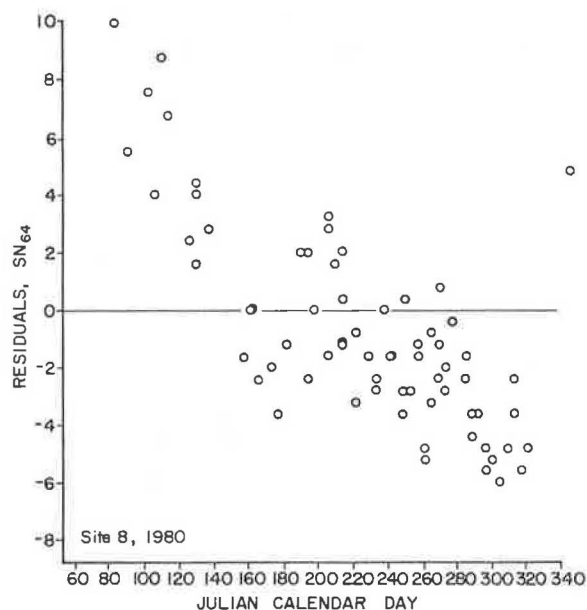
FIGURE 2   Residuals for Pennsylvania Site 8, 1980.
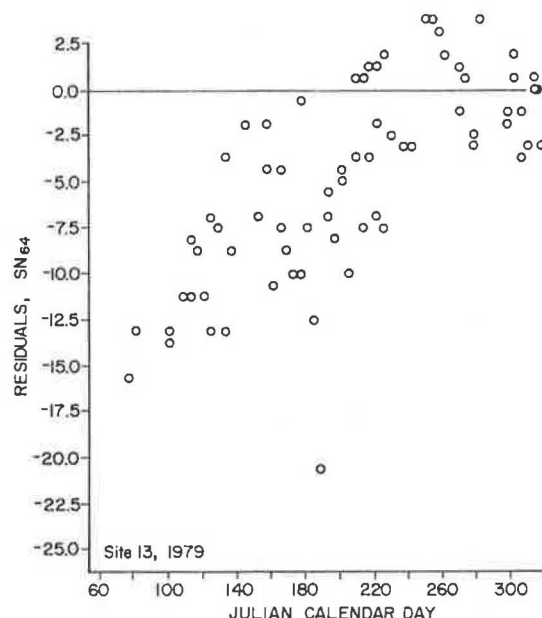
FIGURE 4   Residuals for Pennsylvania Site 13, 1979.
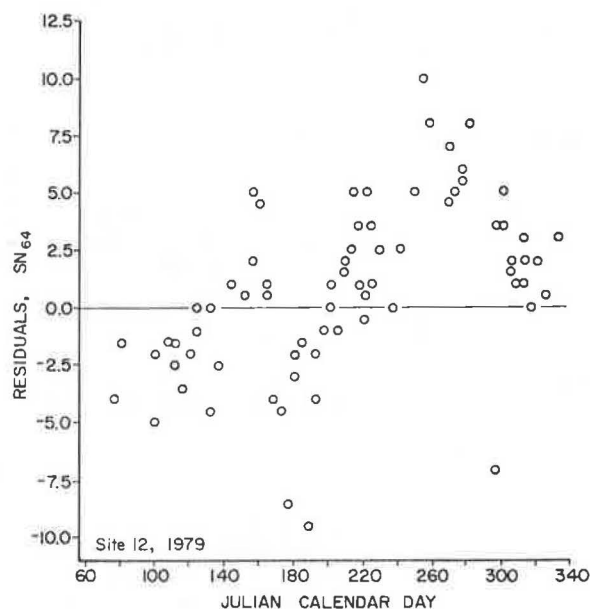
FIGURE 3   Residuals for Pennsylvania Site 12, 1979.

throughout the day on the second, third, and fourth days of the week in order to evaluate within-day variations in skid resistance. Water, pavement, and air temperatures were recorded at the time of each test. Each test consisted of five lock-ups averaged as required by ASTM E274, and measurements were taken with both a ribbed and a blank tire (ASTM Standard Pavement Test Tires E501 and E524, respectively). Summaries of the ribbed tire, skid-resistance measurements for New York, Pennsylvania, and Virginia are given in Tables 2 through 4. Details of the testing program can be found elsewhere (5).

Typical plots of skid resistance versus time are shown in Figure 5 for two Pennsylvania sites. In this figure the skid numbers decrease during the months of June, July, and August but show an increase by September or October. This trend is typical of the data from each state. Average standard deviations for the five lock-ups that constitute a single mea-

surement and the average standard deviations for the multiple measurements taken on any given day are given in Table 5. The standard deviations are approximately two skid numbers with some tendency to decrease during the testing season. Given these standard deviations for testing error, a model should not be expected to predict skid numbers with an accuracy better than plus or minus 2 to 3 skid numbers.

The short-term weather corrections are too small to account individually for the typical variations measured in the field (Figure 1). The authors believe that much of the "noise" in the data is due to measurement error as well as to transverse and longitudinal variations in skid resistance on the surface of the pavement. Average within-run (among the five lockups) standard deviation for SN_{64} is 1.7, whereas the within-day standard deviation among repeat runs is only 2.0 skid numbers (Table 5). These values are of the same order of magnitude as the adjustments as a result of temperature and rainfall.

In order to develop a prediction model, it was necessary to estimate the end-of-season minimum skid number. This was done in three different ways: by examining the trend of the plot of skid resistance plotted versus Julian calendar day for each site, by averaging the skid numbers obtained on the first week of testing, and by using a statistical model that assumes an exponential decay in skid resistance from spring to fall (3). The first technique was unsatisfactory because the noise in the data made it difficult to estimate trends over the season. The nonlinear statistical mode

$$SN_{64}\tilde{F} = \ell SN_{64}e^{-(JDAY-300)/t} \qquad (4)$$

where

$SN_{64}\tilde{F}$ = predicted skid resistance on day 300;
  SN_{64} = skid resistance measured on any arbitrary day, JDAY; and
    t = regression coefficient.

did not provide reliable estimates because the seasonal changes in skid resistance often varied sinusoidally or linearly rather than exponentially with time.

The end-of-season skid numbers that were used in

TABLE 2 Mean Skid Numbers (SN_{64}) and Standard Deviation for Each Week of Testing in New York in 1983—Ribbed Tire (E501)

Site No.	New York								
	June 13–17		July 11–15		Aug. 29–Sept. 2		Oct. 17–21		
	$\overline{X}$	s	$\overline{X}$	s	$\overline{X}$	s	$\overline{X}$	s	$SN_{64}F$
1	43	3.3							40
2	42	4.1							40
3	45	0.9	41	1.5	42	1.7	40	4.0	39
4	40	1.5	37	1.6	39	1.3	38	3.9	43
5	35	1.1	36	0.9	35	1.2	32	2.5	28
6	27	1.6	24	3.3	27	1.2	28	3.3	27
7	34	1.4	32	1.5	30	1.1	29	3.7	26
8	48	2.1	46	1.6	47	1.5	42	4.2	40
9	37	1.6	36	1.3	35	1.0	31	2.8	29
10	28	1.4	29	3.2	26	1.3	24	2.5	25
11	34	1.1	35	3.1	31	1.7	30	4.5	33
12	48	1.5	45	2.3	46	1.0	38	2.4	25
13	23	1.1	22	1.0					42
14	50	3.2	48	1.3	47	1.4	42	2.9	33
15	40	1.5	39	1.0	39	1.4	34	2.4	27
16	35	3.4	35	1.1	34	1.2	31	2.9	27
17	43	2.8	42	1.4	43	1.4	38	2.8	27
18	48	2.8	47	1.0	48	2.6	40	2.9	28
19	40	0.9	40	1.4	40	2.4	34	2.3	33
20	30	1.3	31	4.0	30	1.4	28	3.1	26
Avg		1.9		1.8		1.5		3.2	

Note: N = number of tests, each test consisting of five lockups; $\overline{X}$ = mean of the tests for given week; s = standard deviation of tests for given week; and $SN_{64}F$ = arithmetic average of the skid-resistance measurements for last week of testing; corrected for short-term weather changes before being averaged.

TABLE 3 Mean Skid Numbers (SN_{64}) and Standard Deviation for Each Week of Testing in Pennsylvania in 1983—Ribbed Tire (E501)

Site No.	Pennsylvania								
	May 24-28		June 21-25		Sept. 6-10		Oct. 10-14		
	$\overline{X}$	s	$\overline{X}$	s	$\overline{X}$	s	$\overline{X}$	s	$SN_{64}F$
1	30	1.5	27	1.7	24	3.4	23	1.2	23
2	47	2.2	47	1.3	37	4.8	41	3.0	40
3	44	3.2	43	0.8	39	1.4	39	2.1	38
4	27	2.3	27	1.6	22	0.7	25	1.6	24
5	43	5.5	45	2.3	38	1.2	40	1.6	38
6	34	0.8	34	1.9	28	1.5	34	2.1	33
7	30	0.9	29	1.4	24	0.8	28	2.4	27
8	36	1.3	35	1.0	32	1.0	33	1.9	33
9	33	0.6	33	1.9	31	2.1	32	1.4	32
10	47	2.6	49	2.1	46	1.5	46	2.5	45
11	32	1.3	30	1.4	27	1.4	31	3.4	29
12	36	1.1	34	2.0	32	1.1	32	1.6	31
13	37	3.0	37	1.0	36	0.8	35	4.4	34
14	34	1.9	35	3.5	31	0.7	32	3.9	31
15	40	2.9	39	2.3	36	0.9	37	2.1	36
16	37	1.1	37	1.4	35	0.9	34	1.3	33
17	44	1.7	43	2.2	40	1.8	39	1.9	37
18	44	1.6	43	1.6	40	1.3	39	1.3	37
19	51	2.2	49	1.6	47	1.7	45	2.5	45
20	30	1.0	29	1.2	27	2.8	27	1.2	26
21	27	2.0	26	1.6	22	1.7	24	2.1	24
22	53	1.4	52	3.6	46	2.1	47	1.7	46
23	45	1.4	42	1.9	38	1.4	37	2.3	35
Avg		1.9		1.8		1.6		2.2	

Note: N = number of tests, each test consisting of five lockups; $\overline{X}$ = mean of the tests for given week; s = standard deviation of tests for given week; and $SN_{64}F$ = arithmetic average of th skid-resistance measurements for last week of testing; corrected for short-term weather changes before being averaged.

TABLE 4 Mean Skid Numbers (SN_{64}) and Standard Deviation for Each Week of Testing in Virginia in 1983—Ribbed Tire (E501)

Site No.	Virginia								
	May 9-14		June 27–July 2		Sept. 12-16		Oct. 24-28		
	$\overline{X}$	s	$\overline{X}$	s	$\overline{X}$	s	$\overline{X}$	s	$SN_{64}F$
1	59	1.9	56	1.9	52	1.2	51	3.1	50
2	57	5.3	55	1.3	52	1.4	51	3.4	50
3	43	1.1	41	0.8	39	1.8	36	2.1	35
4	42	1.5	39	1.3	38	2.1	35	3.0	35
5	44	1.3	41	1.6	40	1.4	38	2.1	37
6	47	2.5	41	1.2	40	1.6	37	2.8	35
7	47	2.1	43	1.1	40	1.0	36	2.6	32
8	43	1.9			36	1.5	33	2.1	32
9	42	2.7	37	1.5	37	1.9	34	3.0	33
10	49	2.5	44	1.6	43	1.8	40	2.7	39
11	42	1.4	41	0.7	39	2.0	37	2.8	35
12	46	2.0	46	1.3	43	2.6	42	2.4	40
13	38	1.4	35	1.7	35	1.9	34	2.0	33
14	45	1.0	36	2.4	37	2.6	37	2.4	36
15	43	1.8	40	1.0	37	2.6	35	2.2	34
16	40	1.8	35	0.8	33	1.9	32	3.1	31
17	49	1.5	45	1.1	42	1.7	39	2.8	38
18	49	1.1	45	0.8	44	2.0	40	2.6	39
19	42	1.6	40	0.6	37	2.6	34	2.8	33
20	42	1.4			33	3.1	34	2.7	33
21	49	4.5	4.5	1.0	43	1.8	39	2.9	38
Avg.		2.0		1.2		1.9		2.6	

Note: N = number of tests, each test consiting of five lockups; $\overline{X}$ = mean of the tests for given week; s = standard deviation of tests for given week; $SN_{64}F$ = arithmetic average of the skid-resistance measurements for last week of testing; corrected for short-term weather changes before being averaged.

the development of the model were estimated from the blank skid-resistance measurements collected during the last week of testing. These measurements were first adjusted for short-term changes to a set of reference conditions and then averaged. The adjustments were made with the following regression equation (5):

$$SN_{64} = \exp[\ell SN_{64} - b_1(DSF-DSF_0) + b_2(AIRT-AIRT_0)] + b_3(TMEAN5-TMEAN5_0) \tag{5}$$

where the subscript 0 refers to the reference conditions

AIRT = air temperature at time of test, and
TMEAN5 = average of median temperature for the 5 days before the day of test and standard conditions are as follows:
DSF_0 = 2.08, and
$AIRT_0$ = $TMEAN5_0$ = 68 F (20 C).

The coefficients for Equation 5 were calculated on a site-specific basis using the following equation:

$$\ell nSN_{64} = b_{0j} + b_1 DSF + b_2 AIRT + b_3 TMEAN5 + b_4 ADT + b_5JDAY + e \tag{6}$$

were b_{0j} indicates the jth site.

Rainfall data were obtained from the nearest weather station and from rain gages installed at selected test sites. All rainfall data were corrected to a 24-hr observation period ending at 8:00 a.m. Temperature data were also obtained from local weather stations and from measurements taken at the time of test. Traffic data were obtained from the respective state departments of transportation and from spot traffic counts by the skid-testing crew. Traffic on the test sites ranged from less than 100 vehicles per day to nearly 20,000 vehicles per day.

REFINEMENT OF THE MODEL

The 1983 skid-resistance data were examined critically for normality before any statistical work was done to refine the prediction model. No serious exceptions were found except for the presence of several obvious outliers that were removed from the data base. A full discussion of the extensive statistical analyses that were conducted with the data is given elsewhere (5).

Three measures of air temperature were considered for use in the final model: the air temperature mea-
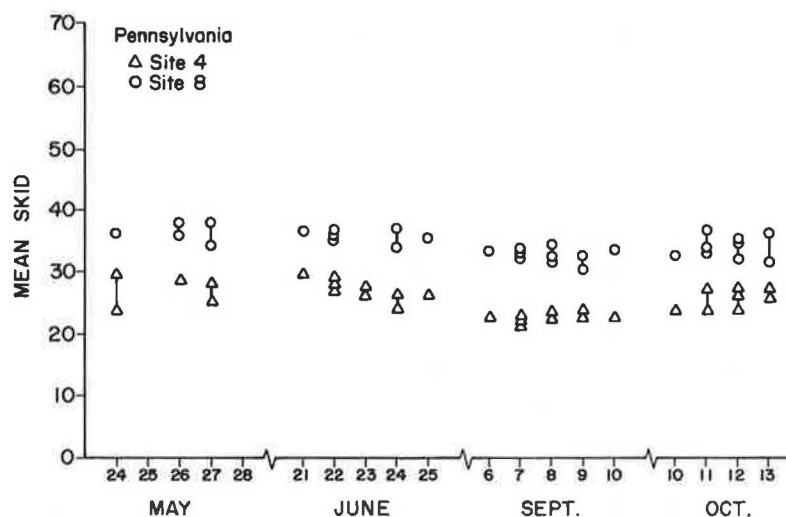
FIGURE 5   Mean SN_{64} versus calendar day of 1983 for Pennsylvania Sites 4 and 8.

TABLE 5   Standard Deviation of SN_{64} for Ribbed Tire (E501) on Bituminous Concrete

State	Week	Between-Run Standard Deviation	Within-Run Standard Deviation
New York	6	2.3	2.1
	10	2.0	1.9
	17	1.4	1.7
	24	3.4	1.6
Avg		2.3	1.8
Pennsylvania	3	2.4	2.6
	7	1.9	2.4
	18	1.6	1.9
	23	1.5	1.6
Avg		1.9	2.1
Virginia	2	2.4	2.0
	8	1.3	1.9
	19	2.0	1.6
	25	2.3	1.4
Avg		2.0	1.7

sured on the tester at the time of test (AIRT), the 5-day arithmetic average of the daily mid-range temperatures as recorded at the weather station nearest the site (TMEAN5), and an exponentially weighted 30-day average temperature (T30), also calculated from weather station data. The three temperature variables were highly correlated, and it was found that any one of the variables gave equally good prediction of $SN_{64}F$. Therefore, the air temperature at the time of test (AIRT) was chosen as the preferred variable because it is simple to measure and it does not require the acquisition of data from outside the user agency.

Julian calendar day crossed with average daily traffic was also considered a variable because it represents the cumulative traffic during the season. This variable was statistically significant but not to the extent that its inclusion in the model is warranted (R^2 increased from 0.862 to 0.864). More accurate ADT data, that is, actual counts taken during the season, and the development of techniques to properly account for the relative effects of automobile and truck traffic may make this a more significant variable.

The average daily traffic (ADT), Julian calendar day (JCD), dry spell factor (DSF), and air temperature (AIRT) at the time of test were found statistically significant and were retained in the final form of the model

$$\ln SN_{64} = b_0 + b_1 SN_{64}F + b_2 ADT + b_3 JDAY + b_4 DSF + b_5 AIRT + error \qquad (7)$$

Site-specific changes in seasonal skid resistance had been observed in the 1979-1980 data, and similar trends were found in the 1983 data. Texture classifications, obtained visually at the time the sites were selected, and blank-ribbed tire data were used in various ways as variables in an attempt to explain site specificity (5). No further improvement in the correlation was obtained and therefore no further use of these data was made. However, it is believed that future research should include blank-ribbed tire measurements to further define site specificity. Alternate treatment of the data and more careful measurements might provide more worthwhile correlations. For example, the blank and ribbed tire measurements in this project were separated by 2 to 4 hr rather than being taken simultaneously. Also, the measurements with the two tires should be taken in the same wheel track, and care must be taken to obtain them at the same location.

PREDICTION PROCEDURE FOR END-OF-SEASON SKID NUMBER

The average skid numbers corrected for short-term weather effects from the last week of testing using the procedure described previously were used as the end-of-season minimum skid numbers for each site. These values were then used as predictors in the generalized model of Equation 7, which was fit separately for bituminous and portland cement concrete pavements. The estimated coefficients using the data from the three states (New York, Pennsylvania, and Virginia) are given in Table 6, along with the standard errors of estimate.

Calculation of the predicted end-of-season skid number, $SN_{64}\tilde{F}$, is accomplished by inverting Equation 7 such that $SN_{64}\tilde{F}$ is a function of measured SN_{64} and the other independent variables, ADT, JDAY, DSF, and AIRT

$$SN_{64}\tilde{F} = (\ln SN_{64} - b_0 - b_2 ADT - b_3 JDAY - b_4 DSF - b_5 AIRT)/b_1 \qquad (8)$$

In order for a highway agency to calculate adjusted end-of-season skid numbers, it would be first necessary to determine the regression coefficients in Equation 8. This would be done by selecting a set

TABLE 6 Estimated Coefficients of the Prediction Model for Individual States and All States Combined

Variable	Site-Specific Model Coefficients, $b_j \pm s(b_j)$[a]			Combined
	New York	Pennsylvania	Virginia	
Bituminous Concrete				
Observations	461	832	623	1,916
Intercept	$2.82 \pm .0838$	$2.71 \pm .0276$	$2.95 \pm .0401$	$2.71 \pm .022$
$SN_{64}F$	$.0353 \pm .00097$	$.0338 \pm .00044$	$.0295 \pm .00097$	$.0346 \pm .000385$
$ADT/1,000$[b]	$.0115 \pm .0116$	$.0130 \pm .0131$	$.0275 \pm .0039$	$.0395 \pm .00419$
JDAY	$-.00139 \pm .000176$	$-.000918 \pm .000053$	$-.00118 \pm .000042$	$-.0011 \pm .00004$
DSF	$-.027 \pm .00679$	$-.0358 \pm .00371$	$-.0176 \pm .00345$	$-.026 \pm .0023$
AIRT	$-.00044 \pm .00053$	$-.000727 \pm .000235$	$-.000799 \pm .000238$	$-.00035 \pm .00017$
Portland Cement Concrete				
Observations	199	231	150	580
Intercept	$3.55 \pm .124$	$2.87 \pm .0417$	$3.22 \pm .228$	$2.84 \pm .032$
$SN_{64}F$	$.023 \pm .00108$	$.0273 \pm .000616$	$.0204 \pm .00434$	$.0275 \pm .00037$
$ADT/1,000$[b]	$-.300 \pm .0604$	$-.121 \pm .0418$	$-.0176 \pm .0398$	$.0435 \pm .0052$
JDAY	$-.00149 \pm .000198$	$-.00069 \pm .0000688$	$-.000894 \pm .000076$	$-.00088 \pm .000058$
DSF	$-.00587 \pm .000904$	$-.0194 \pm .00407$	$-.00637 \pm .00602$	$-.0052 \pm .0035$
AIRT	$-.0019 \pm .000587$	$-.000707 \pm .000305$	$-.00077 \pm .000416$	$-.00052 \pm .00025$

Note: Model: $\ell nSN_{64} = b_0 + b_1 SN_{64}F + b_2 ADT/1,000 + b_3 JDAY + b_4 DSF + b_5 AIRT + \epsilon$.

[a] $b_j \pm s(b_j)$, where b_j is state-specific coefficient of variables in model and s is the standard deviation of associated coefficient.

[b] $ADT/1,000$ is used so that coefficient values are not intractably small.

of 12 to 16 pavement test sites with varying levels of traffic. Portland cement and bituminous pavements should be considered separately. Initially it may also be advantageous to consider different aggregate types separately, depending on the range in properties of the aggregates used in the state. Skid data would then be obtained at least four times throughout the testing season for each of the test sites. The coefficients in Equation 8 would then be determined by regressing the data with Equation 7. The coefficients should be verified in subsequent years to confirm that they do not vary excessively from year-to-year. Until a better understanding of the mechanisms that cause changes in skid resistance are understood, it will be necessary to determine the coefficients on a state or regional basis. Specific details regarding the use of this predictive technique are given in ASTM Test Method format in an associated report (6).

Assessment of the accuracy of the predicted final skid number, $SN_{64}F$, was made by using Equation 8 to predict an end-of-season skid number from each measurement made during the first full 3 weeks of testing in New York, Pennsylvania, and Virginia. A summary of the deviations of the predicted final skid number from the observed values is given in Table 7.

TABLE 7 Summary of Residuals Using State-Specific and Combined Regression Coefficients

State	N	s	Residuals[a] for Given Percentiles			
			5th	25th	75th	95th
Bituminous Concrete						
New York	461	2.53	-3.60	-1.53	1.24	4.69
Pennsylvania	832	2.19	-2.84	-1.46	1.16	3.58
Virginia	623	2.03	-3.30	-1.18	1.14	3.72
Three states combined	1,916	2.34	-3.51	-1.50	1.34	3.88
Portland Cement Concrete						
New York	199	3.00	-4.64	-1.78	1.76	4.66
Pennsylvania	231	1.82	-2.67	-1.19	.98	2.98
Virginia	150	1.51	-3.45	-1.28	1.24	3.71
Three states combined	580	2.30	-3.75	-1.33	1.27	3.54

Note: Number of observations and s = standard deviation of observation.

[a] A residual is the difference between the measured values and the predicted value.

According to the table, 90 percent of the predicted values are within -3.51 and $+3.88$ skid numbers of the measured values for the bituminous sites and within -3.75 and $+3.54$ skid numbers for the portland cement concrete sites. This is considered very good given that the standard deviation of the measurements is two skid numbers.

To illustrate the magnitude of the changes in SN_{64} afforded by the variables ADT, JDAY, DSF, and AIRT, Equation 7 was raised to the exponent e

$$SN_{64} = \exp(b_0 + b_1 SN_{64}F + b_2 ADT + b_3 JDAY + b_4 DSF + b_5 AIRT) \qquad (9)$$

The following reference values were inserted into Equation 9: ADT = 5,000 vehicles/day; JDAY = 200; DSF = 0; and AIRT = 68°F. Changes in skid number were then calculated by varying each of the variables, ADT, JDAY, DSF, and AIRT independently, creating Figures 6 through 9, respectively. A separate set of calculations was done for four levels of $SN_{64}F$, generating a separate curve for each set of calculations. The results of the calculations, which are presented in Figures 6 through 9, show that JDAY and $SN_{64}F$ are the most significant factors causing changes in skid resistance; air temperature has little effect, and the dry spell factor and average daily traffic have only minimal effect.

The use of paired skid measurements taken on two different days was considered an alternative method for predicting the end-of-season skid number, $SN_{64}F$. It was reasoned that this might bypass the problem of the site specificity of the model coefficients. To determine whether this was the case, 10 pairs of observations were randomly chosen from the first and third weeks of testing in New York. A simple linear extrapolation of the skid numbers was performed to day 300. Differences between the predicted end-of-season skid number and the measured end-of-season average were calculated for 10 pairs of measurements and 17 sites. The differences between the actual and predicted end-of-season skid number for each individual site were large and were inconsistent from site-to-site. This led to the conclusion that this approach is not promising and, consequently, was not pursued further.
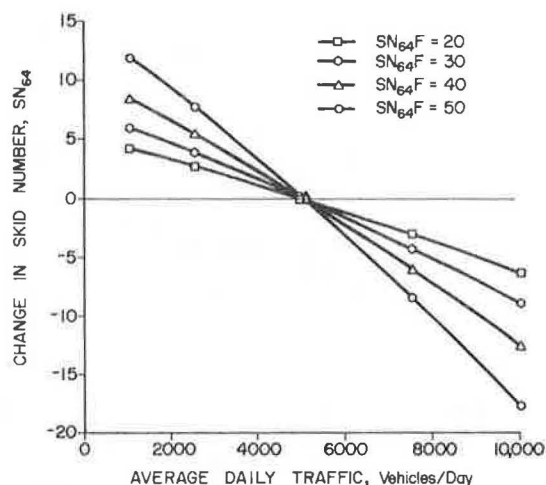
FIGURE 6   Corrections in SN_{64} due to change in ADT.

FIGURE 8   Corrections in SN_{64} due to changes in DSF.

FIGURE 7   Corrections in SN_{64} due to changes in JDAY.
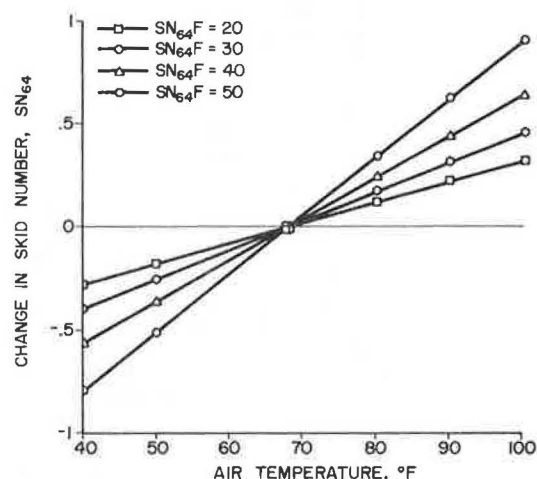
FIGURE 9   Corrections in SN_{64} due to changes in AIRT.

SUMMARY AND CONCLUSIONS

A procedure has been presented that can be used to predict the end-of-season skid number from a single measurement made at any time during the season. The procedure is empirical in that it is based on a prediction equation developed through the regression analysis of data obtained from field test sites. Variables included in the prediction equation are the dry spell factor, air temperature at the time of test, Julian calendar day, average daily traffic, and the skid number measured on any arbitrary day within the test season. The dry spell factor is based on the number of days since the last rainfall.

The end-of-season skid number was not predicted reliably with the exponential seasonal variation model. The skid resistance increases earlier in the season than accounted for by the exponential model.

In the prediction model, short-term (day-to-day) adjustments in skid number are accounted for by the dry spell factor and air temperature, whereas long-term adjustments (within season) are accounted for by Julian calendar day and average daily traffic. Only variables that can be readily obtained were included in the procedure so that it can be implemented by a typical highway agency.

Using the data obtained in this study, the pro-

cedure was used to adjust measurements made on any given day to the end-of-season values. As a result, 90 percent of the adjusted values were within approximately +3.6 to -3.6 skid numbers of the actual end-of-season value. This is considered very good given that the standard deviation of the skid numbers obtained from five consecutive lockups of the test tire on the same test site averaged 1.7 skid numbers and the standard deviation for multiple tests within a given day averaged 2.0 skid numbers.

The coefficients in the prediction equation were site-specific and varied from season-to-season. Blank and ribbed tire data and subjective descriptors of the site did not account for the site specificity. Additional research is needed to adequately understand the mechanisms that cause day-to-day and within-season variations in skid resistance so that more rational predictive models can be developed.

manager, R.R. Hegmon, is gratefully acknowledged. The interpretation of the findings and the conclusions are those of the authors and do not necessarily have the endorsement of the Federal Highway Administration.

NOMENCLATURE

ADT	Average daily traffic, vehicles/ day/test lane,
AGE	Age of pavement surface, years.
AIRT	Air temperature at time of test, °F.
$b_0 \ldots b_i$	Regression coefficients.
DSF	Dry spell factor, $\ln(t_r+1)$, where t_r is number of days since last rainfall of 0.1 in. or more, and DSF $\leq$ 2.08 $t_r \leq$ 7.
e	Base of the natural logarithm.
JDAY	Julian calendar date.
PNG	Percent normalized skid-resistance gradient defined as $-100/SN \cdot [d(SN)/dV]$, where SN is the skid resistance at any velocity V.
Q1, Q3	First and third quartile, respectively.
R	Correlation coefficient or range in observations (maximum-minimum).
s	Standard deviation.
SN_0	Skid number extrapolated to zero speed.
SN_{64}	A skid-resistance measurement made in accordance with ASTM E274.
$SN_{64}F$	Average of skid-resistance measurements for last week of testing, first corrected for short-term weather changes before being averaged.
$SN_{64}\tilde{F}$	End-of-season skid resistance estimated from a predictor model.
t_r	Number of days since last rainfall, $t_r \leq$ 7.
TEMP	Average of maximum and minimum temperatures on the day of test.
TMEAN5	Average of the daily mid-range

temperatures for the 5 days before day of test.

T30   Weighted temperature history, °F defined as

$$1/30 \sum_{i=1}^{30} \left\{ [(29/30)^i T_{j-1}] \right\}, \text{ where}$$

T_{j-i} is the average of the maximum and minimum air temperatures on the Julian calendar date i days before the date of interest.

REFERENCES

1. R.R. Hegmon. Seasonal Variations in Pavement Skid-Resistance--Are These Real? Public Roads, Vol. 42, No. 2, Sept. 1978, pp. 55-62.
2. J.M. Rice. Seasonal Variations in Pavement Skid Resistance. Public Roads, Vol. 41, No. 4, March 1977, pp. 160-166.
3. J.J. Henry, K. Saito, and R. Blackburn. Predictor Model for Seasonal Variations in Skid Resistance. Final Report FHWA/RD-83/005. FHWA, U.S. Department of Transportation, 1983.
4. S.H. Dahir, J.J. Henry, and W.E. Meyer. Seasonal Skid Resistance Variations. Final Report FHWA-PA-80-75-10. Pennsylvania Department of Transportation, Harrisburg, Aug. 1979.
5. D.A. Anderson, W.E. Meyer, and J.L. Rosenberger. Data Collection Procedure for Use with Skid Resistance Measurements. FHWA Report FHWA/RD-84/109. Vol. 1, FHWA, U.S. Department of Transportation, 1984.
6. J.J. Henry and K. Saito. Skid Resistance Measurements with Blank and Ribbed Test Tires and Their Relationship to Pavement Texture. Presented at 64th Annual Meeting of the Transportation Research Board, Washington, D.C. 1984.

International Roughness Index: Relationship to Other Measures of Roughness and Riding Quality

WILLIAM D. O. PATERSON

ABSTRACT

Different measures of road roughness with varying degrees of reproducibility and repeatability have been applied by various agencies in the world, but the exchange of roughness information has been hampered by a lack of an acceptable reference and a quantitative basis for relating the different measures. Presented in this paper is such a basis developed from an analysis of data from the International Road Roughness Experiment (IRRE) and other sources. The International Roughness Index (IRI), developed from the IRRE as a suitable calibration standard for all response-type and profilometric instruments, is the transferable reference scale. It is the metric equivalent of a reference inches/mile index. Two-way conversion relationships and confidence intervals are presented for the Quarter-car Index (QI), British Bump Integrator trailer index (BI), and various profile numerics of the French Analyseur de Profil en Long (APL) (longitudial profile analyzer) profilometer from the IRRE, and for the Serviceability Index from other sources. The characteristics of each scale, and the sources of variation and range of application of the conversions are discussed.

Road roughness is a major determinant of riding quality and the economic benefits from maintenance (1), and is thus an extremely important measure in the road condition inventory of a highway network. The quantification of the benefits and the prediction of roughness trends in the future under any given maintenance policy, however, are dependent on the ability to relate the measure of roughness to the measures used in major empirical studies that have been conducted in various countries.

Three primary scales have been used in the major studies of road deterioration and road user costs, which form the basis of economic models at present (1,2). In the studies in Kenya, the Caribbean, and India, roughness was referenced to the Bump Integrator trailer (BI) of the Transport and Road Research Laboratory (TRRL) (United Kingdom) in units of mm/km. In the Brazil study, roughness was referenced to the Quarter-car Index (QI), a profile-based scale in units of counts/km, often abbreviated simply to units of QI (2-4). In addition, in North America, riding comfort and vehicle cost data have been related to the Serviceability Index of pavement condition originating at the AASHO Road Test (5).

In road condition surveys worldwide, many more different roughness measures are being used. Most come from response-type measuring systems mounted in a passenger car or on a trailer and measuring the relative axle-body displacement of the rear axle in units such as mm/km, inches/mile, counts/unit length, and so forth, including, for example, the Bump Integrator, Mays ride integrator, Mays ride meter, Cox meter, National Association of Australian State Road Authorities (NAASRA) meter, BPR Roughometer, and other variations. In many francophone countries, dynamic profilometry systems such as the Analyseur de Profil en Long (APL) trailer of the Laboratoire Central des Ponts et Chaussées (LCPC), France, and the Viagraphe have been used. The extent to which all

these systems have been calibrated and controlled to be reproducible and repeatable over time has varied considerably. Although some local standards have been developed, there has been difficulty in relating the roughness measures to one of the three primary scales mentioned previously, and the profile numerics developed for the French profilometry systems are unique to those systems.

To provide a common quantitative basis with which to reference these different measures of roughness, both for the purposes of instrument calibration and for comparison of results, the World Bank initiated the International Road Roughness Experiment (IRRE) (6) held in Brazil in 1982. The IRRE included 10 different methods and the involvement of and sponsorship by organizations from Brazil, the United States, the United Kingdom, France, Belgium, and Australia. This experiment resulted in the establishment of the international Roughness Index (IRI), an independent profile-related index appropriate as a reference scale for all profilometric and response-type systems (6), and the issuance of guidelines on the calibration and measurement of roughness (7).

The IRI mathematically summarizes the longitudinal surface profile of the road in a wheeltrack, representing the vibrations induced in a typical passenger car by road roughness. It is defined by the reference average rectified slope ($RARS_{80}$, the ratio of the accumulated suspension motion to the distance traveled) of a standard quarter-car simulation for a traveling speed of 80 km/h. It is computed from surface elevation data collected by either topographical survey or mechanical profilometer. The computational method and mathematical equations are described by Sayers et al. (7) with further background provided by Sayers, Gillespie, and Queiroz (6). The index is expressed in units of m/km IRI and is the metric equivalent of the reference inches/mile statistic from an earlier NCHRP study (8).

In this paper, the data from the IRRE and other sources are used to develop a basis for relating the major roughness scales to one another in order to

facilitate the use of previous and current research findings and road inventory data. The ultimate result is a chart and series of equations that can be used for converting between any two scales, with the IRI scale serving as the reference.

ROUGHNESS MEASURES

Roughness is the variation in elevation of a road surface that typically has a complex profile comprising a spectrum of different wavelengths and amplitudes. The spectrum tends to vary with the type of surface. For example, asphalt-paved surfaces have little short wavelength roughness, whereas surface treatment, gravel, and earth surfaces have a mixture of short, medium, and long wavelengths (earth surfaces in particular can have high concentrations of short wavelengths and large amplitudes).

The measures of roughness fall into three categories as follows [elaborated on with respect to accuracy by Sayers et al. (7)]:

1. A profile numeric defined directly by mathematical function from the absolute profile of road surface elevations in one or two wheelpaths (when the profile is measured dynamically, some loss of accuracy usually occurs);

2. Summary numerics measured through response-type systems calibrated to a profile or other numeric by correlation (usually the cumulative axle-body relative displacement averaged over a given distance and expressed as a slope); and

3. Subjective ratings of riding quality or pavement serviceability, usually made by a panel of raters within a scale defined by subjective descriptors.

Differences arise between roughness measures due partly to the way the measuring instrument responds to the road profile and partly to the way the data are processed. In the case of profile numerics, the numeric represents either some measure of the displacement amplitude relative to a moving average amplitude (in which case the result varies with the baselength chosen), or else it represents the response of a standard vehicle through a mathematical model of the way a vehicle responds to roughness (in which case the result varies with the mathematical definition and the simulated speed of travel).

In the case of response-type systems, the differences arise primarily through the frequency response

TABLE 1 Summary Descriptions of Some Major Road Roughness Measures

Measures	Symbol	Units	Description
International roughness index	IRI	m/km IRI	Reference index summarizing the road profile by a mathematical model representing the response of a traversing vehicle (6). Computed from elevation data in a wheelpath (7) for use as a profile numeric for profilometric methods and a calibration standard for response-type instruments. Defined by reference average rectified slope ($RARS_{80}$) of axle-body displacement of quarter-car simulation with fixed-vehicle constants and a simulated speed of 80 km/h (6,7). Scales from 0 (perfect) upward to about 20 (poor unpaved road).
Referenced Response Measures			
Quarter-car index	QI QI_m QI_r	Counts/km QI	A profile-related measure developed for Brazil Road Costs Study and since applied elsewhere (3,4). Originally defined by a quarter-car simulation of vehicle response at 55 mph on wheelpath profile elevations measured by (GMR) surface dynamics profilometer and used as a calibration standard for response-type systems. No longer exactly reproducible except as redefined. Subscripted by m (QI_m) represents the calibrated Mays meter estimate of QI used as a basis for all Brazil road costs study data (2), or by r (QI_r) represents profile index redefined in terms of root mean squared vertical acceleration (RMSVA) of 1 and 2.5 m baselengths of elevation data by correlation (4).
Bump integrator trailer (TRRL)	BI BI_r	mm/km	Single wheel trailer (based on BPR roughometer) standardized by TRRL, towed at 32 km/h and measuring axle-body displacement by unidirectional frictional clutch sensor. Used in road costs studies of Kenya, Caribbean, and India and in several developing countries. Usual application is vehicle-mounted sensor calibrated to one of several standard trailer units. Responses of trailer units have possibly varied over time; a profile index (BI_r) based on root mean squared deviation of elevations on a 1.8-m baselength and 300 mm sample interval ($RMSD_{300, 1.8}$) was recently defined by correlation to one trailer unit (6). Scales from low positive value upward to about 16,000 (poor unpaved road).
Inches per mile (reference quarter-car simulation)	IM_r (RQCS)	in./mile	A calibration reference used for response-type systems by some North American agencies, identical in definition to the IRI scale but expressed in units of inches/mile (note: 63.36 inches/mile = 1 m/km). Roughness expressed in these units usually represents response-type system measures, which may not have been calibrated to this reference. Scale from 0 (perfect for reference) upward.
Profile Numerics for Dynamic Profilometers			
Waveband energy (APL72)	W_{sw} W_{mw} W_{lw}	(L^2) (L^2) (L^2)	Numerics developed by LCPC for the APL profilometer traveling at a speed of 72 km/h, defining the mean-square energy values of short (1 to 3,3 m), medium (3.3 to 13 m), and long (13 to 40 m) wavelength bands, computed by squaring and integrating the filtered signal value over a section length of 200 m for a speed of 72 km/h (6). Scales from 0 (perfect) upward. Sometimes presented in combination as a rating index, I, from 1 (worst) to 10 (best) by unit increments.
Coefficient of planarity (APL72)	$CP_{2.5}$	0.01 mm	Profile numeric developed by Center for Road Research (CRR) Belgium for the APL profilometer towed at 72 km/h, defined by an analysis of the deviation of the profile from a moving average reference line (6). Computed for standard baselengths of 2.5, 10, and 40 m for every 100 m (expressed in the subscript); the IRRE indicated that $CP_{2.5}$ correlated most highly with IRI and most response measures. Scales from 0 (perfect) upwards.
Coefficient APL_{25}	$CAPL_{25}$	(L)	Profile numeric developed by LCPC for the APL profilometer towed at 21.6 km/h, computed as the average absolute value of the profile signal over section lengths of 25 m (6). Scales from 0 (perfect) upward.
Relating to Subjective Rating			
Serviceability index	SI	PSI	Mathematical function representing subjective panel rating of pavement serviceability; that is, ride quality and the need for maintenance, defined at the AASHO Road Test in terms of slope variance of the surface profile, mean rut depth, and areas of cracking and patching by statistical correlation. Difficult to reproduce, usually redefined by a local panel rating. Scales from 5.0 (excellent condition) to 0 (worst).

characteristics of each system. A vehicle typically has two resonant frequencies: one at 1 to 2 Hz for resonance of the body on the suspension, and the other at 8 to 12 Hz for the resonance of the wheel-axle system between the stiff springs of the tires and the suspension. The amplitude of road roughness in these ranges is exaggerated by the vehicle. Thus for certain combinations of roughness wavelength and vehicle speed, the amplitude is exaggerated and at others it is attenuated. Hence, two response-type systems operating at different speeds, or two systems with differing resonance characteristics, will tend to exaggerate or "see" different aspects of roughness on a given road and give different results.

The eight measures of road roughness considered in this paper cover the three categories previously defined and are described in detail in Table 1. For further discussion of these measures, see Sayers et al. (6). The measures include

1. IRI, the International Roughness Index, in m/km IRI;

2. IM_r, the inches/mile equivalent of IRI used in North America and sometimes called reference quarter-car simulation (RQCS), or Golden car;

3. QI_m, the Quarter-car Index of the Brazil road costs study as measured by calibrated Mays meters, in counts/km;

4. BI_r, the response of the TRRL Bump Integrator trailer used during the IRRE, in mm/km;

5. W_{sw}, the short-wavelength energy numeric defined by LCPC for the APL profilometers;

6. $CP_{2.5}$, the coefficient of planarity on a 2.5-m-baselength defined by the Belgian Centre des Recherches Routières (CRR), in 0.01 mm;

7. $CAPL_{25}$, the coefficient of the APL25 profilometer analysis defined by LCPC; and

8. SI, the present serviceability index usually defined by regional panel ratings to be similar to the SI defined at the AASHO Road Test, in PSI (present serviceability index).

Comparable data for individual response-type systems not calibrated to one of the foregoing measures were not available. Although the Australian NAASRA meter was tested at the IRRE, the mounting vehicle differed from the Australian standard vehicle so the data cannot be used to develop a valid conversion.

RELATIONSHIPS AMONG PHYSICAL ROUGHNESS MEASURES

International Experiment Data

The IRRE was conducted in Brazil on a series of 49 road sections each 320 m long (6). The sections consisted of asphalt concrete, surface treatment, gravel, and earth surfaces in nearly equal amounts. The roughness on each section was measured by rod and level surveying, TRRL 3-m-beam profilometer, APL profilometer trailer (at both 72 and 21.6 km/h), and various response-type systems, including a TRRL Bump Integrator trailer, three Chevrolet sedans mounted with Mays meter sensors (an adaptation of the Mays ride meter), and a sedan mounted with a Bump Integrator and NAASRA meter sensors in parallel. Each instrument was used according to the standard procedure specified for it under the control of the relevant agency.

The range of values and bivariate linear correlations between different measures observed at the IRRE are given in Table 2 for the scales just described, with the exception of the Serviceability Index, which was not measured in the experiment. The observed data for the same scales are given in Table

TABLE 2 Bivariate Linear Correlation Coefficients and Ranges for Major Roughness Scales, as Observed at the International Road Roughness Experiment

Roughness Index[a]	IRI	QI_m	BI_r	$CP_{2.5}$	W_{sw}	W_{mw}	$CAPL_{25}$
IRI	1.000						
QI_m	0.962	1.000					
BI_r	0.973	0.933	1.000				
$CP_{2.5}$	0.958	0.923	0.927	1.000			
W_{sw}	0.937	0.921	0.893	0.942	1.000		
W_{mw}	0.768	0.629	0.702	0.692	0.686	1.000	
$CAPL_{25}$	0.719	0.705	0.644	0.744	0.732	0.851	1.000
No. observations	49	49	49	45	45	45	49
Mean	6.03	77.8	4,724	84.2	21.5	67.0	12.5
Standard deviation	3.30	43.7	3,141	36.6	11.4	51.4	5.0
Minimum	1.90	19.2	1,310	28.0	3.0	7.8	4.6
Maximum	16.6	211.5	16,485	169.0	37.2	181.9	21.7

Note: Further details of the definition of each index given by Sayers et al. (6).
Source: Derived from data of the IRRE from Sayers, Gillespie, and Queiroz (1986).

[a]   IRI = International Roughness Index, m/km IRI.
      QI_m = Quarter-car Index of Brazil Road Costs Study, counts/km.
      BI_r = Bump Integrator trailer of Transport and Road Research Laboratory, mm/km.
      $CP_{2.5}$ = Coefficient of planarity on 2.5 m baselength for French APL72 profilometer, 0.01 mm.
      W_{sw} = Energy index of short wavelengths (1 to 3.3 m) for French APL72 profilometer.
      W_{mw} = Energy index of medium wavelengths (3.3 to 13 m) for French APL72 profilometer.
  $CAPL_{25}$ = Rectified displacement coefficient from French APL25 profilometer.

3, including the reference inches per mile statistic (IM_r), which was computed simply by the dimensional conversion from m/km as 63.36 IRI.

The IRI data were computed as the $RARS_{80}$ statistic from rod and level survey data following the method outlined by Sayers et al. (7).

The QI_m data represent the Mays meter values calibrated to the Quarter-car Index scale by a methodology similar to that used in the original Brazil road costs study (3), so that they would closely represent the empirical foundation of all the vehicle operating cost and road deterioration relationships derived from that study. Separate calibration equations were established for each vehicle from the QI_r profile index computed from rod and level data using only data from asphalt concrete surfaces (4,9) as follows:

$$\hat{QI}_r = 12.155 \ MM_1 \equiv QI_{m1}$$

$$\hat{QI}_r = 10.565 \ MM_2 \equiv QI_{m2}$$

$$\hat{QI}_r = 11.034 \ MM_3 \equiv QI_{m3}$$

where

$\hat{QI}_r$ = least-squares regression estimate of QI_r profile index from calibration of MM_i against QI_r, in counts/km QI;

QI_{m1} to QI_{m3} = calibrated roughness measure for Mays meter vehicle numbers 1 to 3, in counts/km QI; and

MM_1 to MM_3 = three-run average Mays meter count per unit distance for vehicle numbers 1 to 3, in m/km.

Then

$$QI_m = mean \ (QI_{m1}, \ QI_{m2}, \ QI_{m3}).$$

Although the original study used QI instead of QI_r as the calibration standard, it has been shown (2) that the calibration equations were not significantly

TABLE 3 Roughness Data by Various Measures in the International Road Roughness Experiment

Surface	SEC	IRI	IM_r	BI	QI_m	QI_r	$CP_{2.5}$	$CAPL_{25}$	W_{sw}	W_{mw}
Asphalt concrete	CA01	4.1	260	1,970	54	47	56	17.7	9.4	122.2
	CA02	4.6	291	2,340	55	61	65	15.0	12.0	80.4
	CA03	6.3	399	3,690	75	84	91	17.2	29.1	119.3
	CA04	5.3	336	3,280	66	75	80	16.7	21.2	141.5
	CA05	6.2	393	4,220	78	87	90	18.0	30.6	159.6
	CA06	7.3	463	5,025	96	95	108	19.0	29.7	78.9
	CA07	2.5	158	1,785	33	29	49	7.0	6.3	28.5
	CA08	2.6	165	1,775	34	27	42	7.0	6.8	17.4
	CA09	3.5	222	2,420	51	37	60	11.0	10.7	33.1
	CA10	3.3	209	2,235	45	36	62	11.0	16.5	45.5
	CA11	5.4	342	3,545	72	71	69	16.0	17.8	136.3
	CA12	1.9	120	1,310	19	17	28	5.0	3.3	11.2
	CA13	1.9	120	1,325	22	17	28	5.5	3.0	10.5
Surface treatment	TS01	4.3	272	3,335	77	46	70	7.5	19.2	18.4
	TS02	5.1	323	4,060	59	57	73	9.5	18.4	39.8
	TS03	4.7	298	4,245	75	54	80	10.4	22.8	27.4
	TS04	5.5	348	4,010	101	59	89	19.4	25.8	25.0
	TS05	5.7	361	4,685	124	60	94	9.0	29.4	20.8
	TS06	3.3	209	2,485	37	35	50	8.2	8.8	27.3
	TS07	3.3	209	2,555	38	38	51	8.4	9.2	39.0
	TS08	4.0	253	3,045	46	46	50	10.9	11.6	61.5
	TS09	3.9	247	3,150	43	42	60	7.8	14.9	18.0
	TS10	3.8	241	3,335	44	42	61	7.2	16.0	20.7
	TS11	2.5	158	2,210	28	26	36	4.6	6.3	13.6
	TS12	2.5	158	2,315	27	25	40	5.2	4.6	7.8
Gravel	GR01	3.7	234	2,315	36	42	58	5.8	13.3	17.4
	GR02	3.8	241	2,485	38	42	58	7.0	12.9	14.2
	GR03	7.2	456	5,320	90	93	103	17.0	33.4	94.6
	GR04	6.4	406	4,565	77	83	113	14.6	36.0	109.9
	GR05	9.2	583	6,985	133	115	169	20.0	37.2	104.1
	GR06	8.3	526	7,010	117	103	153	20.2	37.2	117.8
	GR07	5.5	348	3,970	80	67	89	7.7	30.6	42.4
	GR08	4.4	279	2,910	54	51	75	7.1	15.3	16.9
	GR09	9.2	583	6,060	105	110	139	16.9	37.2	98.6
	GR10	7.1	450	4,655	94	84	134	13.2	37.2	94.6
	GR11	14.1	893	10,890	187	194	–	13.4	–	–
	GR12	12.7	805	10,385	180	193	–	18.0	–	–
Earth	TE01	4.3	272	3,400	53	50	71	11.4	17.5	51.7
	TE02	4.1	260	3,270	51	48	72	10.7	17.7	35.4
	TE03	7.2	456	6,350	90	90	125	14.5	34.8	93.7
	TE04	7.3	463	7,065	94	89	128	18.6	33.7	181.9
	TE05	13.9	881	13,350	164	187	–	16.8	–	–
	TE06	16.6	1,052	16,485	211	221	–	21.7	–	–
	TE07	4.4	279	3,745	65	54	83	9.5	22.9	43.8
	TE08	5.0	317	3,905	67	58	86	9.0	22.9	30.4
	TE09	8.6	545	6,390	94	109	129	14.7	35.0	107.2
	TE10	10.2	646	9,300	121	138	156	17.3	37.2	155.1
	TE11	9.6	608	8,455	111	134	158	16.8	37.2	155.0
	TE12	9.0	570	7,860	99	140	108	18.1	37.1	148.0

Note: Refer to Table 1 for definition and units of roughness measurement.
Source: Derived from data given by Sayers et al. (6).

affected. A significnt difference does exist, however, between QI_r and QI_m because of the non-zero intercept in the definition of the QI_r profit statistic (as will be seen in Table 4). Hence it was important to use QI_m instead of QI_r in this correlation exercise.

The BI_r data represent the roughness measured by the Bump Integrator trailer at 32 km/h, which were three-run averages of both wheelpaths. These data represent the output of the trailer as it was at the IRRE, under controlled operating conditions, and were considered by TRRL to be representative of its performance in previous studies.

The $CP_{2.5}$, W_{sw}, W_{mw}, and $CAPL_{25}$ numerics for the APL profilometer were the section-mean values (across both wheelpaths) of the values reported at the IRRE [(6), Appendix G].

It can be seen that the data cover a wide range, from very smooth (1.9 m/km IRI) to very rough (16.6 m/km IRI) roads. Further comment on the correlations will be made later.

Analysis

The objective of the analysis was to develop practical conversion relationships among the various mea-

sures. Typically, when two variables are imperfectly correlated, either both are measured with error or the two represent different measures. In this situation, linear regressions of the one variable on the other, and the other on the one are normally not interchangeable because the least-squared deviations differ in the two senses. For this analysis, a conversion relationship was obtained by making linear least-squares estimates of coefficients in both senses between each pair of variables and averaging as follows:

$$y_i = a + bx_i + u_i \tag{1}$$

$$x_i = c + dy_i + v_i \tag{2}$$

The conversion equation should be such that

$$Y = p + qX \text{ and } X = (Y - p)/q \tag{3}$$

take

$$\hat{p} = (a - c/d)/2 \tag{4}$$

$$\hat{q} = (b + 1/d)/2 \tag{5}$$

where

x_i, y_i = the ith pair of values of roughness measures x and y, respectively;

u_i, v_i = residual errors of y and x, respectively;

a, b, c, d = coefficients estimated by linear regression;

p, q = coefficients adopted for conversion equation; and

X, Y = conversion equation estimates of x y, respectively, given the other.

The goodness of fit of Equation 3 as a conversion relationship was quantified by regressing the observed values of y_i on the predicted values Y_i without intercept.

The resulting conversion relationships are given in Table 4. The root mean squared error (RMSE) of the conversion prediction and the estimated bias are given for each. The bias in each case is very small, typically less than 2 percent, and negligible.

A selection of the conversion relationships is plotted with the observed data in Figures 1 and 2. One observation is given per test section, and the surfacing types are distinguished by symbols. Figure 1 shows the relationships between the Brazil QI_m scale, the TRRL BI scale, and the IRI scale, which were pertinent to the major road costs studies. Figure 2 shows the relationships of three numerics of the APL profilometer to the IRI.

Discussion of Relationships

Very high correlations exist between the IRI scale and both the QI_m and BI measures used in the major empirical studies, so that interchange between either of the historical measures and IRI can be made with reasonable confidence. This is shown in Figures 1a and 1c. The standard error for estimating IRI roughness was 0.92 and 0.76 m/km IRI from QI_m and BI measures, respectively. From the plots it can be seen that this error is reasonably uniform over the range of roughness and across all four surface types.

A feature to note in the QI_m data is that two of the measurements on surface treatment pavements are high values that appear as outliers in both Figures 1a and 1b. The high values result not from a shortcoming of the QI scale but from resonance of the wheel-axle system in the specific vehicles used for the Mays meters; this occurred on two sections that had minor surface corrugations at about 2 m spacing. Neither profile statistic, IRI, or $CP_{2.5}$, was unduly affected by the corrugations, which reflects the good damping characteristics incorporated in each one. The Bump Integrator trailer, traveling at the slower speed of 32 km/h compared with the 80 km/h speed of the Mays meter vehicle, was not affected either, as shown in Figure 1c.

The BI trailer tends to be more sensitive to earth roads than passenger cars (or IRI or QI_m) because of the particular characteristics of its suspension system. The system has a resonant frequency that corresponds to a wavelength of about

TABLE 4   Summary of Relationships and Statistics for Conversions Between Roughness Scales

Conversion Relationship	Standard Error	Coefficient of Variation	Bias Slope	Units
E[IRI] = $QI_m/13$	0.919	15.4	0.989	m/km
= $(QI_r + 10)/14$	0.442	7.34	0.975	m/km
= $0.0032\ BI^{0.89}$	0.764	12.7	1.008	m/km
= $CP_{2.5}/16$	0.654	12.4	0.993	m/km
$\cong 5.5\ \log_e (5.0/PSI)$	–	–	–	m/km
= $0.80\ RARS_{50}$	0.478	–	1.002	m/km
= $0.78\ W_{sw}^{0.63}$	0.693		0.994	m/km
= $CAPL_{25}/3.0$ if asphalt				
= $CAPL_{25}/2.2$ if not asphalt	1.050		1.030	m/km
E[QI_m] = 13 IRI	12.0	15.3	0.993	Counts/km
= $9.5 + 0.90\ QI_r$	14.5	18.7	0.985	Counts/km
= {BI/55 if not earth, BI/73 if earth}	11.7	15.0	1.002	Counts/km
= $0.81\ CP_{2.5}$	11.7	17.2	0.986	Counts/km
$\cong 72\ \log_e (5.0/PSI)$	–	–	–	Counts/km
= $7.9\ W_{sw}^{0.70}$	8.78		0.996	Counts/km
= $6.2\ CAPL_{25}$	18.29		1.13	Counts/km
E[QI_r] = $-10 + 14$ IRI	6.32	8.35	1.024	Counts/km
$\cong BI/62$	14.0	18.3	1.006	Counts/km
= $-10 + 0.89\ CP_{2.5}$	13.1	20.3	0.980	Counts/km
E[BI] = $630\ IRI^{1.12}$	694	14.7	0.998	mm/km
= $36\ QI_m^{1.12}$	1100	22.8	0.985	mm/km
= {55 QI_m if not earth, 73 QI_m if earth}	673	14.2	0.976	mm/km
= $62\ QI_r$	850	18.1	0.971	mm/km
E[$CP_{2.5}$] = 16 IRI	10.5	12.4	0.994	0.01 mm
= $11 + 1.12\ QI_r$	14.8	17.6	0.995	0.01 mm
= $1.23\ QI_m$	14.4	17.2	0.986	0.01 mm
= $11.7\ W_{sw}^{0.65}$ (if $CP_{2.5} < 150$)	8.87		1.018	0.01 mm

Note: Roughness scale codes:
  BI = TRRL Bump Integrator trailer at 32 km/h (mm/km).
  $CAPL_{25}$ = APL profilometer coefficient for 21.6 km/h operation.
  $CP_{2.5}$ = APL profilometer coefficient of planarity (.01 mm).
  IRI = International Roughness Index (m/km) [denotes $RARS_{80}$ (7)].
  QI_m = RTRRMS-estimate of QI roughness in Brazil study (counts/km).
  QI_r = Profile RMSVA-function of QI roughness (counts/km).
  $RARS_{50}$ = ARS response of reference roughness simulation at 50 km/h (7).
  W_{sw} = Short wavelength (1 to 3.3 m) energy index W of APL72 profilometer as defined by French LCPC [(6), Appendix G].
Source: Computer analysis of data from the International Road Roughness Experiment (6).
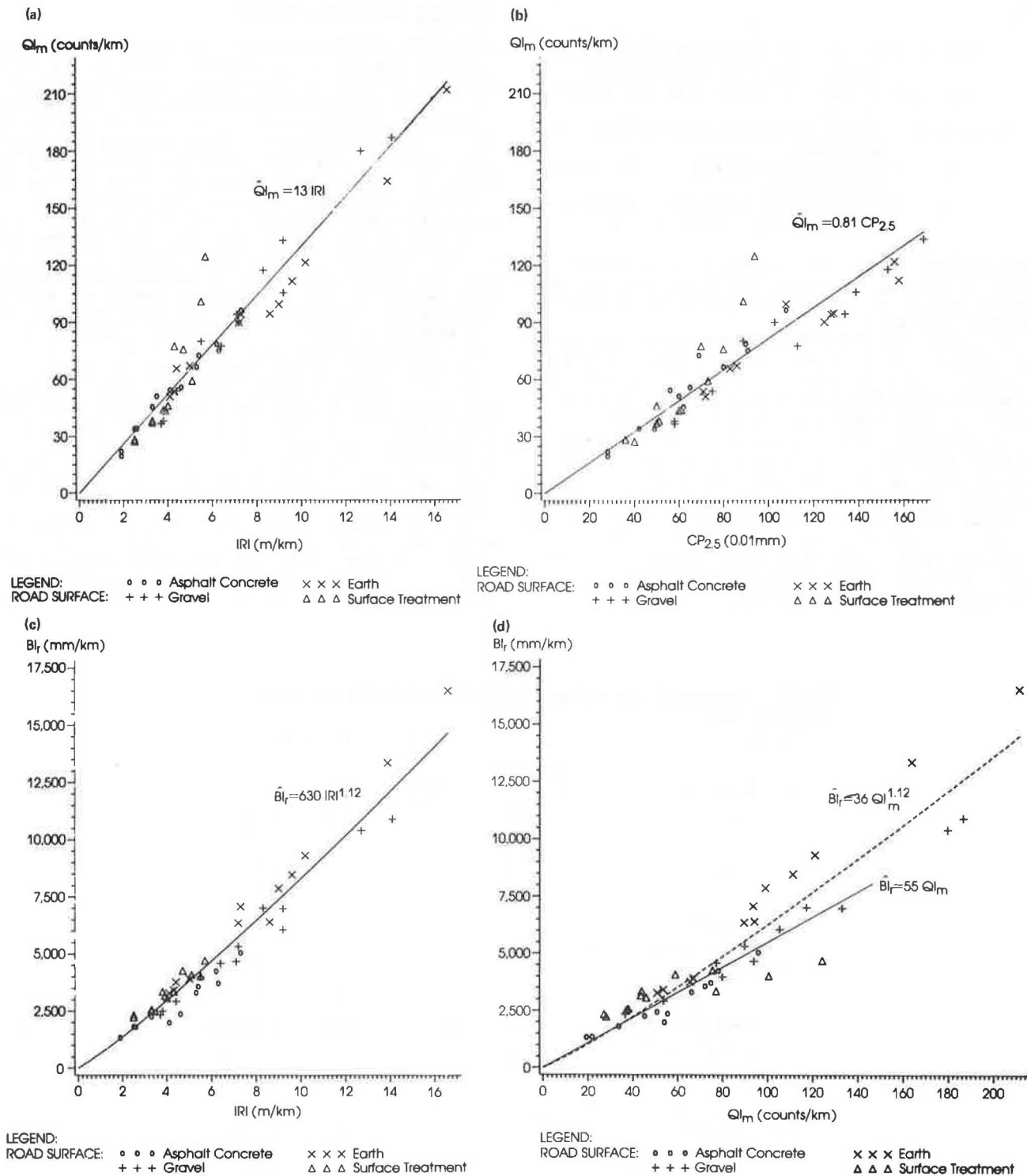
FIGURE 1 Relationships for conversion between QI_m (Brazil road costs study), BI (TRRL Bump Integrator trailer), and $CP_{2.5}$ (French/Belgian APL profilometer) scales of road roughness: (a) Brazil calibrated Mays meter, QI_m, and profile roughness, IRI; (b) Brazil calibrated Mays meter, QI_m, and APL72 profilometer coefficient, $CP_{2.5}$; (c) TRRL Bump Integrator trailer at 32 km/h and profile roughness, IRI; and (d) TRRL Bump Integrator trailer at 32 km/h and Brazil calibrated Mays meter, QI_m.

0.76 m, and the shock absorbers are loosely damped with gain levels 50 to 100 percent greater than typical passenger cars at the resonance frequencies. Thus, the BI trailer responds to the strong short wavelength content in earth surfaces with an exaggerated response, which results in the nonlinearity evident in Figures 1c and 1d for earth surfaces.

This also implies that high roughness measurements coming from the BI trailer probably overstate the response of a typical passenger car (even when traveling at a comparably slow speed), so that the nonlinearity is important when interpreting vehicle operating cost relationships that are related to BI trailer roughness.
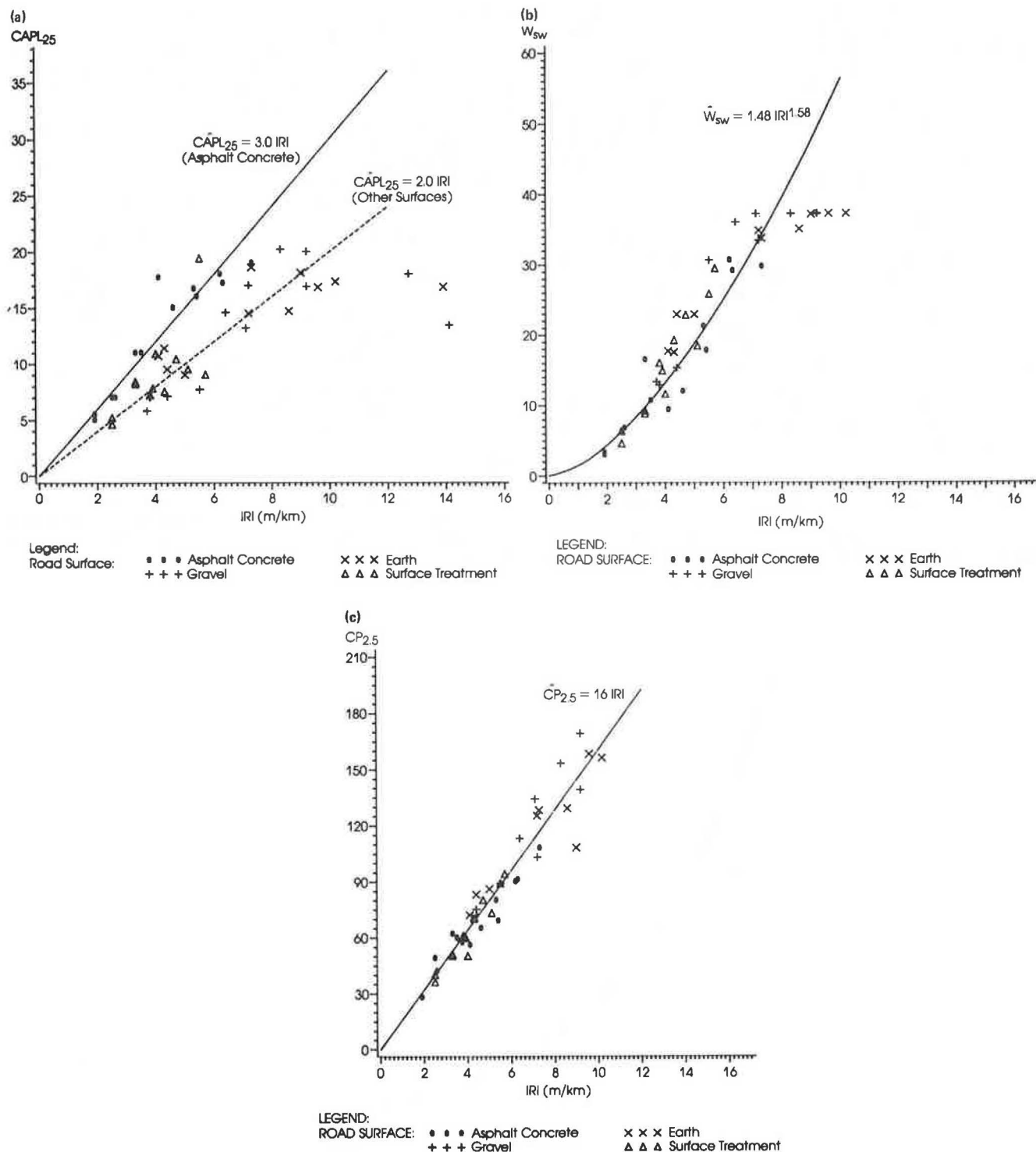
FIGURE 2   Relationships of various roughness coefficients of the French APL profilometer systems APL72 and APL25 to the International Roughness Index: (a) APL25 profilometer coefficient, $CAPL_{25}$, and profile roughness, IRI; (b) APL72 profilometer short wavelength energy, W_{sw}, and profile roughness, IRI; and (c) APL72 profilometer coefficient, $CP_{2.5}$, and profile roughness, IRI.

On surfaces other than earth, the relationship between the BI and QI_m scales is virtually linear as shown by the solid line in Figure 1d. The relationship given as

$$BI \ (mm/km) = 55 \ QI_m \ (counts/km) \qquad (6)$$

was derived in a separate analysis (9). Other studies have indicated that the value of the ratio (55)

can rise to 75 or higher when the BI trailer suspension system is not adequately maintained. Note that when the measurement error is proportional to the square root of the mean value [which is valid here, see Paterson (2)], and no intercept is expected because the measures are essentially similar (i.e., p = 0 in Equation 3), it can be shown that q in Equation 3 is estimated by

$$\hat{q} = \textstyle\sum y_i / \sum x_i = \bar{y}/\bar{x} \qquad (7)$$

where $\bar{x}$, $\bar{y}$ are the mean values of x, y, respectively. This result is particularly useful because it means that a linear conversion under the foregoing conditions can be derived simply from the ratio of the mean values of each scale.

Of the various profile numerics developed for the APL profilometer, the two that correlate the most highly with vehicle response, and in particular the IRI roughness scale, are the $CP_{2.5}$ and short wavelength energy (W_{sw}) indices shown in Figure 2 and Table 2. The APL25 coefficient ($CAPL_{25}$) has a generally poor correlation with IRI and other response-type measures because it is sensitive mostly to long (7 to 15 m) rather than short wavelengths, and the correlation is thus best on asphalt concrete surfaces (see Figure 2a and Table 4). All the APL statistics, except $CP_{2.5}$, tend to reach signal saturation as can be seen from Figures 2a and 2b. For example, the W_{sw} index for the APL25 is not applicable to roughness levels above 8 m/km IRI. In order to avoid mechanical damage, the APL profilometer was not operated on roads with roughness greater than 11 m/km IRI during the IRRE; that is, unpaved roads with moderately high roughness.

RELATIONSHIP OF SERVICEABILITY INDEX TO ROUGHNESS

Roughness defined by a slope variance statistic was included as one component of the Serviceability In-

dex function estimated from panel ratings of pavement serviceability at the AASHO Road Test. Some attempts have since been made to relate roughness to serviceability by calibration of the vehicles to slope variance and application of the original SI function given in the AASHO Road Test (5). However, it has been more common for agencies to relate roughness directly to new local panel ratings of serviceability (PSR). Ratings, however, tend to vary considerably with the expectation of the users and their previous exposure to very high roughness levels, so that the ratings typically vary from country to country. SI was not defined for unpaved roads.

Relationships between PSR and the QI_m and IRI roughness scales are given in Figure 3. These were derived from four panel rating sources: Brazil and Texas [(3), Working Document 10], South Africa (10), and Pennsylvania (11). For the first three, PSR was related directly to the QI profile numeric; in Texas, the panel rating was an estimate derived from a waveband correlation with profile data derived in Texas that was applied to Brazilian road profile data. For the Pennsylvania relationship, an approximate conversion of 1 count/km QI_m = 6.6 in./mi was applied to the roughness data.

Considerable variations exist in the Serviceability Index scales derived from the different sources: the Texas, Pennsylvania, and South Africa ratings represent users who are used to high-standard paved
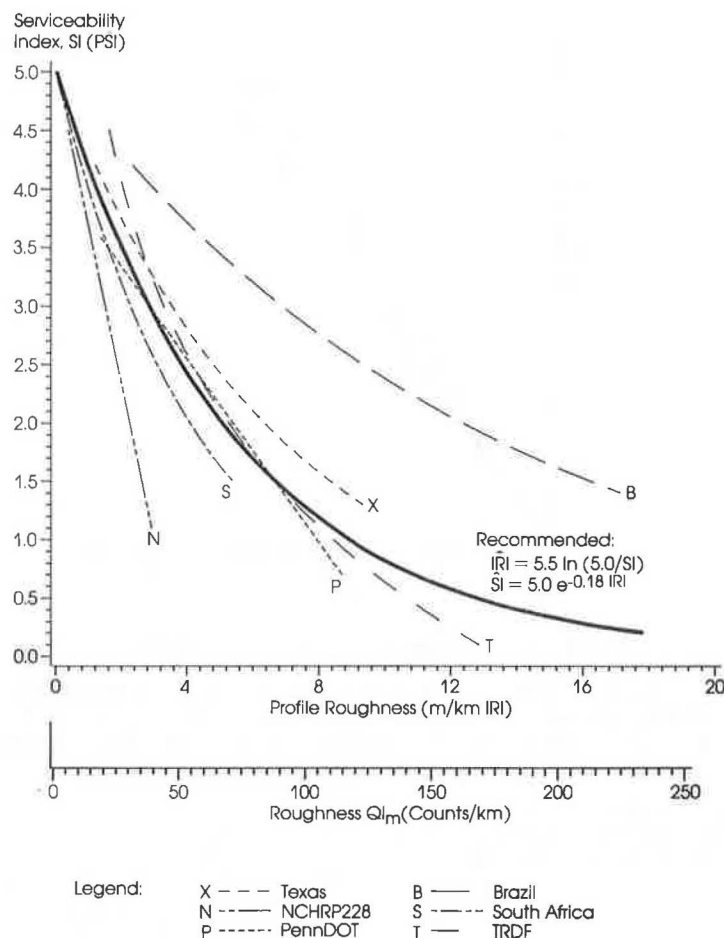

FIGURE 3 Approximate relationships between AASHO serviceability index, PSI, and the QI_m and IRI roughness scales, based on panel ratings from four sources.

roads, but the means nevertheless vary by up to one rating interval when rating a given roughness, whereas the Brazilian raters attach much higher ratings to rough roads than do the other groups. A linear relationship between rating and roughness may be adequate over the range of two to four rating units on paved roads as claimed by Janoff et al. ([12]) but does not apply more generally. By extrapolation, the scales indicate that a roughness of 130 to 175 QI is equivalent to 0 PSI, except for the Brazilian panel, which included unpaved roads and rated a roughness of 175 as better than 1 PSI. The best continuous function meeting the perfect score of 5 on the SI scale at a roughness of zero is as follows:

$$QI_m = 72 \log_e (5.0/SI)$$

$$IRI = 5.5 \log_e (5.0/SI)$$

However, the linear function may be just as appropriate over normal ranges of paved road roughness, that is

$$QI_m = \max [136 - 33 \, SI; \, 0]$$

$$IRI = \max [10.5 - 2.5 \, SI; \, 0]$$

The slope of the QI_m/PSI relationship varies from -20 for serviceability above 3.5 PSI to -33 for serviceability below 3.0 PSI. The common initial and terminal levels of serviceability are therefore approximately

4.2 PSI $\simeq$ 13 counts/km QI_m $\simeq$ 1.0 k/km IRI

2.5 PSI $\simeq$ 50 counts/km QI_m $\simeq$ 3.8 m/km IRI

2.0 PSI $\simeq$ 65 counts/km QI_m $\simeq$ 5.0 m/km IRI

1.5 PSI $\simeq$ 86 counts/km QI_m $\simeq$ 6.6 m/km IRI

CONVERSION CHART

For convenience of application, the results of the foregoing analyses are presented in the form of a conversion chart in Figure 4. The IRI scale is used as a reference on each side of the chart, and for North American users, the equivalent reference scale in inches/mile units (IM_r) is presented alongside.

For all other roughness measures shown on the chart, the bars have three sets of graduations, the estimated value on the centerline, a low value on the left, and a high value on the right. The low and high values are defined by the 15th and 85th percentiles of the preceding data and indicate the range over which the actual value for a specific road section can be expected. For example, to estimate the roughness of 6 m/km IRI in terms of the QI_m scale, an estimated value of 78 counts/km QI_m is obtained, and the authors are about 70 percent confident that the actual value will be between 66 and 90. For converting between two of the nonreference scales, the centerline of the given scale is used, and the estimated low and high values of the desired scale are read. For calculator applications, the conversion functions and confidence intervals are listed at the bottom of the chart.

The ranges of validity of the conversion functions are shown by the length of the bars on the chart. Individual observations may exceed the ranges shown on the IRI, QI_m, BI, and IM_r scales, but typically such high levels of roughness are confined to short sections. In the case of the APL numerics,

the ranges are limited by the mechanical capability of the equipment and by the signal processing method to cases of paved roads and unpaved roads of low to moderate roughness.

A chart such as the one shown in Figure 4 meets a practical need, but there are two important caveats. First there is the potential inference that the various roughness measures are interchangeable and measure the same thing. The IRRE showed clearly that, while different response-type systems were highly correlated when operated under identical conditions, significant variations do exist between the scales on some surfaces. These arise from differences in the operating conditions, equipment, wear, and interpretation of the diverse spectrum of wavelengths in a road profile. These variations are accommodated in the chart through the confidence intervals, which indicate that the conversions are approximate and give the range within which the actual value may vary. Second, there is no guarantee that the data collected at the IRRE are exactly representative of the historical data collected in previous studies. Not all these studies will have been conducted with the recommended degree of control as was done at the IRRE, although there is reasonable confidence in this respect for the QI_m, BI_r, and APL measures.

CONCLUSION

An acceptable basis for comparing the roughness measures used in past and present major studies has been established for use where one of the following calibration references exist: $BI_r QI_m$, $CP_{2.5}$, IM_r or IRI. However, the various roughness measures sense, filter, and amplify the road profile characteristics in different ways so that exact equivalences do not exist between them. The conversion chart and relationships, shown in Figure 4, present the means for comparing a number of scales that have been in use and for relating them to the International Roughness Index. These conversions and their inexactness were based primarily on data from the international experiment conducted in Brazil, and they are generally valid only over the range of asphalt, surface treatment, gravel, and earth surface types included in the experiment. That validity, however, covers a wide range, and significant deviations are only likely on extremely different surface types, including surfaces with periodic defects, such as corrugations, or strong short wavelength content such as potholed roads, earth roads, surfaces placed by manual labor (macadams, cobbles, set-stones, etc.), and coarse-gravel roads.

The degree to which the conversions presented here are applicable to either historical or present measurements made with a system similar to one of those described, depends largely on how the operating conditions compare with those existing at the IRRE. In the case of the profile-related systems (QI_m, W_{sw}, and $CP_{2.5}$), which are time-stable, the degree of confidence is high. In the case of the Bump Integrator trailer, and other systems using hardware as a reference, the applicability depends on the degree of similarity of the hardware to the system used at the IRRE, which can differ in extreme cases by up to 40 percent when out of calibration.

The widespread adoption of IRI as a reference and calibration standard is being encouraged worldwide to improve the reliability of exchanging information related to road roughness. The IRI would then be a common denominator, in some cases existing in parallel with a local index or series of profile statistics.

IRI (m/km IRI)	QI_m (count/km)	BI_r (mm/km)	CP_2.5 (0.01 mm)	W_SW	CAPL_25	SI (PSI)	IM_r (in/mile)	IRI m/km

Notes:
On the 3-line scales, the center line represents the estimated value, and the left and right margins represent the low (15th percentile) and high (85th percentile) limits of individual values about the estimated value.

ESTIMATING IRI SCALE
Low value
Estimated value
High Value

ESTIMATING OTHER SCALE
Low Value
Estimated value
High value

NOTES:
Conversions estimated on data from the International Road Roughness Experiment, (Sayers, Gillespie and Queiroz, 1986) as follows:

1. IRI — International Roughness Index (Sayers, Gillespie and Paterson, World Bank Technical Paper 46, 1986)

2. QI_m — Quarter-car Index of calibrated Maysmeter, Brazil-UNDP Road Costs Study
$IRI = QI_m/13 \pm 0.37\sqrt{IRI}$ $IRI < 17$

3. BI_r — Bump Integrator trailer at 32 km/h, Transport and Road Research Laboratory, UK
$IRI = 0.0032\ BI_r^{0.89} \pm 0.31\sqrt{IRI}$; $IRI < 17$

4. $CP_{2.5}$ — Coefficient of planarity over 2.5m baselength for APL72 Profilometer, Centre de Recherches Routiers, Belgium:
$IRI = CP_{2.5}/16 \pm 0.27\sqrt{IRI}$; $IRI < 11$

5. W_{sw} — Short Wavelength Energy for APL72 Profilometer, Laboratoire Central des Ponts et Chaussées, France
$IRI = 0.78\ W_{sw}^{0.63} \pm 0.69\ IRI$; $IRI < 9$

6. $CAPL_{25}$ — Coefficient of APL25 Profilometer, Laboratoire Central des Ponts et Chaussées, France:
$IRI = 0.45\ k\ CAPL_{25} \pm 16\%$; $IRI < 11$
where k = 1 for general use, k = 0.74 for asphalt concrete surfaces, k = 1.11 for surface treatment, earth or gravel.

7. SI — Serviceability Index, American Association of State Highway and Transportation Officials:
$IRI = 5.5 \ln (5.0/SI) \pm 25\%$; $IRI < 12$

8. IM_r — Inches/mile equivalent of IRI from Reference Quarter-Car Simulation at 50 mile/hr (see 'HSRI-reference' in Gillespie, Sayers and Segel NCHRP report 228, 1980; and 'RARS_{80}' in Sayers, Gillespie and Queiroz, World Bank Technical Paper 45, 1986):
$IRI = IM_r/63.36$

FIGURE 4   Chart for approximate conversions between the International Roughness Index and major roughness scales.

REFERENCES

1. A.D. Chesher and R. Harrison. Vehicle Operating Costs: Evidence From Developing Countries. Highway Design and Maintenance Standards Study, Vol. 1, Transportation Department, World Bank, Washington, D.C., 1987 (in press).

2. W.D.O. Paterson. Prediction of Road Deterioration and Maintenance Effects: Theory and Quantification. Highway Design and Maintenance Standards Study, Vol. III. Transportation Department, World Bank, Washington, D.C., 1987 (in press).

3. GEIPOT. Research on the Interrelationships Between Costs of Highway Construction, Mainte-nance, and Utilization (PICR). Final Report, 12 volumes. Empresa Brasileira de Planejamento de Transportes, Brasilia, Brazil, 1982.

4. C.A.V. Queiroz, W.R. Hudson, A.T. Visser, and B.C. Butler. A Stable Consistent, and Transfer-able Roughness Scale for Worldwide Standardization. In Transportation Research Record 997, TRB, National Research Council, Washington, D.C., 1984, pp. 46-55.

5. The AASHO Road Test (7 Vols.). Special Reports 61A to 61G. HRB, National Research Council, Washington, D.C., 1962.

6. M. Sayers, T.D. Gillespie, and C.A.V. Queiroz. The International Road Roughness Experiment: Establishing Correlation and a Calibration Stan-

dard for Measurements. Technical Paper 45. World Bank, Washington, D.C., Jan. 1986.

7. M. Sayers, T.D. Gillespie, and W.D.O. Paterson. Guidelines for Conducting and Calibrating Road Roughness Measurements. Technical Paper 46. World Bank, Washington, D.C., Jan. 1986.

8. T.D. Gillespie, M.W. Sayers, and L. Segel. Calibration of Response-Type Road Roughness Measuring Systems. NCHRP Report 228. TRB, National Research Council, Washington, D.C., 1980, 81 pp.

9. W.D.O. Paterson, A.D. Chester, and S.O. Lo. Conversion Between BI and QI Roughness Measures Used in Road Costs Studies. Unpublished report. Transportation Department, World Bank, Washington, D.C., Jan. 1984.

10. A.T. Visser. A Correlation Study of Roughness Measurements with an Index Obtained from a Road Profile Measured with Rod and Level. Technical Report RC/2/82, National Institute for Transport and Road Research, Pretoria, South Africa, March 1982.

11. J.B. Nick and M.S. Janoff. Evaluation of Panel Rating Methods for Assessing Pavement Ride Quality. In Transportation Research Record 946, TRB, National Research Council, Washington, D.C., 1983, pp. 5-13.

12. M.S. Janoff, J.B. Nick, P.S. Davit, and G.F. Hayhoe. Pavement Roughness and Rideability. NCHRP Report 275, TRB, National Research Council, Washington, D.C., 1985, 66 pp.

The Implication of the International Road Roughness Experiment for Belgium

M. B. GORSKI

ABSTRACT

The International Road Roughness Experiment (IRRE) has had a double impact on the current practice of roughness evaluation. First it has upgraded the moving average statistics (CP) developed and used in Belgium for the assessment of evenness. The latter is based on a dynamic profilometer monitoring of the longitudinal profile of the road surface. Its scale of representation can be interpreted from different points of view (acceptability criteria associated with comfort and security, maintenance levels associated with structural integrity, and methods of assessment such as visual inspection). The link between CP scale and the roughness measures generated by response-type road roughness measurement systems (RTRRMS) adds a new dimension to the interpretation of the Belgian scale. It enables roughness to be predicted or estimated in terms of vehicle behavior because the RTRRMS results are expressed in scales simulating quarter-car response. The second impact is a consequence of the first. The IRRE demonstrates the need for further development of roughness evaluation and enhances the pavement management systems approach developed in Belgium in such a way that economic considerations can be assessed through relations between roughness and users' costs.

In order to appreciate the consequences of the International Road Roughness Experiment (IRRE), particularly for Belgium, a brief but complete review of the Belgian state of the art and current practices is necessary. The objectives of road roughness evaluation must be recalled, together with the methodology and the roughness scale used in Belgium. The acceptance of the latter will be stated. In this sense, the IRRE is more than just an exercise aimed at establishing a reference calibration procedure. It has enhanced the vision of what a roughness scale is designed for. In the case of the roughness (or evenness) scale developed in Belgium, a new dimension has been added to its interpretation. Beyond the ability of the roughness scale to contribute to problems linked with the maintenance of structural integrity of roads or with the comfort and safety of road users, the IRRE has opened the door to problems

Centre de Recherches Routières, 42 Boulevard de la Woluwe-B, 1200 Brussels, Belgium. Current affiliation: Transportation Department, World Bank, 1818 H St., N.W., Washington, D.C. 20433.

of a different order. These problems concern economic considerations such as users' costs and management of networks.

ROAD ROUGHNESS EVALUATION: OBJECTIVES AND ACTIVITIES

Road roughness evaluation achieved through longitudinal profile measurements on pavements is prompted by three major goals:

• To monitor, on roads in service, the evolution of surface evenness characteristics with time, and locate defects;
• To serve as a contractual test for the acceptance of a newly constructed pavement layer;
• To be used as a research tool for assessing the performance of the laying machines and for studying the construction factors that affect surface characteristics.

The Belgian Road Research Centre (BRRC) is closely cooperating with the Belgian Road Administration, contractors, and consultants to meet these goals through research contracts, technical assistance, and training. More recently these activities have been extended abroad. The roughness scale developed in Belgium has been implemented in France (Laboratoire Central des Ponts et Chaussées) and Morocco (1) (Direction des Routes et de la Circulation Routière). International projects have been completed (IRRE) (2) or are still active [Road Profilometer Evaluation, University of Michigan Transportation Institute (UMTRI) and the Federal Highway Administration].

CURRENT PRACTICE IN BELGIUM

The test method used by the Belgian Road Research Centre to qualify the longitudinal evenness of road pavements is based on

• The continuous measurement of surface irregularities by means of the twin track longitudinal profile analyzer (APL) (two scanning trailers) constructed by the French Bridge and Pavement Laboratory (LCPC); and
• An original numerical processing method developed by the Belgian Road Research Centre, which makes it possible to quantitatively and specifically assess evenness from longitudinal profile irregularities detected by the APL. The signal is recorded on magnetic tape during the measurement, and computer processing takes place afterwards in the laboratory.

The APL Trailer

The longitudinal profile analyzer trailer, shown in Figure 1, is an instrument developed by the French Bridge and Pavement Laboratory to obtain a signal proportional to profile over the frequency range 0.5 to 20 Hz. The trailer consists of three mechanical elements: a frame that acts as a sprung mass, a follower wheel, and a horizontal pendulum. The trailer frame and the suspension serve only to keep the follower wheel on the road by reducing bouncing and oscillations. Compared to a passenger car, the suspension is soft and exhibits high damping. The observed resonance of the sprung mass is well below 1 Hz, and the damping is close to critical.

Unlike the dynamic response-type road roughness measuring devices, the APL does not measure the deflection between the axle and frame. Instead, (Figure 2) a displacement transducer is located be-
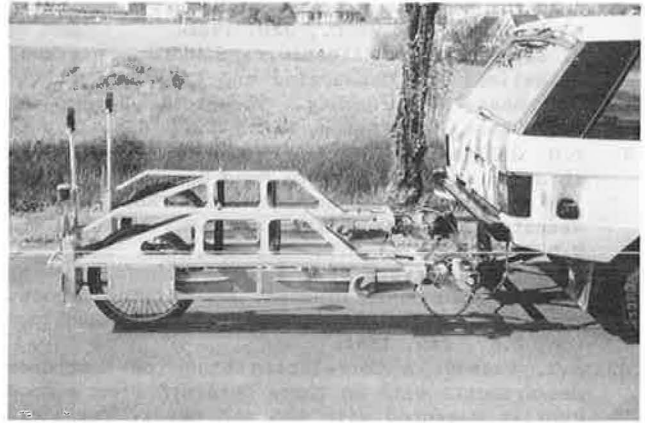
FIGURE 1 The longitudinal profile analyzer of the Belgian Road Research Centre.
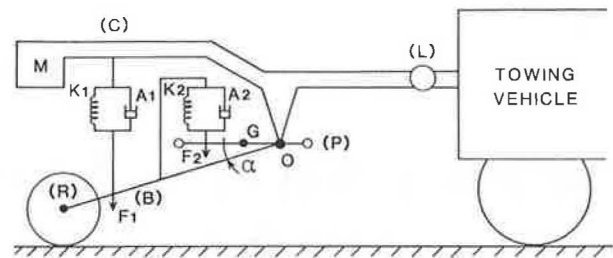
FIGURE 2 APL schematic principle.

tween the trailing arm (B) that supports the follower wheel (R) and the horizontal pendulum (P). The horizontal pendulum consists of an arm with weights at each end, supported in the center by a Bendix-type pivot with crossed blades. One of the weights can be repositioned, allowing adjustment of the rotational moment of inertia. The pendulum is centered by a coil spring, and damping is provided magnetically. Together, the pendulum, spring, and damper constitute a mechanical system that is tuned in the laboratory to provide a unity gain for input frequencies greater than 0.5 Hz. (Lower input frequencies result in an attenuated response.)

The displacement that is measured is designed to replicate the wave-number content of the longitudinal road profile over the wave-number range that corresponds to the frequency range of 0.5 to 20 Hz at the measurement speed. The upper limit is imposed by the dynamic response of the follower-wheel assembly, which will attenuate any inputs at frequencies above 20 Hz (Figure 3).

The trailer is certified when it is manufactured by placing a dynamic shaker under the follower wheel and measuring the ratio of the output signal amplitude to the input amplitude for sinusoidal inputs. The locations of the shock absorber and coil spring in the suspension are adjusted to optimize the response. The shaker is also placed under the towing hitch to assure that the trailer is acceptably unresponsive to these movements. Indeed, the geometry that is built into the trailer, and particularly that of its low-frequency pendulum used as a reference, has been designed in such a way that it permits perfect decoupling between the oscillations of the arm carrying the measuring wheel, which follows the fluctuations of the road profile, and the oscillations of the trailer frame due to the influence of the movements of the hitch point of the towing vehicle. This, in fact, is the original concept of the APL.

FIGURE 3 Frequency response of APL trailer to displacement input.

The effectiveness of this feature is actually verified in the course of the adjustment and calibration of each APL trailer on the shake table: the hitch system of the trailer is itself excited by a vibrator, and it is ascertained that this excitation has no influence on the transducer's response. The trailer is considered to be correctly adjusted only when the transducer response to an excitation of the hitch is less than 0.2 perce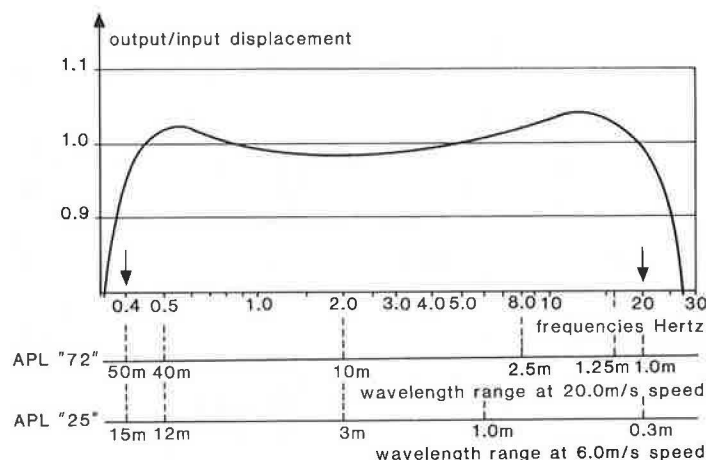nt of the response to an excitation of the measuring wheel with the same amplitude. Each APL trailer is adjusted in this manner at construction, and those used in Belgium are recalibrated periodically (every 2 to 3 years).

Today, the calibration procedures are further refined by verifying the linearity of the transfer function of the APL trailer under signals representing the true conditions of very good and very poor road profiles, in addition to the conventional harmonic type of response curve that is also being determined. Furthermore, no test tracks are imperatively required.

Method of Measurement

Because the amplitude transfer function of the APL is constant to within 5 percent in the frequency range 0.5 to 20 Hz (Figure 3), the wavelength range of the defects detected by the APL, which is proportional to the speed of measurement, is as follows: (a) 1 to 40 m at 72 km/h (20 m/s) on motorways and other roads according to traffic possibilities; (b) 1 to 30 m at 54 km/h (15 m/s) on roads with limited traffic possibilities (cross-town links, speed limits of 60 km/h, bends, etc.); and (c) 0.3 to 15 m at 21.6 km/h (6 m/s) on construction sites, and rural roads.

Because the speed of measurement cannot be increased to infinity, it is, of course, admitted that the APL cannot completely describe a road profile in the sense that it certainly is no absolute leveling device. As far as is known, this is true for all dynamic road profilometers; however, this is not a hindrance. Indeed, those involved in maintenance and rehabilitation of road networks are essentially interested in the profile defects that can affect road users and the modification of which does not necessitate a modification of road alignments. With this objective in mind, the APL is perfectly capable of providing a sufficiently accurate image of the road, for all practical purposes, with the localization and quantification of irregularities up to 40 m long.

The results of measurement are processed to coefficients of evenness, CP (Belgian method, BRRC) (3).

This analysis consists of producing a geometric representation of the measured longitudinal profile. The mean surface area of the deviation of the measured profile from a reference line formed by the same profile after smoothing is determined (average of bump and hollows). This area is calculated by sampling the measured profile at intervals of 1/3 m or 1/6 m (for the speed of 21.6 km/h).

This calculation leads to the definition of a coefficient of evenness (CP), the dimensions of which are 1 CP = 10^{-5} m (10^4 mm^2/km). It is determined in relation to the base length chosen for smoothing and the division of the scanned section into blocks of equal length, which has been set at 100 m.

Interpretation of CP Values

The coefficient of evenness for a given base smoothing length and a given block length is directly proportional to the mean surface area of the deviation of the measured longitudinal profile from the smoothed profile. The higher the coefficient of evenness for a given base length and a given block length, the poorer the quality of longitudinal evenness.

The use of the sliding-mean concept (moving average) to calculate CP values (smoothing of the profile) amounts to filtering the measured longitudinal profile. The result of this filtering is to eliminate the deformations with a longer wavelength than the base length chosen for smoothing. Thus the effect of short-span deformations is separated from that of long-span deformations, which makes it possible to characterize and locate the detected irregularities.

The use of one and the same evenness scale (CP values restricted to spans of 2.5 m and to medium spans of 10 to 15 m) makes it possible to ensure a transition between the "zero point" (acceptance test) and later tests carried out for monitoring purposes (4).

Acceptability Criteria

As stated earlier, the scale of evenness coefficients makes it possible to distinguish short-span irregularities (base lengths of the order of a few meters) from relatively longer medium-span deformations (base lengths of the order of 10 to 15 m).

A remarkable fact appears when comparing the different acceptability thresholds for evenness set in the various scales obtained for the different apparatus used in Belgium and in various other countries (Great Britain, France, Switzerland): they are

in agreement when translated into values on the scale of coefficients of evenness. This holds true when comparing the acceptability thresholds for deformations with short spans (< 2.5 m) (Table 1) and with mean spans (Table 2). This was established through experiments on Belgian road sections designed to correlate CP values with the results obtained on the same sections by the APL from the Laboratoire Central des Ponts et Chaussées (France), the Swiss Winkelmesser, the Laser Profilometer from the Transportation and Road Research Laboratory (TRRL) (United Kingdom), and the Viagraph of the Belgian Road Administration.

The existence of such substantial consistency in the choice of acceptability thresholds can lead to the choice of acceptance level for contractual purposes. This is currently taking place in Belgium.

Management System for the Maintenance and Strengthening of Roads

Evenness measurements are integrated into a management system for the maintenance and strengthening of roads. The Belgian national report on Question II at the XVIIth Permanent International Association of Road Congresses (PIARC) World Road Congress (5) contains a concise description of the road assessment method that is currently being set up.

The final objective is to develop a management system for the maintenance and strengthening of the motorways and roads administered by the Roads Department of the Ministry of Public Works. The maintenance decision is based on a ranking system of evaluation.

The quality of the routes making up the motorway and road network is characterized by an overall index that reflects various assessment parameters collected by high yield apparatus and a factor representing the condition of the road surface. There is an intervention threshold for each of these data while the decision to carry out maintenance work to replace the pavement or to provide stronger structural elements is taken on the basis of the overall index, which characterizes both the quality of the route (or road link) under consideration and the type of interven-

tion required (intervention affecting the surface, pavement, or structure). In the event of an intervention affecting the pavement or the structure, an individual project must be designed. The preparation of this project may require further assessment (borings through the structure, sampling of materials, evaluation of the bearing capacity of the soil etc.) in order to make a more thorough diagnosis.

The Belgian Road Administration has adopted the CP scale, which has been divided into five classes for the management of maintenance and strengthening activities on the Belgian state road network. The intervention thresholds for each base length selected for the calculation of CP correspond to the limits between the third and fourth class of evenness (Table 3 gives the partial quality criteria that are currently being used). It should be noted that visual assessment of road roughness versus the CP scale has been evaluated.

During a visual inspection campaign conducted in several Belgian state road maintenance districts, inspectors were asked to give visual appreciation of evenness ("good" or "poor"). The visual survey was conducted on foot by four independent teams of inspectors. A comparative study of the coefficients of evenness measured with the APL for the respective base lengths of 2.5, 10, and 30 m has shown that the judgment of visual inspection is best reflected by the CP_{10m} scale. The class of evenness visually categorized as good corresponds to Class A of the CP scale (Table 3), whereas the class categorized as poor corresponds with class B of the CP scale.

The Belgian Road Research Centre has conducted surveys of the national network to monitor road roughness on behalf of the Belgian Road Administration.

BELGIAN PARTICIPATION IN THE IRRE

The Belgian Road Research Centre has cooperated with the Laboratoire Central des Ponts et Chaussées of France by participating in the IRRE. The profile measurements made by a French APL were translated to the Belgian scale. The experiment consisted of comparing the results of measurements made with various

TABLE 1 Acceptance Level Thresholds Expressed in CP Values for Short Spans (< 2.5 m)

Hectometric Section	HSP Laser Profilometer, TRRL (Base 3 m) Threshold 1 mm r^b = 0.916	APL LCPC Evenness Marks 1 - 3.3 m Threshold 6.5 r = 0.920	BI TRRL 32 km/h Threshold 17.6 ARV (mm/s) r = 0.928	Swiss Winkelmesser Threshold $\hat{s}_w$ = 2.2‰ r = 0.776
Evenness coefficient, CP^a Base 2.5 m	32	34	32 (65 < v < 80 km/h)	27 (v < 80 km/h)

[a]Identical for all of the three APL speeds of measurement: 6, 15, and 20 m/s.
[b]r = correlation coefficient.

TABLE 2 Acceptance Level Thresholds Expressed in CP Values for Mean Spans (10 - 15 m)

Hectometric Sections	Viagraph Belgian Road Administration Threshold		HSP Laser Profilometer, TRRL (Base 10 m) Threshold 2.6 mm r^b = 0.922	APL LCPC Evenness Marks 3.3 - 13 m Threshold 7 (NR Inquiry) r = 0.993
	20 CDI	10 CDI		
Evenness coefficients, CP^a				
Base, 10 m	111	93	90	88
Base 15 m (restricted to 21.6 km/h)	124 (r = 0.806)	103	_[c]	_[c]

[a]Identical for all of the three APL speeds of measurement: 6, 15, and 20 m/s.
[b]r = correlation coefficient.
[c]Not determined.

TABLE 3 Longitudinal Evenness, Classes and Limit Values for Coefficients of Evenness

Classes and Limit Values	CP_{40}/CP_{30}	CP_{10}	$CP_{2.5}$
Class A (very good)	< 160	< 80	< 40
Class B (good)	160 << 320	80 << 160	40 << 80
Class C (average)	320 << 480	160 << 240	80 << 120
Intervention threshold	480	240	120
Class D (poor)	480 << 640	240 << 320	120 << 160
Class E (very poor)	640 <	320 <	160 <

Notes: For the three base lengths of 40, 10, and 2.5 m and for blocks of 100 m measured with the APL (Belgium) at 20 m/s. Base 40 is replaced by 30 at 15 m/s.

devices on 49 sections of paved and unpaved roads in Brazil representing a wide range of evenness levels. The following devices were used: three Mays meters and one BPR Roughmeter (originating from the United States) used by the Brazilian Transportation Planning Agency (GEIPOT); one Bump Integrator trailer (United Kingdom), one vehicle-mounted Bump Integrator (United Kingdom), and one National Association of Australian State Road Authorities (NAASRA) meter (Australia) used by the TRRL (United Kingdom); two static profilometers—one conventional telescope and straight-edge leveling system (used by GEIPOT) and one TRRL beam (United Kingdom); two dynamic profilometers—the APL (longitudinal profile analyzer) of the LCPC (France); and one General Motors (GM) profilometer (United States) used by GEIPOT.

The computations performed at the Belgian Road Research Centre concerned the APL signals recorded in Brazil at a measurement speed of 72 km/h (20 m/s). The sampling step length used was 1/3 m, and the coefficients of evenness (CP) were determined for 2.5, 10, and 40 m base lengths, which are the conventional values used. The coefficients of evenness were evaluated for hectometric sections. The figures given for the experimental section tracks of asphaltic concrete (CA), surface treatment (TS), gravel surfaced (GR), and earth (TE) were obtained from the mean value of three contiguous hectometric blocs, at the beginning of each section track (the test sections were 320 m long).

Linear regressions were also calculated at the Belgian Road Research Centre between the response type road roughness measurement systems (RTRRMS) average rectified velocity (ARV) numerics (for each surface type and speed of measurement) and the CP for the three bases $CP_{2.5}$, CP_{10}, and CP_{40}.

Correlations defined by the correlation coefficient are given in Table 4 for the purpose of illustrating the results of comparison with the response-type road roughness measurement systems driven at the speed of 50 km/h. The results of comparison versus the ARV scale [average rectified slope (ARS) = ARV x 360/v, where v is speed in km/h; ARV is in mm/s; ARS is in mm/km] reveal the following:

• The coefficients of correlation decrease in general when the base of determination of the CP value increases.
• Significant and high values are obtained for CP (base 2.5 m) with all RTRMMS devices on all test sites and for all the test speeds.
• By merging all data belonging to a given RTRMMS device and calculating the linear regression coefficients and the correlation coefficient for each test speed, the effects of speed and site factors that could influence a calibration plot needed to estimate the CP 2.5 numerics from measurements made with one of the RTRMMS can be expected to be evaluated. This case has been examined for both the Mays meter 2 and the bump integrator trailor. It has been found that the best fit for the CP 2.5 values is obtained through correlation with both devices traveling at 50 km/h and that no site type influences the correlation. The two examples are illustrated in Figure 4. Both correlations are significantly high (r > 0.95) and yield quasi-identical linear regression equations.

A comparison was also made with the Quarter-car Index (QI) scale. The Quarter-car Index was accepted as a standard measure of roughness on a previous Brazilian project (research on the interrelationships between the costs of highway construction, maintenance, and utilization, United Nations Development Program). Figure 5 shows the correlation between QI determined for right and left tracks on all sites (CA, TS, GR, and TE) measured with the TRRL beam and the CP 2.5 values obtained from the APL. The value of the coefficient of correlation reveals a significant linear relationship between the two scales without systematic effects induced by surface types.

The CP numerics have been demonstrated to be well correlated with both the ARV (ARS) scale and the QI

TABLE 4 Correlation Coefficient Values for the APL Results Expressed in Coefficient of Evenness and the RTRRMS (ARV) Measures Made at 50 km/h

	MM 01	MM 02	MM 03	BI CAR	NAASRA	BI TRL	BPR
Asphaltic Concrete Test Sites							
$CP_{2.5}$	0.9663	0.9369	0.9558	0.9803	0.9776	0.9678	0.8929
CP_{10}	0.9543	0.9486	0.9711	0.9292	0.9507	0.8836	0.8440
CP_{40}	0.8677	0.8823	0.8940	0.8475	0.8697	0.7877	0.7954
Test Sites with Surface Treatment							
$CP_{2.5}$	0.9717	0.9615	0.9591	0.9787	0.9818	0.9795	0.8770
CP_{10}	0.8451	0.8479	0.7931	0.8505	0.8429	0.7995	0.7255
CP_{40}	0.0331	0.0695	0.0574	0.0609	0.0517	0.0255	0.0656
Gravel Surfaced Test Sites							
$CP_{2.5}$	0.9659	0.9695	0.9716	0.9599	0.9652	0.9675	0.8667
CP_{10}	0.9312	0.9356	0.9199	0.9331	0.9389	0.7996	0.8809
CP_{40}	0.3547	0.3479	0.2644	0.3661	0.3542	0.3985	0.5646
Earth (Clay) Surface Test Sites							
$CP_{2.5}$	0.9452	0.9517	0.9523	0.9289	0.9510	0.9091	0.9435
CP_{10}	0.9226	0.9486	0.8466	0.9350	0.9398	0.9720	0.9701
CP_{40}	0.5111	0.5791	0.4299	0.7325	0.6091	0.6813	0.7260
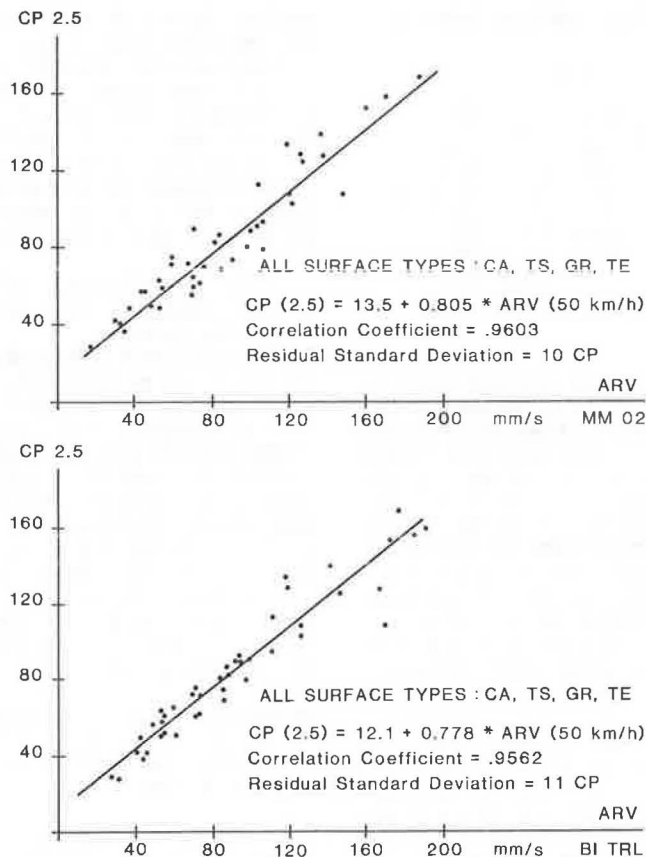
FIGURE 4 Comparison of APL 72 CP (2.5) values with RTRRMS measures made at 50 km/h.

ALL SECTIONS INCLUDED CA, TS, GR, TE

CP (2.5) = 14.0 + 1.06 * QI
correlation coefficient =.9281
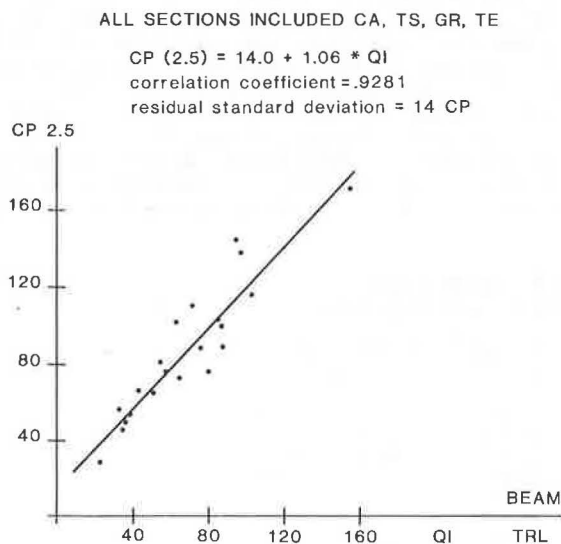residual standard deviation = 14 CP

FIGURE 5 Comparison of QI values calculated from TRRL beam profiles with CP (2.5) derived from APL 72 signal.

scale, provided that a short basis of 2.5 m was used in its determination. It is expected that the choice of another basis, perhaps 3 m, could yield higher correlation coefficients with the QI scale.

In the same manner, optimization of correlation with the ARV scale obtained with different speeds could probably be achieved with a corresponding ad-

justment of the choice of the base for the CP determination. Nevertheless, from the practical purpose of comparing the different scales, the CP 2.5 has been demonstrated to be an acceptable roughness indicator. Of all the APL results, it is the CP 2.5 m numerics that produced the best correlation with the RTRRMS.

The issue of the experiment regarding the APL measuring equipment and the CP statistics associated as a roughness scale can be stated as follows: the APL trailer is validated as a profilometer against rod and level and that it falls within the Class 2 of measurement methods enabling the estimation of reference average rectified slope (RARS) using an independently calibrated instrument (2). In the particular situation in which CP 2.5 statistics are available for the APL, it can be used to estimate RARS using correlated statistics.

CONCLUSION

The IRRE has demonstrated that in order to carry a standard procedure to calibrate the RTRMMS, true roughness values must be assigned to the sites used as references for the measuring devices. It is commonly accepted that this true roughness numeric must be defined by a statistic based on profile geometry. This has triggered the interest in profilometric devices and has set a new trend in research concerning the performance of currently available devices and future needs. Among these, projects are underway at the Belgian Road Research Centre to thoroughly study the compatibility between topographic survey and dynamic profile measurement using the APL, particularly as an automatic leveling device during

Sensation — **Perception**

Experimenter Effects · Experiment Instructions · Stimulus (S) · RATER · Rater Reaction (P) · Rater Judgement (J)
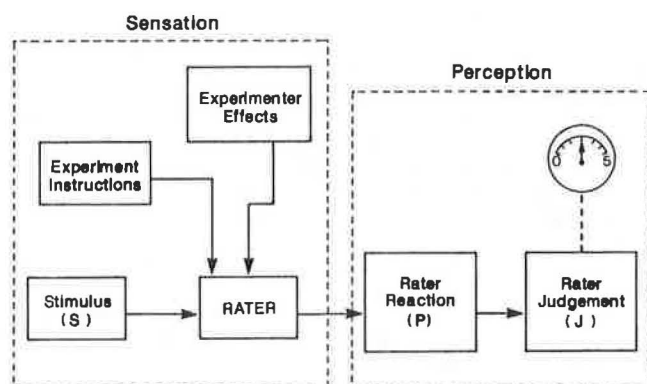
FIGURE 1 Systematized concept of rating.

suggested ways to avoid them) were kept in mind during the planning stages of the study so as to minimize or do away with them completely:

1. The error of leniency, which refers to the constant tendency of a rater to rate too high or to low for whatever reasons; remedied by statistical transformation of rater variance.

2. The halo effect, which refers to the tendency of raters to force the rating of a particular attribute in the direction of the overall impression of the object rated; avoided by accuracy and exactness in definitions.

3. The error of central tendency, which refers to the fact that raters hesitate to give extreme judgments of stimuli and tend to displace individual ratings toward the mean of the group; taken care of by introducing the judgment continuum as distinct from the sensory continuum.

4. The error of anchoring, which refers to the endpoints of the scale being rated; overcome by using accurate definitions.

EXPERIMENTAL DESIGN

In laying out the experiment design, the first step was to look through the "window" of applicability, the inference space. This is defined as that space within which the results of the study may be applied. When selecting the panel, if a wide distribution of members from various parts of Texas are chosen randomly, then the panel could be considered as representative of the people of the state of Texas.

Considerations such as the type and number of variables to include in the statistical analysis relating the profile data to the panel rating data are significant for future applications of the serviceability formulas. It is important to choose pavement test sections that include a wide range of wavelengths, as well as to consider this range of wavelengths as they influence Texas raters' judgments of ride quality. With these ideas in mind, 17 factors, along with their corresponding levels, were enumerated by a research team and a group of pavement engineers from the Texas SDHPT who were familiar with pavement roughness. To reduce the complexity of the analysis, some of the factors were studied in screening experiments and the remainder were studied in the main rating sessions.

SCREENING EXPERIMENTS

The following factors and corresponding levels were considered to be studied in screening experiments:

Factor	Level 0	1
Vehicle type	Car	Van
Position in car	Front	Rear
Rater's age	< 35 years	> 35 years
Rater's sex	Male	Female
Time	Night	Day

Factors associated with the type of pavement sections are listed as pavement variables as follows:

Factor	Level 0	1
Pavement type	Black	White
Surface texture	Coarse	Fine
Location of road	Rural	Urban
Maintenance	Unpatched	Patched
Functional class	Low	High
Surroundings	Poor	Good
Road width	Narrow	Wide
Lane position	Inside	Outside

In order to simplify the analytical procedure and also to make the computational procedure amenable to mainframe computer capacities, it was decided to drop the factors (a) functional class and (b) lane position. A panel of four engineers surveyed existing sections to obtain information about these factors using a form designed for this purpose. Definitions and clarifications as to the levels of each factor were provided. The need to locate more sections was realized. The objective was to fill the full factorial (2^6 or 64 sections) as completely as possible, recognizing that certain sections are impossible to exist or simply do not exist and then to run analyses of variance (ANOVAs), knowing that the factorial is not balanced. The sections used in the factorial for screening the experiments are shown in Figure 2.

			Patched				Unpatched			
			Wide		Narrow		Wide		Narrow	
			Good	Poor	Good	Poor	Good	Poor	Good	Poor
White	Fine	Urban					B4, B17			
		Rural					B6, B7, B16			
	Coarse	Urban			B24, B15		B2, B8	G1, B20		
		Rural	B12, B13				B3, B11	B14		
Black	Fine	Urban	A7, A20	A6, A25	A3	A9	5, B19	A11	A5	
		Rural		G2	A8	40, A10	7, 33	A4, A15	A14	35, 44
	Coarse	Urban	A24, C1	A1	A23	A13	19, 23, B18	37, A2	A21	15
		Rural	A22	A18, B1	39, A16	6, B22	36, 9	A12, A19	8, 38	2, 3

FIGURE 2 Sections used in the factorial for screening experiments.

MAIN RATING SESSIONS

The factors considered for analysis were

1. Rater profession,
2. Function in car,
3. Vehicle wheelbase,
4. Time of day,
5. Rater fatigue, and
6. Vehicle speed.

Selection of the Rating Panel

The selection of the panel was dictated by the strictest considerations as follows:

1. Panelists should represent the typical Texas traveling public,
2. Panelists should have a wide range of highway travel experience, and
3. Panelists should have no undesirable (biased) attitudes toward road travel in general.

Members of the rating panel consisted of personnel from the State Department of Highways and Public Transportation, the Center for Transportation Research (CTR), and volunteers from the general public.

The maximum size of the rating panel was 20, with 15 raters (5 vehicles, 3 to a car) and 5 drivers. The rating panel included both men and women of different ages with a wide range of driving and riding experience.

Selection of Vehicles

Two types of vehicles were selected to study the effect of vehicle wheelbase length: a subcompact model (Plymouth Horizon) and a mid-sized model (Mercury Zephyr and Ford Fairmont). These vehicles were taken as representative of typical vehicles owned and operated by an average middle class Texan. Two subcompacts and three mid-sized vehicles were used in the main rating sessions. Equal wear and tear of the vehicles (within each size category) was considered in their selection.

Selection of Sections

For the main rating sessions, the specific combination of characteristics in a section was not so important as the range of roughness of the section itself. The idea here is that to be able to predict serviceability indices from different kinds of roughness characteristics, it is essential to incorporate sections with these (and all other possible) characteristics. One important need, therefore, was to obtain as wide a range of roughness (serviceability indices) as possible. Because the existing pavement sections did not span the roughness spectrum, it became necessary to launch a search. With this objective in mind, roads in eight counties were surveyed. This search resulted in the location of 100 sections in all 8 counties, 77 of which were flexible and 23 of which were rigid pavement sections.

Rating Sessions

The rating method employed was similar to that used in the screening experiments, except for some improvements. The instructions to the raters were revised, based on experience from the screening sessions as to words or cues that were obfuscating and

that raised a number of questions. The same instructions given to drivers in the screening sessions were given to drivers in the main rating sessions. Of course, because the drivers were required to rate the sections according to the experimental plan, they were also required to attend the training session.

A major enhancement in the training session was the use of videotaped instructions. By using videotaped instructions, the researcher hoped to achieve higher reliability through consistency and standardization. Again, the script for the videotape had to be carefully drafted to ensure the minimization of miscues and vague definitions. This technique was also used to alleviate some of the possible errors arising from scale construction such as anchoring effect, and so forth. After the classroom briefing, the panelists were driven over some of the sections. This orientation session was more extensive than the one in the screening experiments. The same rating form (see Figure 3) was used, except for the "age" column.

To analyze the factors vehicle speed and rater fatigue, seven sections with two levels of roughness were chosen, and runs were made corresponding to the levels of the variables. (The "tired" level of the variable rater fatigue corresponded to runs in which raters were at a continuous rating stretch of more than 2 hr, whereas the "fresh" level corresponded to less than 1.5 hr.) Rater profession and vehicle wheelbase could also be included in the factorial. To examine the effect of vehicle wheelbase, raters in the subcompact cars were switched to the mid-sized cars (and vice versa) and thus rated nine sections in both cars. Eight sections were chosen to be rated both in the morning and afternoon so that the effect of time (morning versus afternoon) could be investigated.

Of the 171 sections that were rated, 129 were flexible and 42 were rigid pavement sections. A maximum panel of 20 raters rated these sections in 5 vehicles over a period of 13 days.

Roughness Measurement

The profilometer was set for normal operating conditions, specifically the following:

1. Accelerometer filter wavelength: 200 ft,
2. Sampling frequency: 6.00 in.,
3. Profiling distance: 0.2-mi sections, and
4. Profiling speed: 20 mph.

Roughness measurements were also made using the Mays meter and the SIometer. Runs were made after proper calibration procedures were followed and under normal specified operating conditions.

ANALYTICAL PROCEDURES

Individual rater performances were examined by plotting the mean individual ratings against the mean panel ratings for each rater (Figure 4 shows a typical plot). The mean individual rating represents the average rating (mean over runs) for each section for that rater. The mean panel rating (PSR) is obtained by taking the mean of all the mean individual ratings of all the raters for a particular section. Thus each point on a rater performance graph corresponds to a test section wherein the vertical axis value represents the individual's mean rating for that section and the horizontal axis value represents the mean rating of the panel as a group (for that same section).

construction of relatively thin overlays for reha-
bilitation of pavements. A precise knowledge of the
profile of a road surface needing maintenance is an
important asset in determining the choice of tech-
nical solution for overlaying.

The maintenance and strengthening management sys-
tem (PMS) developed in Belgium is based on the com-
parison of high-yield assessment parameters with the
results of visual inspection. Moreover, unlike other
management strategies for maintenance and strength-
ening that are based on the characterization either
of the evenness or the bearing capacity of the
existing pavement, the proposed system considers
both criteria complemented by other parameters for
the appreciation of the overall quality of the
assessed route (or road link). The interplay of the
overall index with the intervention thresholds them-
selves makes it possible to combine actions--often
of a simple or inexpensive nature--that must be car-
ried out locally or urgently (skid resistance) with
actions of a general type, taking into account over-
all budgetary restrictions. In order to justify
budgetary allocations, there is a growing need to
present the technological arguments together with
the economical arguments. This can be provided by
the link created between roughness evaluation and
users' costs; the roughness scale implemented in the
PMS being the CP statistics. This scale can perform
a significant estimation of a quarter-car simulation-
type based roughness scale.

Road roughness is an important factor in pavement
management systems, which are essentially aimed at
an economic objective. Using PMS procedures can bring
about a retroaction at the technical level condi-
tioned by the sensibility of global rehabilitation
costs to certain parameters such as roughness, thus
encouraging designers and technicians to produce
maximum efficiency. A good understanding of the mean-
ing of roughness in such a context is particularly
helpful for Belgian engineering consultants and con-
tractors. In this respect, proper evaluation of ex-
periments carried out by the World Bank in Kenya,
Brazil, and India is of primary importance together
with knowledge and the ability to use the highway
design model. Acquaintance with the CP statistics
used for the roughness scale can contribute to the
translation of roughness data for use in existing
foreign networks. Road roughness is the key inter-
face between road structures and transportation
performance.

REFERENCES

1. Dahbi Abdelaziz Gerard Lul. Relevé de l'état des
   Routes au Moyen d'appareil de Mesure et Utilisa-
   tion d'un Paramètre pour la Programmation de
   l'Entretien Routier Préventif. Ler Congrès
   National de la Route, Marrakech, Ministère
   Direction des Routes et de la Circulation
   Routière, Ministère de l'Equipement, Royaume du
   Maroc, 1984, pp. 295-344.
2. M.Sayers, C.A. Queiroz, T.D. Gillespie, W.D.O.
   Paterson, P. Autret, and J. Reichert. The Inter-
   national Roughness Index for Calibration and
   Correlation of Measuring Systems: Results of an
   International Experiment. 10th International
   Road Federation World Meeting, Rio de Janeiro,
   Brazil, Oct. 1984, pp. 339-352.
3. M.B. Gorski. Étude de l'uni Longitudinal des
   Revêtements Routiers CR 15/81. Centre de Re-
   cherches Routières, Bruxelles, Belgium, 1981.
4. M.B. Gorski. L'exploitation à grand Rendement de
   l'Analyseur de Profil en Long et ses Possibilités
   d'Adaptation aux Différentes Techniques de
   Chaussées dans Différents Pays. 10th Interna-
   tional Road Federation World Meeting, Rio de
   Janeiro, Brazil, Oct. 1984, pp. 237-246.
5. Question II, Construction and Maintenance of
   Pavements. Belgian Report. Theme A: General
   Questions. XVIIth World Road Congress, Sydney,
   Australia. Permanent International Association
   of Road Congresses, Paris, France, 1983.

Serviceability Prediction From User-Based Evaluations of Pavement Ride Quality

SUKUMAR K. NAIR and W. R. HUDSON

ABSTRACT

Presented in this paper are the results of research conducted to develop predictive serviceability equations to upgrade those currently in use by the Texas State Department of Highways and Public Transportation (SDHPT). The method has been based on the serviceability-performance (S-P) concept. Experiments were designed to study two types of variables, one associated with the rating process and the other related to pavement characteristics. The rated sections were profiled using the new Model 690D surface dynamics profilometer (SDP). From the profile data, a family of profile summary statistics called root-mean-square vertical accelerations (RMSVAs) was computed. A calibrated Mays meter and Walker accelerometer device (SIometer) were also operated on these sections. A multiple linear regression procedure was used to develop reliable serviceability equations (with good predictive capabilities) by regressing the mean panel ratings on the set of RMSVA indices. Correlation analysis of the Mays meter and SIometer measurements with the panel ratings showed that the calibrated Mays meter predicts panel ratings better than the SIometer. The best prediction of the panel ratings, however, is achieved by the 690D profilometer.

Road riding quality or roughness has special significance as it has been shown to directly affect vehicle operating costs and road safety. In previous studies, relationships have been developed between pavement serviceability and user costs. Sponsored by the World Bank, recent studies in developing countries have provided valuable quantification of road deterioration, vehicle operating costs, and road maintenance policy on road roughness. In this light, the importance of accurate and reliable measurement of road roughness cannot be overemphasized.

The serviceability of a pavement is largely a function of its roughness. Results from the AASHO Road Test (1) have shown that nearly 95 percent of the information about the serviceability of a pavement is contributed by the roughness of its surface profile. Roughness has been defined as the distortion of the pavement surface that contributes to an undesirable or uncomfortable ride (2). The American Society for Testing Materials has defined roughness as "the deviations of a pavement surface from a true planar surface with characteristic dimensions that affect vehicle dynamics, ride quality, dynamic pavement loads, and pavement drainage (e.g., profile, transverse profile, cross slope, and rutting" (3).

In 1968 the Texas State Department of Highways and Public Transportation (SDHPT) conducted a rating session in order to obtain serviceability equations using the 1965 version of the surface dynamics profilometer (4). Since then, these equations have been the basis for the evaluation of Texas highways. With the recent purchase of the highly sophisticated new Model 690D surface dynamics profilometer, it is necessary to upgrade the roughness evaluation system

by incorporating its new capabilities in updated serviceability equations.

Another significant consideration here is the change in the average passenger vehicle. Over the years there has been a noticeable shift in vehicle population from big, heavy automobiles to smaller, lighter ones. Hence it is essential that the changes in ride-quality judgments be reflected in serviceability predictions.

RATING: A SYSTEMS APPROACH

The rating process that results in an evaluation of pavement ride quality is a complex phenomenon. Examining it from a systems standpoint, the process involves three subsystems: the vehicle, the road surface profile, and the rater (highway user). The dynamic interactions between these subsystems are responsible for the output responses and characteristics of the system. In order to understand the rating process, it would appear appropriate to study the interactions between the stimuli and these receptor systems. Consider a rater in a rating situation (Figure 1) being subjected to the physical stimulus (S), the vibrations that are being imparted to him by the vehicle. Each vibration triggers certain events in his mechanical energy receptor systems. Thus, the physical continuum evokes a corresponding sensory continuum. When the same stimulus (vibration) is presented to the same rater on different occasions, it will not always produce the same magnitude of the variable on the sensory continuum. This is where the subjectivity of the rating process is realized. Three continua are the stimulus or physical continuum (S), physiological or subjective continuum (P), and the judgmental continuum (J).

However, as has been previously reported, there exist certain basic problems typical of serviceability ratings. These possible errors (listed next with

S. Nair, Center for Transportation Research, The University of Texas, Austin, Tex. 78712. W.R. Hudson, Dewitt C. Greer Centennial, The University of Texas, Austin, Tex. 78712.

SERVICEABILITY RATING CARD

FIGURE 3 Rating form used in the screening sessions.

Each graph gives an idea as to how each rater performed in comparison to the group. It is not necessary that all points lie on the equality line, but at the same time a point with a large deviation does indicate that for that section, that rater was at variance with the rest of the group for some reason, mostly subjective differences in perception and judgment.

Careful examination of each of the rater performance plots was made to check for discrepancies or abnormalities. No extreme outliers were singled out although it was noted that some of the raters differed with the panel as a group. For instance, one rater may generally tend to rate most pavements better than the others, but then, that is quite reasonable within the limits of acceptable subjective variation. If, however, this variation was found to be of a consistently high order, then the inclusion of this rater in the panel would be reviewed.

In order to analyze the data, mixed model, nested analyses of variance procedures were used. This technique allowed for the testing of hypotheses about the significant differences of means of various variables. The analysis of rating and pavement-related variables was performed using the generalized linear model (GLM) procedure available in the Statistical Analysis System (SAS). Two levels of roughness were chosen corresponding to sections that had PSRs greater than 2.5 and less than 2.5. The main effects of these variables on rating are given in Table 1. These factors are tested against sections S(G) (sections nested within roughness).

Measurements using the Model 690D surface dynamics profilometer are recorded as a road profile, which provides a complete signature of the road surface. In a previous study (5), a profile summary statistic termed root mean square-acceleration (RMSVA) that simulated the response of a typical Mays meter was developed. As a set of indices, RMSVAs can reveal many of the characteristics associated with road roughness.

Thus, from the left and right wheelpath profiles obtained from the operation of the new profilometer, RMSVA values were computed and the left and right wheelpath RMSVAs for each baselength were averaged. For each section, the indices were computed for baselengths of 0.5, 1, 2, 4, 8, 16, 32, 64, and 128 ft.

In addition to the homogeneity and normality, sometimes the question of additivity arises, and in keeping with a sound statistical approach, a nonadditivity test was performed. Tukey's test for nonadditivity (6) was used for this purpose on the main rating data. The interaction effect turned out to be insignificant, indicating that the effect of raters and sections is not multiplicative and that there is no indication that the data need to be transformed.

Multiple regression models were used to relate the profile summary statistics to the panel ratings, and a rigorous statistical procedure (7) was used to select the best candidate in each case.

In selecting prediction equations obtained through standard least-squares regressions, the following criteria were employed:
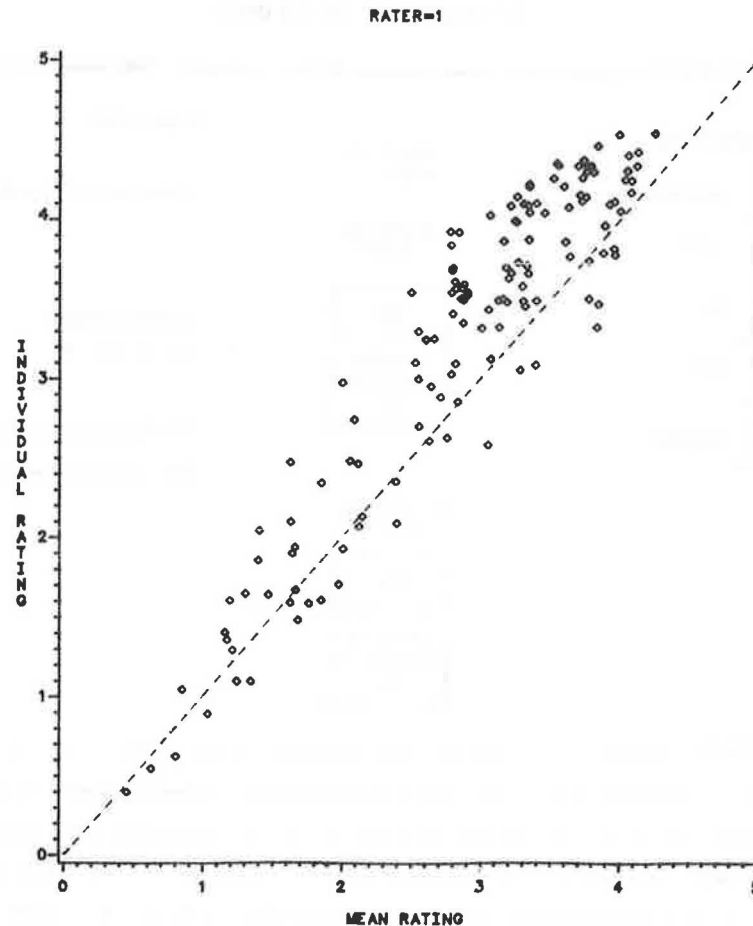
RATER=1

FIGURE 4 Individual rater performance, Rater 1.

TABLE 1 Results of Analysis of Rating Variables

Variable	Effect on Rating
Position in car	Not significant
Rater's sex	Not significant
Rater's age	Not significant
Time (night-day)	Not significant
Rater's profession	Not significant
Function in car	Not significant
Vehicle speed	Not significant
Time (a.m. - p.m.)	Not significant
Vehicle wheelbase length	Significant
Vehicle size	Significant
Rater fatigue	Significant
Pavement type	Significant
Maintenance	Significant
Surface Texture	Not significant
Location of road	Not significant
Road width	Not significant
Surroundings	Not significant

1. The value of R^2 achieved by the least-squares fit;
2. The Mallows' Cp statistic; and
3. The values of s^2, the residual mean square.

The residual sum of squares can be broken up into lack of fit and pure error sum of squares. The Cp statistic is a reflection of the adequacy of the model, that is, whether or not the model is biased. Equations with considerable lack of fit will show up significantly above or below the Cp = p line on a Cp versus p (number of terms in the model) plot.

The residual mean square, s^2, provides an estimate of the variance about the regression, which is presumed to be a reliable unbiased estimate of the error variance. For this study, this presumption is valid, considering the large number of degrees of freedom. This procedure alleviates the problem of unreliable inferences that result from using stepwise regression. Before running the regressions, the individual regressor variables were plotted against the PSRs. Figure 5 shows the relationship between the mean panel ratings and one of the independent variables, VA_4. Overall, it may be observed that as the RMSVA increases, the rating decreases; here again, the physical meaning of the RMSVA .concept is manifested in that, with higher amplitudes, the degree of discomfort (or roughness) as perceived by the user is greater.

Linear multiple regression analyses were performed on the data with the mean panel ratings as the independent variable and the RMSVAs (average of the mean left and right wheelpath values) in the base-lengths of 0.5, 1, 2, 4, 8, 16, 32, 64, and 128 ft as dependent (regression) variables. Separate analyses were carried out as follows:

1. Overall data,
2. Overall data with a forced dummy variable for pavement type,
3. Flexible sections, and
4. Rigid sections.

For each analysis, all possible numbers and combinations of terms were included in the regression
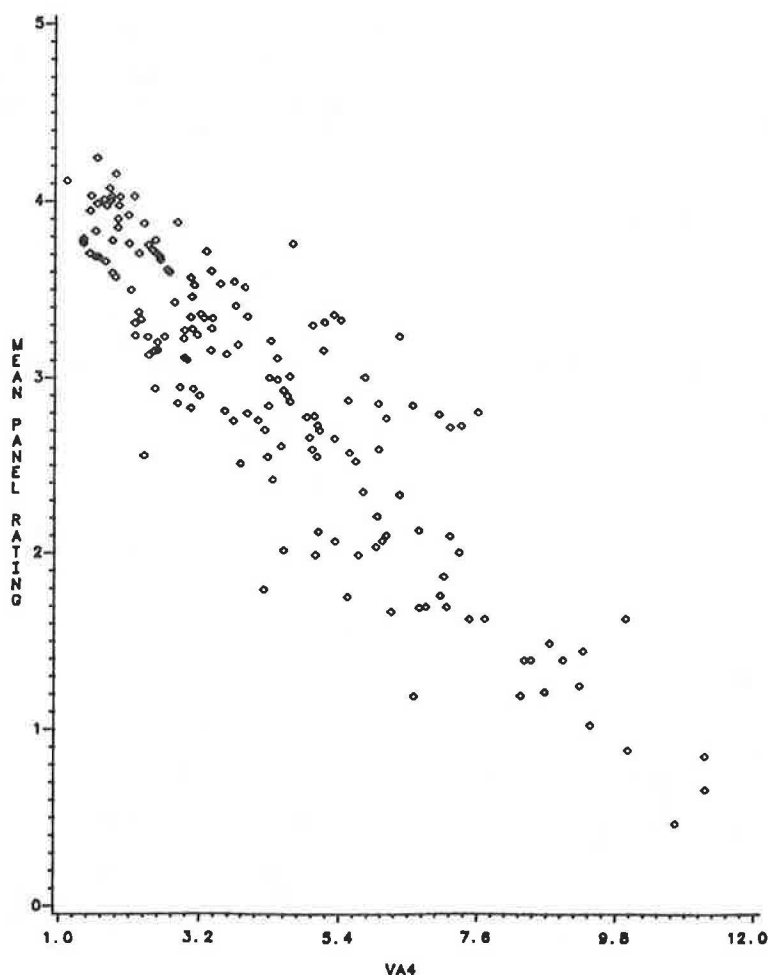
FIGURE 5 PSR versus VA$_4$.

models and R^2 and Cp values were generated for each model. From this list, the best model was selected based on the R^2, Cp, and s^2 criteria. Diagositc checks were made on each of the selected equations to verify that the assumptions of regression were fulfilled satisfactorily. Plots of the predicted values and the residuals were examined and the normality of errors was checked using the W-statistic or the D-statistic, as appropriate.

FINDINGS AND CONCLUSIONS

Based on the controlled experiment designs discussed earlier in this paper, the main effects of the variables associated with the rating process were found to be significant or not significant at the 0.01 α-level as shown in Table 1.

The conclusion is that the position of the rater in the car (whether in the front or rear) does not influence the rating. Similarly, it can be concluded that whether the rater is male or female, young or old, riding in the vehicle or driving the vehicle, or is a technically experienced person or not, has no effect on his or her rating; also, whether the rating is done during any particular time of day has no effect on the rating. These findings support the relationship between roughness (as manifested through the road surface and vehicle characteristics) and the rating of ride quality. The finding that vehicle speed has no effect on rating appears contrary to

expectation; however, it should be expected that the interaction between vehicle speed and road roughness would be significant. The conclusion here is that the rater's receptor system adjusted for the range of levels considered (30 mph versus 50 mph) in such a way that there was no significant difference in his or her ratings.

The variables that indicated a significant effect on rating at the 0.01 α-level were vehicle wheelbase, vehicle size, and rater fatigue. The effect of different vehicle characteristics on the perceptions of ride quality is exemplified here. It was found that raters expressed lower ratings (as much as 1.5 serviceability units) while riding in short wheelbase vehicles compared with longer wheelbase vehicles. The role played by vehicle characteristics in the rating process has been shown by the significance of the effect of vehicle size on rating. The significance of rater fatigue as a variable demonstrated the sensibility of the rater via-à-vis the condition of his or her receptor system.

Two pavement-related variables, pavement type and maintenance, were found to have significant effects at the 0.01-level, whereas surface texture, location of road, road width, and surroundings had no significant effect on ratings. Using regression analyses, a set of serviceability prediction equations was developed. The best formulas obtained are listed next (PSI refers to present serviceability index and VA$_b$ is the measure of root-mean-square vertical acceleration associated with baselength b, ft).

Overall (167 sections):

$$PSI = 4.42 + 1.55 \; 10^{-3} \; VA_{0.5} - 0.311 \; VA_4$$
$$- 3.35 \; VA_{64}$$
with $R^2 = 0.86$, $s^2 = 0.10$.

Overall (with dummy variable PTYPE):

$$PSI = 4.31 = 0.039 \; VA_2 - 0.504 \; VA_8 - 822 \; VA_{128}$$
$$+ 0.366 \; PTYPE$$
with $R^2 = 0.88$, $s^2 = 0.09$.

Flexible (125 sections):

$$PSI = 4.43 - 0.016 \; VA_2 - 0.237 \; VA_4 - 0.4 \; VA_{32}$$
$$- 10.4 \; VA_{128}$$
with $R^2 = 0.89$, $s^2 = 0.10$.

$$PSI = 5.00 - 0.0029 \; VA_{0.5} - 0.2609 \; VA_4$$
$$- 5.006 \; VA_{64}$$
with $R^2 = 0.82$, $s^2 = 0.15$.

Rigid (42 sections):

$$PSI = 4.34 - 0.092 \; VA_4 - 0.47 \; VA_8$$
with $R^2 = 0.73$, $s^2 = 0.03$.

The Mays meter data and the mean panel ratings showed good correlation for flexible sections (correlation coefficient $r = -0.91$). The correlation coefficient for rigid sections was found to be much lower ($r = -0.513$). Regression analysis on the overall sections indicated an R^2 value of 0.79, compared with 0.859 for the profilometer [refer to Nair (7) for prediction equations]. From this it was concluded that

1. The Mays meter can predict PSR better on flexible sections (with an R^2 of 0.83) than on rigid sections (R^2 of 0.26),
2. The SIometer can predict PSR better on flexible sections (with an R^2 of 0.56) than on rigid sections (R^2 of 0.11), and
3. The 690D SDP is by far the best overall predictor of PSR.

For all of the foregoing discussions, it should be remembered that Mays meter and SIometer data correlations have been obtained only after properly calibrating these devices.

The major development of this research study is a set of equations relating the ride quality of pavement sections to pavement roughness. This was achieved by relating a set of roughness summary statistics (RMSVAs associated with different wavelengths) obtained from the pavement profiles to the mean panel ratings. The study showed that up to 88 percent of the variation in PSR can be explained by the roughness variables; this a very high degree of linear association (a correlation coefficient of -0.94) between PSR and roughness as characterized by the set of RMSVAs. Thus, this study further attests to the serviceability-performance (S-P) concept in general, and to the validity of using road profile measurements to predict PSRs and to obtain indices of serviceability in particular.

REFERENCES

1. The AASHO Road Test: Report 5, Pavement Research. HRB Special Report 61-E, HRB, National Research Council, Washington, D.C., 1962.
2. W.R. Hudson. High-Speed Road Profile Equipment Evaluation. Research Report 73-1. Center for Highway Research, University of Texas, Austin, Jan. 1966.
3. Standard Definition of Terms Relating to Traveled Surface Characteristics. ASTM E867. American Society for Testing and Materials, Warrendale, Pa., 1982.
4. F.L. Roberts and W.R. Hudson. Pavement Serviceability Equations Using the Surface Dynamics Profilometer. Research Report 73-3. Center for Highway Research, University of Texas, Austin, April 1970.
5. D.W. McKenzie, W.R. Hudson, and C.E. Lee. The Use of Road Profile Statistics for Maysmeter Calibration. Research Report 251-1. Center for Transportation Research, University of Texas, Austin, Aug. 1982.
6. V.L. Anderson and R.A. McLean. Design of Experiments. Marcel Dekker, Inc., New York, 1974.
7. S.K. Nair, W.R. Hudson, and C.E. Lee. Development of Realistic and Up-to-Date Pavement Serviceability Equations Using the New 690D Surface Dynamics Profilometer. Research Report 354-1F. Center for Transportation Research, University of Texas, Austin, Aug. 1985.

Discussion

R. M. Weed*

This discussion pertains to both the paper and the project report (1) summarized in the paper. The authors have done many things extremely well and, in several ways, have illustrated how a thorough statistical analysis should be performed. However, there is one particular area in which a further refinement may be desirable. This involves the use of multiple linear regression and a perplexing result that obviously was of concern to the authors. After commenting on certain aspects of mathematical modeling,

*New Jersey Department of Transportation, 1035 Parkway Avenue, Trenton, N.J. 08625

I would like to suggest what might be a more appropriate theoretical model.

The primary goal is to find the mathematical model that most accurately describes the process being investigated. To this end, it is appropriate to use every resource available, including any prior knowledge of that process. In the case of pavement serviceability rating (PSR, the Y data) versus vertical acceleration (VA, the X data), it can be reasoned that if a pavement were so smooth that no vertical acceleration could be detected, it would be appropriate to rate it at a value of PSR = 5. At the other extreme, there is essentially no difference between a very high VA value and a slightly higher VA value; for all practical purposes both would correspond to PSR = 0. This suggests that the appropriate mathematical model will originate at (VA = 0, PSR = 5) and decline in some way to eventually become asymptotic to the X axis. (This assumes, of course, that the roughness-measuring device is sufficiently responsive to justify such a relationship. This must be confirmed by an examination of the data. If the device is not sufficiently responsive, it is unlikely that any mathematical model would be very useful, and the use of a different device would be indicated.)

A further consideration is a philosophical one. It is believed by many analysts that known prior knowledge (the engineering constraints on the intercept and the asymptote in this case) should take precedence over empirical statistical measures. In other words, if it were believed that a model of a particular form was fundamentally correct, it would be chosen in favor of a competing model that happened to have a higher correlation coefficient. The rationale is that, while the competing model might appear to have greater predictive power for this particular data set or range of data, the more theoretically appropriate model is likely to perform better in the long run (especially if, as so often happens with published research findings, it should be used outside the range of data from which it was generated).

A basic exponential decay function that is capable of satisfying the constraints on the intercept and the asymptote is given by Equation 1 in which A and B are constants and e is the base of natural logarithms. Other similar forms may also be used. If several different wavelengths of VA must be accounted for, then Bx in this expression would be replaced by a function f(x). Figure 6 illustrates three general shapes that these functions can take.
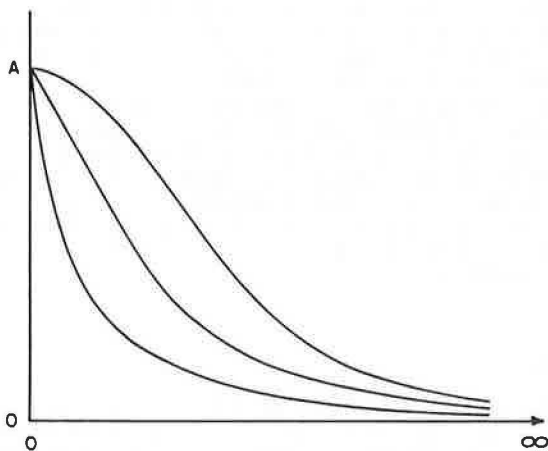
$$y = Ae^{-Bx} \qquad (1)$$

FIGURE 6 Examples of exponential decay curves.

If possible, because of the collinearity problem that the authors have duly noted ([1],p.115), it might be both practical and desirable to choose a single wavelength on which to base the equation. All the data plots ([1],pp.116-124) exhibit the same general trend and PSR versus VA_8, for example, would appear to have the most uniform variability about a fitted line.

The decision to use a linear model was apparently made by visual inspection ([1],p.115) of the data plots. However, in most of the plots presented in the report, it is very easy to visualize how the exponential forms in Figure 6 might more appropriately be fitted. (It should be noted that failure to locate the Y axis at VA = 0 in these figures tends to mask this effect.) One of the figures, PSR versus VA_{16}, is reproduced here as Figure 7 to illustrate an approximate exponential fit. (Actual exponential fits obtained by least squares with similar PSR data may be seen in the discussion of the paper by Janoff elsewhere in this Record.)

It is always disconcerting whenever an analysis produces a result that is inconsistent with a (presumed) known fact. The authors are appropriately concerned about the positive coefficient for $VA_{0.5}$ in the overall equation for PSI, reproduced here as Equation 2. This implies that, if VA_4 and VA_{64} were held constant, the PSI improves as $VA_{0.5}$ increases, an obviously incorrect conclusion as they have noted. Although the authors state that there is no evidence of incorrect specification of the model, this result in itself may be an indication that the chosen form of the model (linear) is inappropriate. Their attempt to obtain a better model was unsuccessful, most likely because only linear models were considered.

$$PSI = 4.42 + 0.00155\ VA_{0.5} - 0.311\ VA_4 \\ - 3.35\ VA_{64} \qquad (2)$$

The authors' investigation of a model with the intercept forced to be at PSI = 5.0 was certainly sound and logical but, unfortunately, had little chance for success unless it was also recognized that an exponential model was needed. In the form given by Equation 1, for example, this would involve setting A = 5 and determining the coefficient B by regression.

Still another troublesome factor may come into play. Figure 8 shows an example illustrating how data conforming to the same fundamental exponential relationship can produce two distinctly different equations when linear regression is used. If flexible pavements tend to be smoother than rigid pavements (as is the case in the state of New Jersey), they lie farther up on the exponential curve. If analyzed by linear regression, they produce a steeper slope than that obtained from the data representing rigid pavements. In this case, depending on where these lines cross, either could be falsely perceived to serve better than the other. An effect similar to this may also be present in the Texas data.

A final point is very speculative. Roughness measurements produced by wavelengths that are similar in length are stated to be correlated ([1],p.115), resulting in a collinearity problem among the several independent variables of the multiple regression. Because the measurements in question deal with a vibrational phenomenon, there may also be some sort of harmonic relationship between wavelengths that are integral multiples of each other. It is possible that the positive coefficient in Equation 2 is the result of correlation among the measurements obtained from different wavelengths. If it is absolutely necessary to include more than one wavelength, perhaps
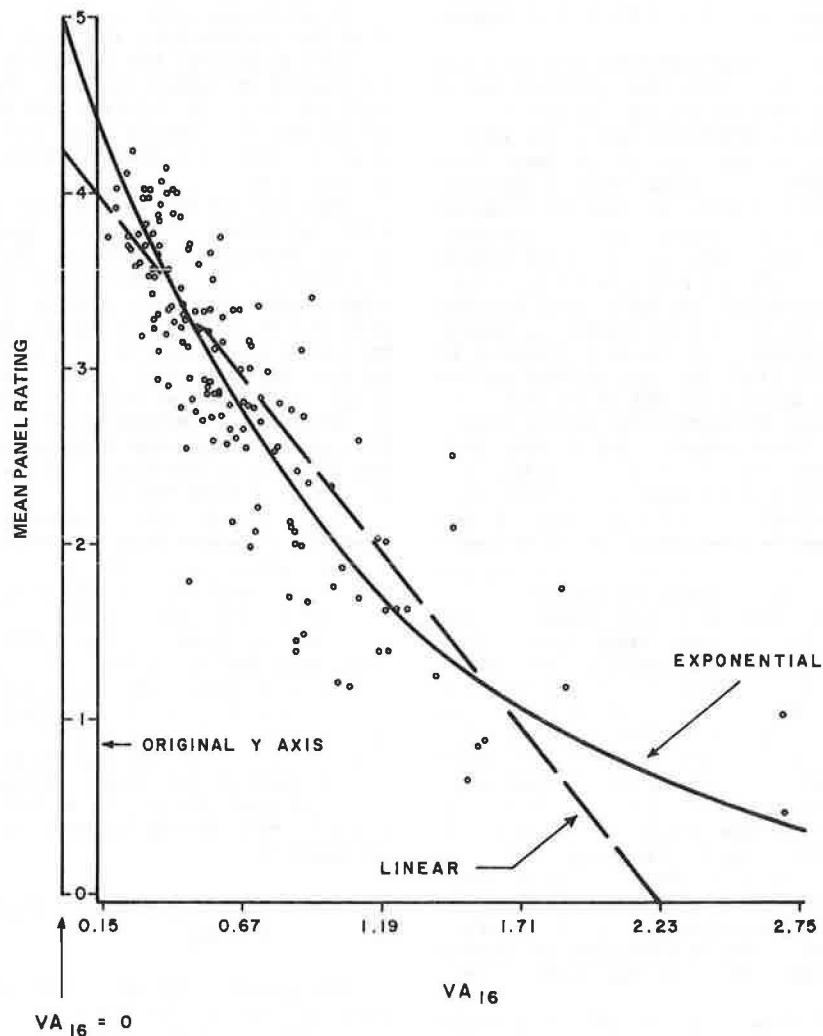
FIGURE 7 Approximate linear and exponential fits.
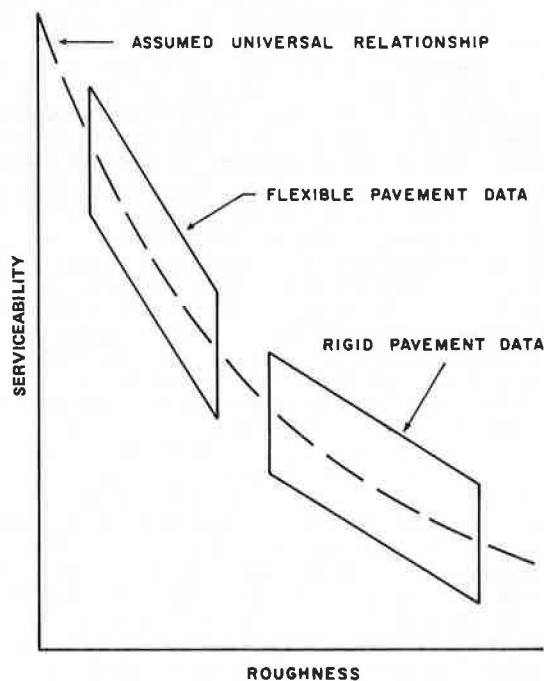
FIGURE 8 Conceptual illustration of a condition that can produce different linear regression lines.

it would be better to choose wavelengths that cannot produce harmonic frequencies.

In view of the apparent problem with a linear model, as well as the possible collinearity problem, it may be inappropriate to conclude that rigid pavements are perceived to serve better than flexible pavements ($\underline{1}$,p.133). The use of a dummy variable representing pavement type in the PSI equation ($\underline{1}$,p.130) may be unnecessary if an exponential model is used. It is also conceivable that some of the other conclusions regarding performance of the various types of equipment might be altered to some extent with an exponential model.

In summary, the authors have conducted a very thorough experiment and have made an important contribution to the understanding of the perception of pavement serviceability. Consideration of exponential models that satisfy the fundamental engineering constraints, and a concerted effort to avoid the collinearity problem, may serve to further enhance their efforts.

REFERENCE

1. S.K. Nair, W.R. Hudson, and C.E. Lee. Realistic Pavement Serviceability Equations Using the 690D Surface Dynamics Profilometer. Research Report 354-1F. Center for Transportation Research, University of Texas, Austin, Aug. 1985.

Authors' Closure

We are most appreciative of Weed's discussion of our paper. In general, we agree with his comments and thank him for his very careful review of our work. It is generally true that every available modeling resource should be used in conceptualizing a problem and we did attempt to do this.

It is not necessarily true that boundary conditions such as proposed of VA = 0, PSR = 5 will always govern such concepts and it presumes too much knowledge of the problem. In reality, a VA = 0 may not, for example, be attainable on a pavement nor may it be considered perfect by the average rater. Furthermore, any time individual raters are forced to use a scale that is bounded, such as 0 to 5, it is almost precluded that the average of a set of 10 or more raters can ever equal 5.0. For these reasons, it is difficult, in our opinion, to consider forcing the model through an origin of VA = 0, PSR = 5.0.

We concur wholeheartedly that the exponential form should be considered. We chose to consider and use the basic linear form because we were replacing an existing equation with the linear form, and the sponsors desired minimum acceptable change. We do agree, however, that the exponential model is a worthwhile model to examine, and we will examine that possibility as time permits. There is not sufficient time, however, to do so for this closure.

Review of the relationship between vertical acceleration and serviceability rating leads to the conclusion that several wavelengths are necessary to fulfill the correlation. Therefore, Equation 1 as proposed by Weed will involve a more complicated function of X.

The comments about the relative smoothness of rigid and flexible pavements in the state of New Jersey are not applicable to Texas pavements. In general, Texas pavements in the study exhibited similar roughness ranges for rigid and flexible. We will certainly attempt to further investigate the concept of nonharmonic wavelengths as further work is permitted.

In summary, we greatly appreciate Weed's contribution and his thoughtful review and ideas in extending this work. We will certainly take them into account as additional work progresses.

The International Road Roughness Experiment:
A Basis for Establishing a Standard Scale for
Road Roughness Measurements

M. W. SAYERS, T. D. GILLESPIE, and C. A. V. QUEIROZ

ABSTRACT

With the general lack of equivalence between the many methods and measures by which road roughness is characterized, standardized indices offer the means to achieve a time-stable data base that can be utilized by all. The International Road Roughness Experiment (IRRE) was organized in Brasilia, Brazil, to find a suitable index and to quantify the relationships between different equipment and roughness indices in use. Roughness measurements were made on 49 test sites by diverse types of equipment in common use. The data were analyzed to determine the equivalence between the roughness measures that could be obtained with each type of equipment and whether one common measure was applicable to all. The results from the IRRE showed that a standard roughness index is practical and measurable by most of the equipment in use today, whether of the profilometer or road meter type. As a result of the IRRE, a standard index was selected that is based on the quarter-car analysis method with standard parameter values and a reference speed of 80 km/h. Provided in this paper is the background on the fundamental of roughness characterization that guided the selection of the standard road roughness index.

Roughness is an indicator of road condition and is useful for making objective decisions related to the management of road networks. Today roughness is measured by many methods (ranging from rod and level surveys to instrumented vehicles) and may be quantified by any of a number of measures or indices. With the growth of the base of roughness data in recent years, it has become painfully clear that the many different methods and indices used for characterizing road roughness are generally not equivalent. Many early methods came into existence as a consequence of what could be measured, although progress is being made today in identifying what should be measured (1). In many cases, the measures are determined by the performance of hardware that cannot be adequately controlled to achieve time-stable data. Thus, utilization of roughness data can be difficult, particularly when considering roughness data obtained by more than one method. Establishing standard roughness indices is a way to eliminate most of these problems. Yet, it should be recognized that more than one index may ultimately be needed to satisfy the differing needs to quantify roughness influence on ride comfort, vehicle vibrations, surface distress, and other factors.

The International Road Roughness Experiment (IRRE) was proposed by the World Bank and the government of Brazil to find a standard roughness index appropriate for the many types of roughness measuring equipment now in use, and to provide a basis for comparing roughness measures obtained by different procedures

and instruments. The IRRE was held in Brasilia, Brazil, in 1982, and was conducted by research teams from Brazil, the United Kingdom, France, the United States, and Belgium. Forty-nine road test sites were measured using a variety of test equipment and measurement conditions. The sites included a full roughness range of asphaltic concrete, surface treatment, gravel, and earth roads. The data acquired were analyzed to determine the extent to which the different types of equipment could be used to obtain a common measure of roughness and how the different measures of roughness in common use could be related quantitatively.

The results from the IRRE showed that a standard roughness index is, in fact, practical, and an index was proposed that is measurable by most of the equipment now in use, including road meters and profilometers (2). This selected measure has been denoted as the International Roughness Index (IRI). The IRI is based on the quarter-car analysis method, with standardized parameter values and a reference simulation speed of 80 km/h. Guidelines have recently been published for measuring the IRI with the various instruments currently available throughout the world (3).

This paper is intended to provide some of the background relevant to the selection of the IRI, concentrating mainly on the concept of roughness as a property of the longitudinal profile of the traveled wheeltracks of the road. It is also intended to cover the fundamental similarities and differences between the different approaches that have been taken toward calculating a single roughness index from the measured profile of the road.

M.W. Sayers and T.D. Gillespie, Transportation Research Institute, The University of Michigan, 2901 Baxter Rd., Ann Arbor, Mich. 48109. C.A.V. Queiroz, Instituto de Pesquisas Rodoviarias, Departmento Nacional de Estradas de Rodagem, Centro Rodoviario, Km 163-Rodovia Presidente Dutra, 21240-Rio de Janeiro-RJ, Brazil.

TYPES OF ROUGHNESS-MEASURING EQUIPMENT

The equipment in common use for measuring roughness falls into two generic categories. In the first--

profilometric methods--the longitudinal elevation profile of the road is measured and then analyzed to obtain one or more roughness indices. Both manual quasistatic methods and high-speed profilometers are in use, with the high-speed profilometer systems being more popular in developed countries and the manual methods being a practical alternative in developing countries. In the second category--response-type road roughness measuring systems (RTRRMSs)--a vehicle is instrumented with a road meter device. The road meter produces a roughness reading as the result of the vehicle motions that occur while traversing the road. RTRRMSs offer a means to rapidly acquire roughness data with relatively inexpensive equipment. However, the roughness measure is intimately tied to vehicle response, which varies among vehicles and also varies with time, vehicle condition, and weather. Thus, the RTRRMS measures are less accurate in general, and require a fairly complicated calibration to convert the measures to a standard scale.

Today, the majority of roughness data are obtained with RTRRMSs, and therefore the IRI must be compatible with the RTRRMS-type of measure if it is to be widely used. For this reason the IRRE included three Mays meter cars (4), a car with Bump Integrator (5) and National Association of Australian State Road Authorities (NAASRA) road meter (6), a Bump Integrator trailer (5), and a Bureau of Public Roads (BPR) roughmeter (7). The use of profilometric methods is rapidly growing, however, offering greater measuring capabilities and accuracy. Thus, it is also essential that the IRI be compatible with instruments that can measure the profile directly in order to avoid premature obsolescence. Four profilometer methods were included in the IRRE: rod and level surveys, the French Bridge and Pavement Laboratory (LCPC) longitudinal profile analyzer (APL) (8), the Transport and Road Research Laboratory (TRRL) Beam, and a General Motors Research (GMR)-type inertial profilometer (9).

ROUGHNESS MEASURES

There was complete agreement among the participants in the IRRE that the IRI should be defined as a property of the true road profile so that it can be measured directly with profilometers. At the same time, the index should be strongly correlated with the measures obtained with RTRRMSs so that their measures can be converted to the IRI scale with maximum accuracy.

Analyses of the IRRE data showed that all of the RTRRMSs give highly correlated measures when they are operated at the same test speed and that all could be calibrated to a single roughness scale without compromising their accuracy. Thus, the selection of an IRI was largely a matter of choosing a standard RTRRMS speed, and then choosing an analysis by which the profile can be reduced to a single index that is highly correlated with the RTRRMS measures obtained at that speed. Although it would appear that there are many existing and possible roughness indices that may be considered, in actuality, many are equivalent in the fundamental properties that are being quantified. The equivalence can be best understood by considering the ways in which a profile may be reduced to a summary index.

Techniques for Calculating Roughness from Profile

What exactly is road roughness? A qualitative definition is that roughness is "the variation in surface elevation that induces vibrations in traversing

vehicles." Thus, texture properties that contribute to tire noise vibrations are a form of road roughness. At the other extreme are long undulations that cause low-frequency bounding vibrations in a vehicle at high speeds. In order to quantify the roughness of the longitudinal profile of a wheeltrack, an analysis is needed to reduce the continuous profile to a single summary index. For use as an IRI, a profile analysis must include those roughness components that affect the RTRRMS measures, while excluding the components that are unrelated. Some profile analyses are essentially incompatible with the RTRRMS measure, so that good correlations (r^2 values of 0.9 and higher) cannot usually be obtained in the field. In this paper, only those analyses are considered that are closely linked with RTRRMSs.

Summary Statistics: Root-Mean-Square and Average Rectified Values

Because vertical deviations in a profile occur both in the positive and negative direction, they tend to average out over distance. Two methods of profile analysis are widely used to avoid this cancellation and meaningfully summarize the deviations. One of the methods is to square the amplitude of the variable so that it will always be positive. The result is a mean-square average of the variable of interest. The statistical properties of squared variables are well known, and therefore this method is a convenient first choice of statisticians. Often, the square root of the average--the root-mean-square (RMS) average-- is used to keep the original units of the variable. The second method is to take the absolute value of the variable (rectify it) so that it will always be positive and use the average rectified (AR) value. Indices obtained using this technique are sometimes called absolute mean values or mean absolute values. This method is easier to apply directly during measurement and has been implemented by using either one-way mechanical clutches or electronic counters in nearly all road meters used in RTRRMSs.

In published studies, there has been little difference in the results obtained using RMS summary measures versus AR measures (10). The main difference will occur when roughness varies along the length of the road, in which case the RMS method will tend to weight the rougher section more when averaging than will the AR method. For example, consider two adjacent sections of road, each 1 mi long, with the second mile twice as rough as the first. The mean-square roughness for the second mile will be four times that of the first, and the RMS roughness for the combined 2-mi section will be 1.58 times the roughness of the first mile. Using the AR method, the combined roughness would be the simple average, being 1.50 times the roughness of the first section.

Variation in Profile Elevation

A logical first choice for characterizing the roughness of a profile might be to use the RMS or AR value of the profile elevation itself. Unfortunately, such a simple measure proves to be strongly dependent on the measurement method used. The reason for this is that all roads have a characteristic distribution of the profile variation over wavelengths. Although it is true that different surface types will have unique signatures in their roughness distribution, all surface types are alike in that elevation amplitudes increase by many orders of magnitude over the wavelength range of interest, while the slope amplitudes are approximately constant over all wavelengths. (In this context, the word constant means that the amplitudes are within several orders of magnitude.) This

leads to some useful generalities, which apply now only to analyses based on profile elevation, but also to those based on profile slope and profile vertical acceleration. Some of these generalities will now be illustrated by example, based on profiles obtained by rod and level survey (vertical precision = 0.001 ft; longitudinal interval = 1.0 ft).

Before examining the profiles, it is worth noting that the true variation in profile elevation is not suitable as a measure of roughness. The inclusion of hills would yield roughness measures that are dominated by the height of the hills. If the road happens to be going up a hill, even if the road is perfectly smooth, the elevation will change considerably, and a high variation would be obtained because of the hill, not the road surface. Therefore, in the example, the underlying hill (as determined by the mean slope value) was removed before the plots were prepared.

Figure 1a shows the measured elevation profile of one wheeltrack of a relatively smooth pavement (plotted with different scale factors in the longitudinal and vertical directions in order to show the profile details). The variation may be summarized in a roughness index using the AR method by the average height of the cross-hatched area (area divided by length).
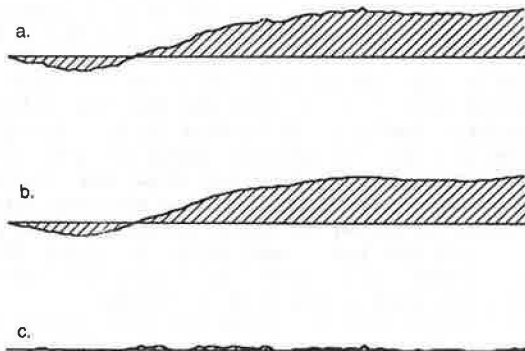

FIGURE 1 Effect of long and short wavelengths on roughness derived from profile elevation. (a) Full profile: roughness is indicated by cross-hatched area. (b) Reduction of short wavelengths has almost no effect on roughness. (c) Reduction of long wavelengths has a very strong effect on roughness.

The profile can be processed mathematically to filter out certain wavelengths, as is commonly done with some roughness measurement methods. Figure 1b shows that when the short wavelength variations caused by texture and localized defects are removed from the profile, the area (the roughness measure) is essentially unaffected. On the other hand, Figure 1c shows that when the longer wavelengths are removed, most of the area is eliminated and that the roughness would be much lower. The variation in elevation is strongly influenced by the longest wavelength included in the measurement. High-speed profilometers, such as the APL trailer and the General Motors (GM)-type inertial design, generally have a limit as to the longest wavelength that can be measured, determined by the design of the particular instrument and (usually) the travel speed during profile measurement. Because each has different limits on wavelength, they would not measure the same roughness (the largest values being obtained by the instrument that sees the longest wavelengths). When profile is measured with rod and level, there is no limitation of the type observed with profilometers

because even the static slope of the road is included in the measure. Practically speaking, however, the longest significant wavelength is largely determined by the length over which the survey is made, so the roughness becomes a function of length.

Thus, pure elevation variation is unacceptable as a roughness index because it is influenced by the longest wavelength observed by the profilometric measurement method. Even in the case of perfect measurement (rod and level or equivalent), the index is influenced by the length of the profile. In order for a roughness index based on elevation to be valid for more than one particular profilometer or test length, the longest wavelength of interest must be clearly identified and then all longer wavelengths must be attenuated through an appropriate analysis. Several analyses that do this were used in the IRRE and three of those are described later.

Variation in Profile Slope

Traditionally, most roughness measures do not use units of elevation, but instead use units of slope. The early AASHO and rolling straightedge profilometer (CHLOE) instruments produced a measure called slope variance, and most RTRRMSs provide a measure with units of slope, such as mm/km or inches/mi. As with elevation, however, the true slope variance of the road is also an unmeasurable property. Figure 2a shows the slope profile of the same road as used in the previous figure. (The slope was computed by tak-

FIGURE 2 Effect of long and short wavelengths on roughness derived from profile slope. (a) Full profile: roughness is indicated by cross-hatched area. (b) Reduction of short wavelengths decreases roughness. (c) Reduction of long wavelengths decreases roughness.

ing the difference in adjacent elevation values and dividing by the separating distance.) In the slope profile, the shorter wavelengths are seen to be more significant than for the case of the elevation profile. Once again, the roughness, defined by average rectified slope (ARS), is proportional to the average height of the cross-hatched area. Figures 2b and 2c show that the average height is reduced by removing short wavelengths and also by removing long wavelengths. The quarter-car analysis, described later, is able to produce a standard roughness index by limiting both the long and short wavelengths outside of the range of interest.

Although the variation in profile slope is only moderately influenced by the longest wavelength included in the measure, nonetheless, the true slope

variance is an unmeasurable property. Figure 3 shows why. When inspected closely enough, any road profile will change elevation abruptly at some point, showing a change in height that occurs over zero distance. The profile is vertical, and at that point, the true slope is infinite. Consequently, the RMS slope and ARS measures are also infinite. Figure 3 also shows that when the profile elevation is sampled at discrete locations that are a fixed distance (ΔX) apart, the slope values will be finite. The maximum slope measured will be decreased as longer sample intervals are used.

FIGURE 3   Illustration of the infinite slopes that occur in an elevation profile.

Variation in Spatial Vertical Acceleration

Figures 4a, 4b, and 4c show the corresponding profiles for the second derivative of profile--spatial vertical acceleration. In this case, the average height of the cross-hatched area is determined most strongly by the shortest wavelength that is included
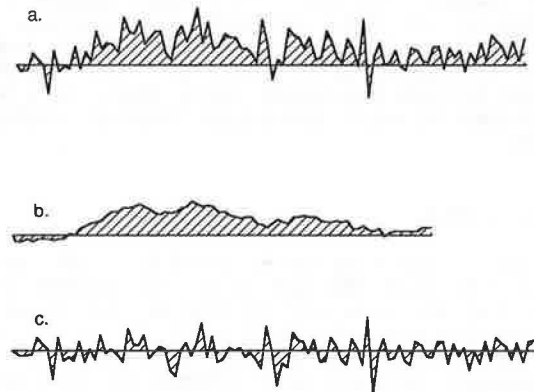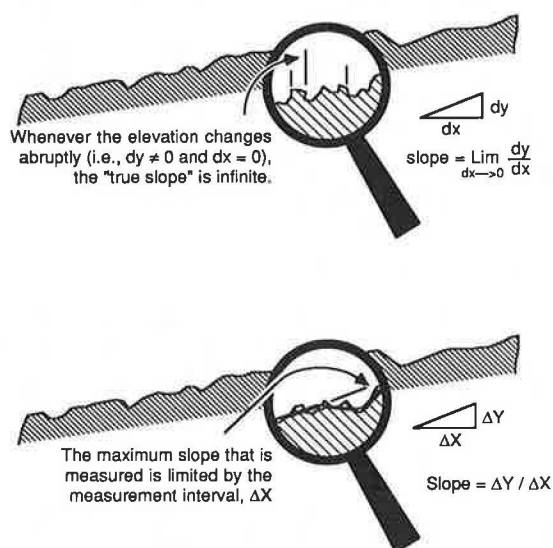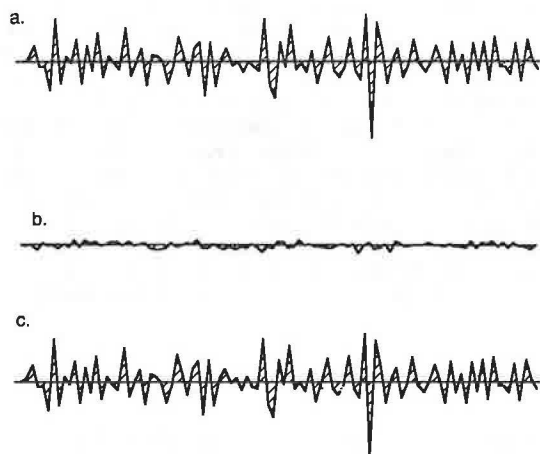

FIGURE 4   Effect of long and short wavelengths on roughness derived from profile spatial acceleration. (a) Full profile: roughness is indicated by cross-hatched area. (b) Reduction of short wavelengths has a very strong effect on roughness. (c) Reduction of long wavelengths has almost no effect on roughness.

in the measure. Figure 3 shows that the true slope of a road profile will be infinite at many points. Similarly, the true vertical acceleration will also be infinite at many points. (It will be infinite if there are discontinuities in slope, even if the slope is itself finite.) In a sense, the vertical acceleration is similar to the elevation; the roles of the long and short wavelengths are reversed. In this case, a valid roughness index must be based on an analysis that clearly identifies the shortest wavelength of interest and attenuates all shorter wavelengths. The RMSVA analysis, which does this, is described later.

Table 1 gives a summary of the sensitivity that each of the three simple roughness indices have to the wavelengths included in the measurement.

Moving Average--The Belgian Coefficient of Evenness Measure

The profiles shown in Figures 1-3 were filtered using an analysis called a moving average. The profile is smoothed by averaging adjacent elevation values together, as shown in Figure 5. With an additional step, the same analysis can be used to eliminate the long wavelengths while leaving the shorter ones. To do this, the smoothed profile is subtracted from the original, such that the long wavelength portion is cancelled out, leaving only the shorter wavelengths. This was done in Figure 1c by using a moving average of 5 m (16 points).

This type of analysis is used by several agencies, including the Belgian Road Research Center (CRR), as a means for quantifying roughness based on an elevation profile ($\underline{11}$). In Belgium, the roughness index is calculated by using the AR method, and the measure is called the coefficient of evenness (CP). It is reported in CP units, where one CP unit is 0.020 mm. The moving average analysis is dependent on the baselength used in the averaging, and therefore it is customary to subscript the baselength used, for example, $CP_{5.0}$.

When there are many samples included in the baselength (10 or more), the effect of sample interval is negligible if the same baselength is kept. By processing the same profile using different baselengths, information about different wavelengths can be extracted. The CP value is most sensitive to wavelengths that are close to the baselength used to define the moving average. For example, the $CP_{2.5}$ numeric primarily indicates roughness over the wavelength range of 1.2 to 5 m, with maximum sensitivity at the wavelength corresponding to the baselength of 2.5 m.

The CP analysis is conceptually that of the AR elevation shown in Figure 1. The problem with the true AR elevation being sensitive to profile length (and unmeasurable with a high-speed profilometer) has been eliminated by intentionally filtering out wavelengths longer than the band of interest.

APL 72 Short-Wave Energy Index

The French Bridge and Pavement Laboratory (LCPC) uses the mean-square method for summarizing the energy of variations in profile elevation and eliminates the effect of wavelengths outside of the desired range using electronic band-pass filters ($\underline{8}$). Typically, the profile is measured electronically and stored as a voltage on an FM tape recorder. The tape is played back in the laboratory into three independent filters that summarize the short, medium, and long wavelength components of the measured signal. Each one of these filters acts similarly to two moving averages: one

TABLE 1 Effect of Wavelengths on Profile Variations

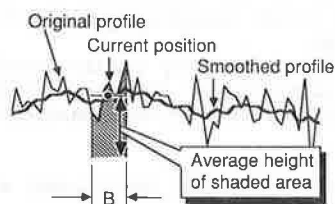| Effect of Including	On Elevation	On Slope	On Vertical Acceleration
Longest wavelengths	Increases variation greatly	Increases variation	Negligible effect
Shortest wavelengths	Negligible effect	Increases variation	Increases variation greatly

FIGURE 5 Illustration of the process of filtering with a moving average.

eliminating the long wavelengths and one eliminating short wavelengths. The short-wave index, covering wavelengths from 1.0 to 3.3 m/cycle correlates well with the RTRRMS measures.

Although the details of this electronic technique share little in common with the numerical moving average method, the results are nearly identical because the theoretical responses of the two forms of analysis are similar for the longest wavelengths included in the analyses. The analyses treat short wavelengths very differently (the APL 72 system completely eliminates short wavelengths, whereas the CP analysis leaves them intact), but because the short wavelengths have, at most, only a slight effect on the summary index, this has a negligible influence when the analyses are applied to real road profiles.

RMSD--The TRRL Beam Analysis

The British Transport and Road Research Laboratory (TRRL) overseas unit has developed an instrument for statically measuring profile in developing countries that has been called the TRRL Beam. The beam measures elevation profile along individual 3-m sections and includes a microcomputer that is programmed to compute a roughness statistic based on an analysis that is, in concept, similar to the moving average (2).

In the RMSD analysis, the profile is processed in discrete sections equal in length to a standard baselength, such as 1.8 m. A linear regression line is computed for the profile length yielding an equation of the form

$$\ddot{y} = a + b \cdot x \tag{1}$$

where x is the longitudinal distance, $\ddot{y}$ is the estimate of the profile elevation at position x, and a and b are determined by a least-squares fit. At each position, there will be a deviation between the measured elevation value and the estimate from the linear regression line. The RMS deviation (RMSD) is used as the roughness index. The profile is processed one segment at a time, but the RMSD is accumulated over the entire profile. The TRRL overseas unit recommends that both the baselength and the measurement interval be standardized, with values of 1.8 m and 300 mm, respectively.

The RMSD analysis is approximately similar to the RMS value of elevation. The problem with true RMS

elevation being dependent on measurement length has been controlled by using the linear regressions over a 1.8-m baselength to eliminate wavelengths outside of the range of interest.

Because most roughness data have units of slope instead of displacement, a conversion equation is used by TRRL to rescale the RMSD measure to an estimate of an idealized RTRRMS [the TRRL Bump Integrator (BI) trailer, as it performed in the 1982 IRRE]. The conversion is based on a quadratic equation derived by correlating RMSD values with the ARS measures from the RTRRMS. The equation is

$$RBI_{32r} = 472 + 1437 \cdot RMSD + 225 \cdot RMSD^2 \tag{2}$$

where RBI is the reference bump integrator (RBI) index, based on a travel speed of 32 km/h and estimated from RMSD. RBI is assigned arbitrary units of mm/km to match the BI trailer, and RMSD has units of mm.

Quarter-Car Analysis

For the last 10 years, roughness measures similar to those obtained from RTRRMSs have been computed from profile measurements using a quarter-car simulation (QCS). A QCS is a mathematical model found in many dynamics textbooks. The response of this model is influenced by several parameters that describe the vehicle being simulated, including two masses, two spring rates, a damping rate, and a simulation speed. The first quarter-car simulation was intended to replicate the measures from RTRRMS developed by the Bureau of Public Roads, called the BPR roughometer. In 1979, a standard set of vehicle parameters selected to maximize correlation with RTRRMSs was proposed in an NCHRP research project (12). Details about the QCS analysis have been described many times (2,3,12-14) and will not be repeated here.

Unlike the preceding three analyses, the QCS is close in concept to an average slope measure, rather than elevation. Basically, the analysis acts as a filter that removes both long and short wavelengths outside of the range of interest so that the AR slope that is reported can be independent of the method used to obtain the profile measurement. Using the standard model parameters from the NCHRP project (12), this measure is called reference average rectified slope (RARS). The measure included an effect due to simulation speed, and therefore the speed is usually subscripted. For example, measures made by using a simulation speed of 80 km/h are reported as $RARS_{80}$.

RMSVA

Root-mean-square vertical acceleration (RMSVA) is an analysis illustrated in Figure 6. Figure 3 shows that an approximation of the first profile derivative-- the slope--is calculated as $\Delta Y/\Delta X$, where ΔY is the change in profile elevation and ΔX is the distance between those elevation measures. In Figure 6, the slope is calculated by using an arbitrary baselength B, which is an integer multiple of ΔX. Re-

a.

$$S1 = [y(x) - y(x - B)] / B$$
$$S2 = [y(x + B) - y(x)] / B$$

Slope = $\Delta y / B$
"V.A." = ΔSlope / B

$$VA = (S2 - S1) / B$$
$$= [y(x + B) + y(x - B) - 2y(x)] / B^2$$

b.

$$MCD = y(x) - \frac{1}{2}[y(x + B) + y(x - B)]$$
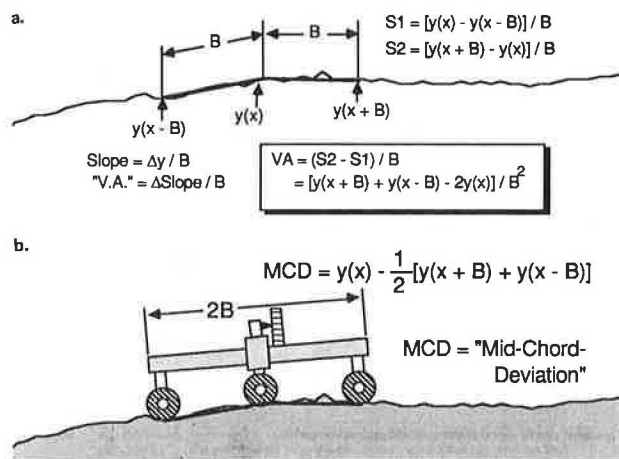
MCD = "Mid-Chord-Deviation"

FIGURE 6 Analysis of the RMSVA and its equivalence to mid-chord-deviation. (a) The RMSVA analysis is obtained by applying a finite-difference slope equation to the profile to compute slope and then applying the same equation again to obtain a form of vertical acceleration. (b) The RMSVA analysis is a rescaled version of the mid-chord-deviation, as measured with a rolling straightedge.

peating the difference equation again gives an approximation of the second derivative--the vertical spatial acceleration. This variable will approach the vertical acceleration of the profile as the baselength B approaches zero. When B has larger values, the analysis attenuates the short wavelengths contributing to vertical acceleration. Because the baselength affects the index, the baselength should be subscripted, for example, $RMSVA_{2.5}$.

The RMSVA statistic can be considered as the RMS value of vertical acceleration with wavelengths outside of the range of interest attenuated by the use of a long baselength. This is somewhat confusing, however, because the attenuation is not as simple as with all of the other analyses mentioned earlier. As a result, most of the roughness included in the RMSVA numeric comes from wavelengths outside of the region where the analysis approximates vertical acceleration. As will be shown later, the analysis is identical to a rolling straightedge, and the RMSVA statistic is perhaps better understood by thinking of it as the mid-chord-deviation obtained from a rolling straightedge.

RMSVA is not actually used directly as a roughness index, but as a building block for defining an index. Two such indices are in use: the quarter-car (QI) index developed in Brazil, and the reference Mays meter (MO) index developed in Texas.

QI_r

The QI_r analysis was developed by Brazilian researchers as a means for using profiles measured with rod and level to calibrate RTRRMSs (10). The analysis was needed to replace a quarter-car index measured with a specific profilometer system, which experienced hardware problems that made its reliability suspect. Using a data base consisting of QI measures from the profilometer and RMSVA measures from rod and level, the following equation was derived:

$$QI_r = -8.54 + 6.17 \cdot RMSVA_{1.0} + 19.38 \cdot RMSVA_{2.5} \quad (3)$$

where RMSVA is to have units of mm/m² = $1/m \cdot 10^{-3}$, and QI_r has the arbitrary units of counts/km. (The r subscript indicates the index derives from RMSVA.)

MO

The MO analysis was developed in Texas, also as a means for calibrating RTRRMSs (14). Following the same method used in Brazil, a correlation was developed between RMSVA measures (from a profilometer) and ARS measures from several RTRRMSs with installed Mays meters. The reference Mays meter index was defined as

$$MO = -20 + 23 \cdot C \cdot RMSVA_{1.2} + 58 \cdot C \cdot RMSVA_{4.9} \quad (4)$$

where C is a constant needed for unit conversion from a spatial acceleration to a temporal acceleration.

The MO index was not considered during the IRRE; it is included here because it has been the subject of several recent publications and because it is so similar to the QI_r index that generalizations about QI_r also apply to the MO.

Rolling Straightedge

One of the earliest approaches to measuring a profile property directly to obtain roughness was the rolling straightedge, sometimes called a profilograph. With this type of instrument, a rolling straightedge is used to establish a reference datum, and deviations from that reference are measured and summarized by using the RMS or AR method to obtain a roughness measure. Figure 6b shows a simple view of such an instrument. The AASHO profilometer, the CHLOE profilometer, and the University of Michigan profilometer were all variations of the rolling straightedge concept. The first validation of the high-speed GM-type of inertial profilometer involved demonstrating that when a profile is processed using a rolling straightedge analysis, agreement is obtained with the measures from a rolling straightedge instrument (9).

Figure 6 shows that the equation describing the mid-chord-deviation from the rolling straightedge is nearly the same as the RMSVA equation. The only difference is in the scale factor of 2/B² used in the RMSVA equation to present the measure with the units of spatial acceleration, rather than simple deviation. Thus, the RMSVA analysis is completely identical to a rolling straightedge with an arbitrary scale factor.

Comparison Between the Roughness Indices

Wavelengths

Each analysis described previously isolates wavelengths of interest from the measured longitudinal profile. Table 2 gives a summary of the parameters used in each analysis to control the wavelengths that contribute to the roughness indices. Given that the amplitudes of profile slope are fairly uniform over wavelength, it is convenient to calculate and plot the response of the roughness analyses to wave number (wave number = 1/wavelength) based on a slope input. By using the same type of input for each, the responses can be compared directly. Also, by choosing slope rather than elevation as the input, the relative significance of the different wave numbers can be easily observed. Figure 7 shows the responses of four of the profile analyses. Although the analyses differ in concept and development, because they have been optimized for correlation with RTRRMSs, they all end up responding to approximately the same wave numbers: 0.05 to 0.7 cycle/m (wavelengths from 1.5 to 2.0 m/cycle). In the IRRE and other experiments, good correlations have been found between RTRRMSs and all

TABLE 2 Summary of Wavelengths Observed by Profile Analyses

	Type of Statistic	Limit of long Wavelengths	Limit of short Wavelengths	Proposed Parameter Values
Moving average (Belgian CP)	Elevation (AR)	Baselength, B (wavelengths > 2B are attenuated)	Interval, ΔX^a	B = 2.5 m
APL 72 waveband	Elevation (RMS)	Filter cut-off Frequency 1	Filter cut-off Frequency 2[b]	Short-waves (1.0-3.3 m/cycle)
TRRL beam RMSD	Elevation (RMS)	Baselength, B (wavelengths > 2B are attenuated)	Interval, ΔX (exact effect is not known)	B = 1.8 m ΔX = 0.30 m
Quarter-car analysis (NCHRP Report 228)	Slope (AR)	Vehicle parameters, simulation speed	Vehicle parameters, simulation speed	NCHRP parameters, V = 80 km/h
RMSVA	Rolling straightedge (RMS)	Baselength, B	—	(See QI, MO)
QI_r (Brazil)	RMSVA (RMS)	Baselength, B	—	B1 = 2.5 m B2 = 1.0 m
MO (Texas)	RMSVA (RMS)	Baselength, B	—	B1 = 1.22 m B2 = 4.88

[a] The sample interval only has an influence when the baselength is less than 10 ΔX.
[b] The short-wavelength cut-off has only a secondary effect because road profiles naturally attenuate short wavelengths of elevation variables.
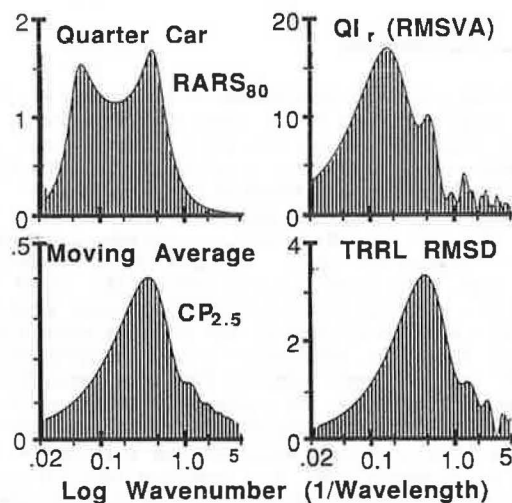

FIGURE 7 Sensitivity of four profile analyses to wave number.

of the analyses mentioned previously when the parameter values given in Table 2 are used.

Sample Interval--ΔX

All of the analyses except the APL 72 wave band can be performed numerically by computer. Thus, they can be applied to profiles measured statically by rod and level or to profiles measured with any high-speed profilometer whose profile signal can be digitally sampled. An important parameter in this process is the distance between samples, ΔX.

The choice of sample interval is usually selected for a profilometer based on hardware considerations, and a standard interval for all profilometers is nonexistent. To require a standard interval would seriously compromise the flexibility associated with profilometers, and in some cases, would also compromise their accuracy. Thus, it is important that the analysis chosen for the IRI be flexible regarding the required sample interval.

In the case of manual methods, such as rod and level, the choice of sample interval has a direct bearing on the work needed to perform a measurement. A small ΔX value means that more elevation measures are needed for a given road length. Because profiling by rod and level is slow and labor-intensive, it is always desirable to select the largest ΔX values that can be used while still obtaining a valid measure.

Table 3 gives a summary of the ranges of ΔX allowed for each of the analyses to provide the associated roughness index with negligible bias. (Although bias is eliminated when ΔX is within the ranges shown, better repeatability and reproducibility are usually obtained as ΔX approaches zero.) The broadest continuous range is allowed by the quarter-car analysis, including intervals up to 700 mm (slightly more than 2 ft). The largest interval is the 1.22 m (4 ft) that would be allowed for the MO analysis, but the range of values is not continuous. The RMSVA analysis essentially uses the baselength parameter as the sample interval, and therefore the analyses based on RMSVA will work for any interval that divides evenly into both of the baselengths. Therefore, while an interval of 1.22 m is valid for the MO analysis, an interval of 1.0 m is not. The TRRL analysis is standardized for 300 mm, and therefore only that interval is valid. Because the APL 72 energy analysis is not numerical, digitizing considerations are not applicable.

TABLE 3 Practical Considerations of Profile Analyses

	Allowable Sample Interval Range (mm)	Averaging Method for Subsections	Loss of Profile Length (m)	Value of Perfectly Smooth Road
2.5 m moving average, $CP_{2.5}$	0-250	Simple	2.50	0
APL 72 short-wave energy	—	RMS	—	0
Reference BI, TRRL beam $RMSD_{1.8,300}$	300	Complicated, (conversion + RMS)	—	472 mm/ km
Quarter-car analysis ($RARS_{80}$)	0-700	Simple	0.25	0
RMSVA (rolling straightedge)	B/k, k=1,2,...	RMS	B	0
QI_r (Brazil)	500, 250, 167, 125,...	No exact method	2.50	−8.54 counts/ km
MO (Texas)	1219, 610, 406, 305,...	No exact method	4.88	−20 in/ mi

Effect of Site Length

It is often convenient to compute roughness for relatively short sections, for example, 200 m long. Later, those measures are combined to apply the same measures to longer sections, for example, 1 km long. The method used to combine the measures from the subsections should give the same result as would be obtained by making a single measure over the entire length.

For an RTRRMS, which is based on the AR method of averaging, roughness measures from sections of equal length are simply averaged. Table 3 shows that the moving average and quarter-car indices are combined in this fashion. As noted earlier, RMS measures are averaged by adding the squares of the measures and then taking the square root of the sum. As indicated in Table 3, the RMSD analysis requires an even more complex method. Because a quadratic equation is used to present the RMSD measures in units of mm/km, there is no simple way to combine the converted indices. They must be first converted back to RMSD, using the inverse of the quadratic equation. Then, the RMSD values can be combined using an RMS average. Finally, that RMSD value must be converted back to mm/km using the quadratic equation.

For the QI and MO analyses, no method exists to combine measures for short sections to obtain the measure that would be calculated for the entire length. To visualize this, consider an unrealistic (but mathematically simple) case in which a section that is 1.0 km long is measured in two sections. In the first half, the $RMSVA_{1.0}$ value is 9.5 whereas the $RMSD_{2.5}$ value is zero. The resulting QI_r is then 50 counts/km. In the second section, the $RMSVA_{1.0}$ value is zero and the $RMSVA_{2.5}$ value is 3.02, also giving a QI_r of 50. For the entire section, the $RMSVA_{1.0}$ value would be 6.7 (the RMS average of 9.5 and 0), whereas the $RMSVA_{2.5}$ measure would be 2.14. Thus, the true QI_r value for the entire length is 74.3, even though both subsections have QI_r values of 50. Thus, the QI and MO indices can be length dependent.

Note that values of zero RMSVA would never be measured in practice; therefore the effect will be smaller and in most cases nonexistent. This example is included to help explain the more plausible scenario in which a 1-mi road with an MO rating of 100 in./mi can be composed of two subsections with MO ratings of 90 and 95.

Loss of Profile Length

The moving average and rolling straightedge (RMSVA) analyses use geometric smoothing, which requires measurement of the profile on either side of the point being considered. In each of these cases, a length equal to 1/2 of the baselength will not be processed at the beginning of the profile. The same is also true at the end of the profile.

Intuitive Understanding of the Scales

The moving average and the rolling straightedge (RMSVA) have been shown to be easily visualized geometric analyses of profile (see Figures 5 and 6). The quarter-car analysis owes much of its popularity to the fact that most practitioners are familiar with the RTRRMS measure that it replicates. The popularity of the RTRRMS-type of measure (ARS) is evident because the RMSD and RMSVA analyses are not used in their direct forms, but are instead converted to an approximation of the RTRRMS statistic and given units of ARS. As indicated in Table 3, these conversions include offsets, such that the roughness indices have arbitrary scales that do not coincide with a simple intuitive concept of roughness. A profile with zero variation will not give a zero roughness reading under the RMSD, QI_r, or MO analysis methods. Further, there is no simple relation between the roughness reading and any single property of the original profile. For example, if one road has twice the roughness of another on the RMSD scale (with units of mm/km), there is no physical property of the road that can be identified as being twice as large in one road as the other. In contrast, with

the quarter-car index if one road is twice as rough as another, it means that the slope amplitudes are twice as high over the wavelengths included.

Compatibility with Profilometric Methods

Perhaps the most critical consideration is the practical one that the IRI must be measurable with most of the profilometric equipment now in use, in addition to the equipment that can be envisioned over the coming years. Clearly, an index that is tailored to a specific piece of equipment is inappropriate as an IRI. In the case of the rod and level method, which is gaining popularity in developing countries as the only viable profilometric method, a sample interval on the order of 0.5 m is a practical limit. If shorter intervals are absolutely required to eliminate bias in the measures, the manpower needed to perform the measurements becomes too great.

The IRRE included paved and unpaved roads, which were profiled using rod and level ($\Delta X = 500$ mm), the TRRL Beam, and an APL trailer operated in two configurations. Of all the analyses described in this paper, only the quarter-car $RARS_{80}$ index could be measured on all types of roads using all of the profilometric methods. Briefly, the problems with the other analyses were as follows:

$CP_{2.5}$

The moving average analysis becomes sensitive to the sample interval when shorter baselengths are used. A baselength of 2.5 m was found to provide much better correlation with the RTRRMSs than the longer baselengths. CP_{10} was measurable by most of the equipment, but did not have the same degree of correlation with the RTRRMSs.

APL 72 Short-Wave Index

This analysis was developed specifically with the APL profilometer in mind, and cannot be applied directly to rod and level methods.

RMSD

This analysis is tailored to the TRRL beam instrument, and would require further development for use with other methods of measuring profile. It was not tested with the APL system and has not been used with any profile measuring method other than the TRRL beam.

QI_r

The APL profilometer was not able to measure QI_r directly for all of the surface conditions covered in the IRRE.

Correlation With the RTRRMSs

When profilometric methods are not possible for whatever reason, it is expected that the roughness measures will be made with an RTRRMS calibrated to the IRI scale. The accuracy of the RTRRMS measure is limited by the correlation between the IRI and the RTRRMS, and therefore a high correlation with RTRRMSs is required. Also, the correlation should be insensitive to surface type, so that practitioners can apply a single calibration equation to all RTRRMS measures.

It was demonstrated that the measures from any two RTRRMSs are highly correlated if they are operated at the same speed and that the correlations drop when the speeds used for the systems differ. Therefore, an essential part of the IRI is the standardization of RTRRMS measuring speed. When all of the factors were considered, it became clear that a relatively high speed suitable for highway use was necessary. A standard speed of 80 km/h (50 mi/h) was selected, as it is already standard for many organizations.

The best correlations were obtained using the quarter-car analysis, $RARS_{80}$. The next closest profile analysis was QI_r, which generally showed the same correlations except in the cases of a few outlier test sites. The measures from the RTRRMSs did not correlate as well with any of the profile references, but the errors observed using the quarter-car were about one-half of those observed using QI_r.

Using a lower standard speed, TRRL obtained high correlations by using the RMSD analysis. However, this analysis was tested (by TRRL) only on the sites that were measured with the TRRL beam--18 sites, of which 10 were measured in both wheeltracks. Thus, the correlations with most of the RTRRMSs were based on only 10 data points (For the BI trailer, 28 wheeltracks were covered.) Even though the RMSD parameters were optimized to obtain high correlation of those sites, the performance of the quarter-car (using the appropriate simulation speed) was just as good.

The quarter-car, the QI_r, the RMSD, and most recently, the MO, have all been developed to provide a reference for calibrating RTRRMSs. Of these, only the quarter-car directly computes the ARS-type of roughness index observed by an RTRRMS. It is also the only analysis based on the mechanics of the measuring process, rather than an empirical correlation. Correlation experiments have been used only to validate its performance. Each of the other analyses used some other instrument as a reference, and those reference instruments no longer exist. But as Figure 7 shows, the correlation methods used with the other analyses result in choices of parameter values that cause those analyses to resemble the quarter-car analysis to the extent possible. For all practical purposes, the quarter-car can be considered as the culmination of the reference RTRRMS concept underlying QI, MO, and the BI trailer.

The success that can be achieved by using the IRI as a standard measure of roughness can be seen when measurements from diverse types of equipment calibrated to that standard are compared. Figure 8 shows the agreement possible between a Mays meter car, a National Association State Road Authorities (NAASRA) car, the TRRL Bump Integrator trailer, and the APL trailer. Included in this plot are results from roughness measurements at speeds other than the standard of 80 km/h (speeds are indicated in the axis labels), and each of the RTRRMSs was calibrated from profile measured by a difference source.

The IRRE included no test sites with portland cement concrete (PCC) surfaces, and therefore it is mentioned here that the IRI had already been tested and validated on PCC sites before the IRRE, as a part of the correlation program reported in NCHRP Report 228 (12). Thus, the IRI has been tested for all conventional road surfaces used in the United States.

CONCLUSIONS

The IRRE added further proof that most problems with compatibility between RTRRMSs can be solved simply by adopting a standard measuring speed and calibrating RTRRMS to the same profile-based roughness index.
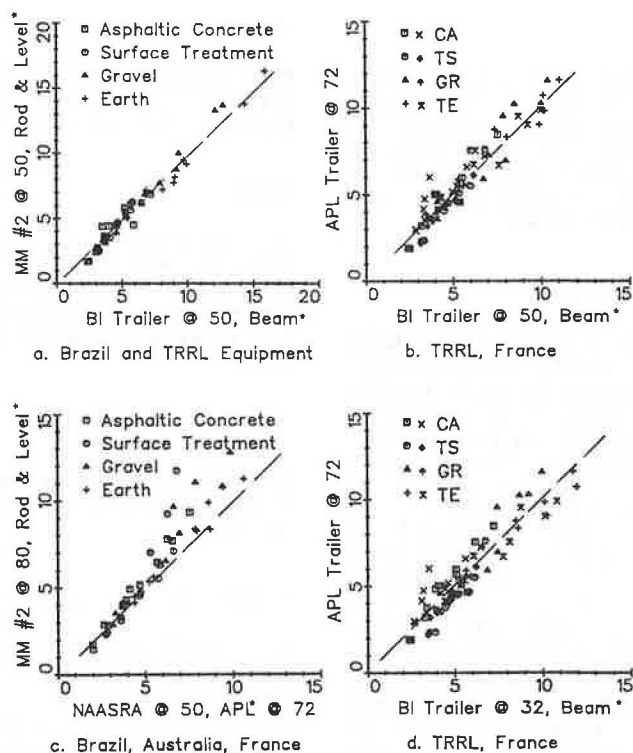
FIGURE 8 Examples of agreement among equipment using the IRI roughness scale.

In choosing a profile-based index to define the IRI, a number of analytic methods were considered. When the parameters are optimized for correlation with RTRRMSs, the analyses become very similar regarding the wavelengths that are emphasized in the roughness indices. Essentially, they begin to resemble a quarter-car analysis. The quarter-car analysis was therefore used to define the IRI roughness scale.

Because the quarter-car analysis most directly measures the profile components contributing to the RTRRMS measures, it avoids some practical problems that arise with the other indices. The QI_r, RMSD, and MO analyses all result in roughness scales that are obtained by conversions that introduce peculiarities into the scales, such as nonzero reading for a perfect road and dependence on the profile length.

Because they respond to approximately the same wavelengths, results obtained using the different analyses are almost perfectly correlated for most types of roads. In special cases (on roads with peculiar properties) differences are observed, with the quarter-car providing the best match with the RTRRMSs.

ABBREVIATIONS AND ACRONYMS

APL	Longitudinal profile analyzer (instrument developed by LCPC)
APL 72	Waveband analysis (roughness index associated with the APL)
AR	Average-rectified (averaging method)
ARS	Average rectified slope (roughness measure)
BI	Bump integrator (instrument developed by TRRL)
BPR	Bureau of Public Roads
CHLOE	Rolling straightedge profilometer (instrument developed by AASHO)
CP	Coefficient of smoothness (roughness index used in Belgium)
CRR	Center for Road Research (Belgium)
ΔX	Sample interval (distance between measures)
GMR	General Motors Research
IRRE	International road roughness experiment (Brasilia, Brazil, 1982)
IRI	International roughness index
LCPC	Central Bridge and Pavement Laboratory (France)
MO	Reference Mays meter index (roughness index from Texas)
NAASRA	National Association of Australian State Road Authorities
QCS	Quarter-car simulation
QI	Quarter-car index (roughness index developed in Brazil)
QI_r	Estimate of QI from RMSVA (roughness index developed in Brazil)
RARS	Reference averaging rectified slope (roughness index from a QCS)
RBI	Reference bump integrator (roughness index developed by TRRL)
RMS	Root-mean-square (averaging method)
RMSD	RMS deviation (roughness index developed by TRRL)
RMSVA	RMS vertical acceleration (roughness index developed in Texas)
RTRRMS	Response-type road roughness measuring system (category of instruments)
TRRL	Transport and Road Research Laboratory (United Kingdom)

REFERENCES

1. M.S. Janoff and J.B. Nick. Effects of Vehicle and Driver Characteristics on the Subjective Evaluation of Road Roughness. Measuring Road Roughness and Its Effects on User Cost and Comfort. ASTM STP 884. T.D. Gillespie and M. Sayers, eds., American Society of Testing and Materials, Philadelphia, Pa., 1985, pp. 111-126.

2. M. Sayers, T.D. Gillespie, and C. Queiroz. International Experiment to Establish Correlations and Standard Calibration Methods for Road Roughness Measurements. Technical Paper 45. World Bank, Washington, D.C., 1986.

3. M. Sayers, T.D. Gillespie, and W.D. Paterson. Guidelines for the Conduct and Calibration of Road Roughness Measurements. Technical Paper 46. World Bank, Washington, D.C., 1986.

4. Mays Ride Meter Booklet. 3rd ed., Rainhart Company, Austin, Tex., 1973.

5. P.G. Jordan and J.C. Young. Developments in the Calibration and Use of the Bump-Integrator for Ride Assessment. TRRL Supplementary Report 604. Transport and Road Research Laboratory, United Kingdom, 1980.

6. W.J. Gray. A Review of Australian Experience with Road Roughness as Measured by the NAASRA Roughness Meter. Presented at the Symposium on Roughness, 60th Annual Meeting of the Transportation Research Board, Washington, D.C., 1981.

7. J.A. Buchanan and A.L. Catudal. Standardizable Equipment for Evaluating Road Surface Roughness. Public Roads, Feb. 1941.

8. J. Lucas and A. Viano. Systematic Measurement of Evenness on the Road Network: High Output Longitudinal Profile Analyzer. Report 101, French Bridge and Pavement Laboratories, France, June 1979.

9. E.B. Spangler and W.J. Kelly. GMR Road Profilometer, a Method for Measuring Road Profile. Research Publication GRMR-452. General Motors Corp., Warren, Mich., Dec. 1964.

10. C.V. Queiroz. A Procedure for Obtaining a Stable Roughness Scale from Rod and Level Profiles. Working Document 22. Research on the Interrelationships Between Costs of Highway Construction, Maintenance, and Utilization, Empresa Brasileria de Planejamente de Transportes (GEIPOT), Brasilia, July 1979.

11. M.B. Gorski. Étude de l'uni longitudinal des revêtements routiers. Report CR 15/81. Centre de Recherches Routières, Belgium, 1981.

12. T.D. Gillespie, M. Sayers, and L. Segal. Calibration of Response-Type Road Roughness Measuring Systems. NCHRP Report 228, TRB, National Research Council, Washington, D.C., 1980, 81 pp.

13. M. Sayers. Development, Implementation, and Application of the Reference Quarter-Car Simulation. Measuring Road Roughness and Its Effects on User Cost and Comfort. ASTM STP 884. T.D. Gillespie and M. Sayers, eds., American Society for Testing and Materials, Philadelphia, Pa., 1985, pp. 25-47.

14. W.R. Hudson, D. Halbach, J.P. Zaniewski, and L. Moser. Root-Mean-Square Vertical Acceleration as a Summary Roughness Statistic. Measuring Road Roughness and Its Effects on User Cost and Comfort. ASTM STP 884. T.D. Gillespie and M. Sayers, eds., American Society for Testing and Materials, Philadelphia, Pa., 1985, pp. 3-24.